IDENTIFYING AND TARGETING CODING/NON-CODING MOLECULAR SWITCHES REGULATING DRUG RESISTANCE AND METASTASIS IN BREAST CANCER

A DISSERTATION SUBMITTED TO

THE GRADUATE SCHOOL OF ENGINEERING AND SCIENCE

OF BILKENT UNIVERSITY

IN PARTIAL FULFILLMENT OF THE REQUIREMENTS FOR

THE DEGREE OF

DOCTOR OF PHILOSOPHY

IN

MOLECULAR BIOLOGY AND GENETICS

By

Umar Raza

September 2017

IDENTIFYING AND TARGETING CODING/NON-CODING MOLECULAR SWITCHES REGULATING DRUG RESISTANCE AND METASTASIS IN BREAST CANCER

By Umar Raza

September, 2017

We certify that we have read this dissertation and that in our opinion it is fully adequate in scope and in quality, as a dissertation for the degree of Doctor of Philosophy.

_____

Özgür Şahin

(Advisor)

_____

Serkan İsmail Göktuna

_____

Ayşe Elif Erson Bensan

_____

Bala Gür Dedeoğlu

_____

Urartu Özgür Şafak Şeker

Approved for Graduate School of Engineering and Science

_____

EZHAN KARAŞAN

Director of the Graduate School of Engineering and Science

ABSTRACT

IDENTIFYING AND TARGETING CODING/NON-CODING MOLECULAR SWITCHES REGULATING DRUG RESISTANCE AND METASTASIS IN BREAST CANCER

Umar Raza

Ph.D. in Molecular Biology and Genetics

Advisor: Özgür Şahin

September, 2017

Breast cancer is the second most common cancer and the leading cause of cancer associated deaths in women worldwide. Despite the availability of large number and various types of therapy agents which are effective in limiting tumor burden at initial stages, cancer cells still manage to resist to therapy treatment and exhibit re-growth of existing tumor or metastasize to distant organs. Therefore, there is a dire need to identify underlying molecular mechanisms to enhance therapy response and to block metastasis. In addition to coding genome, non-coding RNAs have also play active role in controlling proliferation, apoptosis, invasion and drug resistance in cancer. Therefore, I aimed to identify novel coding/non-coding molecular switches regulating drug resistance and metastasis in breast cancer.

In the first part of this dissertation, I identified miR-644a as a novel tumor suppressor inhibiting both cell survival and epithelial mesenchymal transition (EMT) whereby acting as pleiotropic therapy-sensitizer in breast cancer. Both miR-644a expression and its gene signature are associated with tumor progression and distant metastasis-free survival. Mechanistically, miR-644a directly targets the transcriptional co-repressor C-terminal binding protein 1 (CTBP1) whose knock-outs by the CRISPR-Cas9 system inhibit tumor

growth, metastasis, and drug resistance, mimicking the phenotypes induced by miR-644a. Furthermore, miR-644a/CTBP1-mediated upregulation of wild type- or mutant-p53 acts as a 'molecular switch' between G1-arrest and apoptosis by inducing p21 or Noxa, respectively. Interestingly, an increase in mutant-p53 by either overexpression of miR-644a or downregulation of CTBP1 was enough to shift the balance between cell cycle arrest and apoptosis in favor of apoptosis through the upregulation of Noxa. Notably, p53-mutant patients, but not p53-wild type ones, with high CTBP1 level have a shorter survival suggesting that CTBP1 could be a potential prognostic factor for breast cancer patients with p53 mutations. Overall, modulation of the miR-644a/CTBP1/p53 axis may represent a new strategy for overcoming both therapy resistance and metastasis.

In the second part of this dissertation, I performed whole transcriptome sequencing with downstream pathway analysis in the chemoresistant triple negative breast cancer (TNBC) tumors we developed *in vivo.* This suggested a potential role of integrins and hypoxia in chemoresistance. Mechanistically, we showed that our candidate gene is hypoxia-induced and is overexpressed in resistant tumors, and activates integrin subunit alpha 5 (ITGA5). In the meantime, hypoxia-mediated downregulation of a miRNA targeting our candidate gene, leads to further activation of the ITGA5. This culminates in the activation of FAK/Src signaling thereby mediating resistance. Importantly, higher expression of our candidate gene, or lower expression of miRNA was associated with poorer relapse-free survival only in chemotherapy-treated TNBC patients. Finally, inhibition of candidate gene increased the efficacy of chemotherapy in highly aggressive TNBC models *in vivo* providing pre-clinical evidence for testing inhibitors against our candidate gene to overcome chemoresistance in TNBC patients.

Keywords: Breast cancer, chemotherapy resistance, EMT, microRNAs, p53 signaling, integrin signaling, hypoxia, CTBP1, lysyl oxidase, ITGA5

ÖZET

MEME KANSERİNDE İLAÇ DİRENCİ VE METASTAZI DÜZENLEYEN KODLANAN/KODLANMAYAN MOLEKÜLER ANAHTARLARIN TANIMLANMASI VE HEDEFLENMESİ

Umar Raza

Moleküler Biyoloji ve Genetik, Doktora

Tez Danışmanı: Özgür Şahin

Eylül, 2017

Meme kanseri dünyada en yaygın görülen ikinci kanser olup; kadınlarda kansere bağlı ölümlerin önde gelen nedenidir. Çok sayıda ve farklı çeşitte tedavi ajanlarının varlığına rağmen; kanser hücreleri tedaviye direnç geliştirebilir ve var olan tümör büyümeye devam edebilir ya da uzak organlara metastaz yapabilir. Bu noktada, tedavi yanıtını arttırabilmek ve metastazı engelleyebilmek için altta yatan moleküler mekanizmaları belirlemek önemli bir ihtiyaçtır. Genomun kodlanan bölümünün yanısıra, kodlamayan RNA'lar da kanserde çoğalma, apoptoz, invazyon ve ilaç direncinin kontrolünde aktif rol oynamaktadırlar. Bu nedenle, bu tez çalışmasında meme kanserinde ilaç direncini ve metastazını düzenleyen yeni kodlanan/kodlanmayan moleküler anahtarların belirlenmesi amaçlanmıştır.

Bu tezin ilk bölümünde, hem hücre sağkalımını hem de epiteliyal mezenkimal geçişi (EMG) inhibe eden, meme kanserinde birçok ilaca duyarlılığı artıran ve bir tümör baskılayıcı gibi hareket eden miR-644a'yı tanımladım. Hem miR-644a ifadesi hem de gen imzası, tümör gelişmesi ve uzak metastassız sağkalım ile ilişkilidir. Mekanistik olarak, miR-644a doğrudan transkripsiyonel co-repressor (baskılayıcı) olan C-terminale bağlanan proteini (CTBP1) hedef alır ve bu genin CRISPR-Cas9 sistemi ile baskılanması

miR-644a’nın ifadesinin indüklenmesi ile sağlanan fenotipleri taklit ederek tümör büyümesini, metastazı ve ilaç direncini inhibe eder. Ayrıca, miR-644a/CTBP1 aracılığıyla ifadesi artırılan yabanıl tip (wild type) veya mutant-p53 sırasıyla p21 veya Noxa’yı indükleyerek, hücre döngüsünün G1 evresinde tutulması ve apoptoz arasında bir *'moleküler anahtar'* olarak işlev görür. İlginç olarak, miR-644a'nın aşırı ifadesi veya CTBP1'in ifadesindeki azalma aracılığı ile oluşan mutant-p53'teki artışın, Noxa'nın ifadesinin artışı ile hücre döngüsü-apoptoz dengesinin apoptoz lehine kayması için yeterli olduğu görülmüştür. Yalnızca p53 mutant ve yüksek CTBP1 ifadesine sahip hastarın daha kısa sağkalıma sahip oldukları tespit edilmiş olup; bu sonuç p53 mutasyonu taşıyan meme kanseri hastaları için CTBP1'in potansiyel prognostik bir biyobelirteç olabileceğini düşündürmektedir. Özetle, miR-644a/CTBP1/p53 ekseninin modülasyonun hedeflenmesi, hem tedaviye direnci hem de metastazı yenmek için yeni bir strateji oluşturabilir.

Bu tezin ikinci bölümünde, *in vivo* olarak geliştirilen kemoterapi dirençli triple negatif meme kanseri (TNMK) tümörlerde, yeni nesil dizileme ile tüm genom boyutunda gen ifade profili değerlendirilmiştir. Analiz sonuçları, kemoterapi direncinde hipoksinin ve integrinlerin potansiyel bir rolü olduğunu göstermiştir. Seçilen aday genin hipoksi ile indüklendiği ve kemoterapiye dirençli tümörlerde aşırı ifade edildiği; aynı zamanda ITGA5'i aktive ettiği tespit edilmiştir. Diğer taraftan aday genimizi hedefleyen bir miRNA'nın hipoksi aracılığıyla downregülasyonu sağlanarak ITGA5'in daha çok aktifleşmesine yol açtığı gözlenmiştir. Bu olay, dirence aracılık eden FAK/Src yolağının aktivasyonuyla sonuçlanır. Tez çalışmasının bir diğer önemli bulgusu ise aday genin yüksek anlatımının veya miRNA'nın düşük anlatımının, sadece kemoterapi tedavisi uygulanmış TNMK hastalarında kısa nükssüz sağkalımla ilişkili olduğudur. Son olarak, aday genin agresif TNMK *in vivo* modellerinde inhibisyonunun kemoterapinin etkinliğini

artırması; TNMK hastalarında kemoterapi direncinin üstesinden gelmek amacıyla aday genimize karşı inhibitörlerin test edilmesine ilişkin pre-klinik kanıt sağlamıştır.

Anahtar Kelimeler: Meme kanseri, kemoterapi direnci, EMT, mikroRNA'lar, p53 sinyal yolağı, integrin sinyal yolağı, hipoksi, CTBP1, lisil oksidaz, ITGA5

I dedicate this work to my

MOTHER

who sacrificed her present for my future,

who supported me at each stage of my life and

who showed an endless patience for me

شکریہ امّاں

Acknowledgements

I would like to express my deepest appreciation for Dr. Özgür Şahin for giving me this great opportunity, for directing me with his wise academic experience in my PhD's study and for providing a healthy helpful research environment.

I would like to acknowledge Özge Saatci for her life-saving efforts to help me for both experiments and data analyses whenever needed. I would like to thank Erol Eyüpoğlu for his friendship and endless support throughout this study. It would have not been possible without any of them. I would also like to thank Pelin Gulizar Ersan for her valuable help in most of the *in vivo* experiments. I would like to thank Hilal Bal and my intern, Oğuzhan Tarman, for their friendly help and support in the last year.

I would like to thank all present and former members of Şahin Lab: Merve Mutlu, Emre Yurdusev, Ünal Metin Tokat, Özge Akbulut, Selvi Durmuş, Suhail Akhtar Ansari, Rashmi Rekha Mishra, Nevin Belder, Ridho Assidicky and Özlem Şahin for their help and support.

I would like to acknowledge Hayriye Tatlı Doğan for her efforts in immunohistochemistry analyses throughout the study. I would also be grateful to Dr. Jitao David Zhang for his help with analysis of RNA-seq data. I would also like to thank Dr. Yasser Riazalhosseini for his guidance and for sharing inhibitors and shRNA constructs.

I would like to acknowledge Dr. Mehmet Öztürk and Dr. Özlen Konu for recommending me to Dr. Özgür Şahin. I would also like to thank my mates from Dr. Öztürk's Lab: Çiğdem Özen, Dilek Çevik, Umur Keleş and Gökhan Yıldız for their help and support.

I would be thankful to my elder brother, Abdur Rehman Raza Khan, and his family, for always supporting me and pushing me to work hard. I would also be thankful to my dearest and closest friends back in Pakistan, Hassan Ali and Furqan Haider, for being always available to listen to me and support me. I would like to thank Ali Haider, Naveed-ul-Mustafa and Murat Işbilen for all the fun time we spent together at Bilkent.

Lastly, I express a deep sense of gratitude to Higher Education Commission, Pakistan for financially supporting me throughout my PhD.

Contents

List of Figures

List of Tables

Abbreviations

7-AAD	7-Aminoactinomycin D
ACTB	Actin beta
AGO	Argonaute
AML	Acute myeloid leukemia
APS	Ammonium peroxodisulfate
BAPN	β-Aminopropionitrile
BAX	BCL2 Associated X
BCA	Bicinchoninic acid
BLI	Bioluminescence imaging
BRCA1	Breast cancer type 1 susceptibility protein
BrdU	5-bromo-2-deoxyuridine
BSA	Bovine Serum Albumin
CAR	constitutive androstane receptor
Cdc2/CDK1	Cyclin dependent kinase 1
Cdc25C	Cell division cycle 25C
CDH1	E-cadherin
CDK2	Cyclin-dependent kinase 2
CDK4	Cyclin dependent kinase 4
CTBP1	C-terminal binding protein 1
CTBP2	C-terminal binding protein 2
DAPI	4',6-diamidino-2-phenylindole
DAVID	The database for annotation, visualization and integrated discovery
DMEM	Dulbecco's modified eagle medium

DMFS	Distant metstasis free survival
DNA	Deoxyribonucleic acid
dNTP	Deoxynucleotide triphosphate
ECL	Enhanced chemiluminescence
ECM	Extracellular matrix
EGF	Epidermal growth factor
EGFR	Epidermal growth factor receptor
EMT	Epithelial-mesenchymal transition
ER-α	Estrogen receptor alpha
FAK	Focal adhesion kinase
FBS	Fetal bovine serum
FN	Fibronectin
GAPDH	Glyceraldehyde 3-phosphate dehydrogenase
GEO	Gene expression omnibus
GSEA	Gene set enrichment analysis
H&E	Hematoxylin and eosin
HCC	Hepatocellular carcinoma
HCV	Hepatitis C virus
HIF1A	Hypoxia inducible factor A
HIF1B	Hypoxia inducible factor B
HPRT	Hypoxanthine guanine phosphoribosyl transferase
HR+	Hrmone receptor positive
HRP	Horseradish peroxidase
IDC	Invasive ductal carcinoma
IHC	Immunohistochemistry

ILK	Integrin linked kinase
IPA	Ingenuity pathway analysis
ITGA10	Integrin subunit alpha 10
ITGA5	Integrin subunit alpha 5
ITGB5	Integrin subunit beta 5
kDa	Kilo dalton
KRT18	Keratin 18
LNA	Locked nucliec acid
LOX	Lysyl oxidase
MDR	Multi drug resistance
METABRIC	Molecular taxonomy of breast cancer international consortium
MFP	Mammary fat pad
miRNA	microRNA
MMP1	Matrix metallopeptidase 1
MMP9	Matrix metallopeptidase 9
MTDH	Metadherin
mut	Mutant
MYC	MYC proto-oncogene
NOXA	Phorbol-12-myristate-13-acetate-induced protein 1 (PMAIP1)
NSCLC	Non-small cell lung carcinoma
ORF	Open reading frame
OS	Overall survival
P/S	Penicilllin/Streptomycin
p21	Cyclin-dependent kinase inhibitor 1A (CDKN1A)
PBS	Phosphate buffered saline

pCR	Pathological complete response
PDX	Patient derived xenograft
Poly-HEMA	Poly-hydroxyethylmethacrylate
PR	Progesterone receptor
pre-miRNA	Precursor miRNA
pri-miRNA	Primary miRNA
PTEN	Phosphatase and tensin homolog
PUMA	P53-upregulated modulator of apoptosis
qRT-PCR	Quantitative real time polymerase chain reaction
Rb	Retinoblastoma protein
RDX	Radixin
RFS	Relapse free survival
RHOA	Ras homolog gene family, member A
RTCA	Real time cell analyzer
RTK	Receptor tyrosine kinase
SDS-PAGE	Sodium dodecyl sulfate polyacrylamide gel electrophoresis
SERD	Selective ER downregulator
SNAI2	Snail family transcriptional repressor 2
Src	Src proto-oncogene, non-receptor tyrosine kinase
TAE	Tris-acetate EDTA
TBST	Tris buffer saline Tween20
TCGA	The cancer genome atlas
TNBC	Triple negative breast cancer
TP53	Tumor protein 53
UTR	Untranslated region

v/v	Volume/volume
w/v	Weight/volume
wt	Wild type
XPO5	Exportin 5
ZEB1	Zinc finger e-box binding homeobox 1
ZEB2	Zinc finger e-box binding homeobox 2
ZO1	Zona occludens-1 (Tight junction protein 1, TJP1)

Chapter 1

Introduction

1.1. Breast cancer

Although last decades have witnessed a great success in prevention, diagnosis and therapy, cancer is still one of the leading causes of death worldwide with nearly 1.6 million new cases reported only in the United States in 2016 [1]. Breast cancer is the most common malignancy and the second leading cause of cancer deaths among women [2] whose incidence rate is drastically increasing worldwide as compared to other cancer types [3]. It has been estimated that approximately 60,000 women will be diagnosed with non-invasive whereas nearly 250,000 women will be diagnosed with invasive breast cancer only in the United States, of which around 40,000 will die from breast cancer in 2017 [1].

Being a highly heterogeneous disease, breast cancer represents very distinct molecular, morphologic and clinical features among different subtypes. Clinically, it has been classified into 3 major subtypes based on the expression status of specific receptors, namely, hormone receptors (estrogen receptor alpha (ER-α) and progesterone receptor (PR)) and human epidermal growth factor receptor 2 (HER2/ErbB2). These subtypes are 1) hormone receptor positive (HR+) expressing higher levels of ER and PR; 2) HER2-amplified; and 3) triple-negative breast cancer (TNBC) which lacks the expression of all three receptors [4]. At the molecular level, breast cancer has been classified into 5 major subtypes largely overlapping with the clinical subtypes (Figure 1.1) [5] where Luminal subtype A and B are hormone positive, ErbB2 positive is HER2-amplified, and the most of Basal subtype is TNBCs.

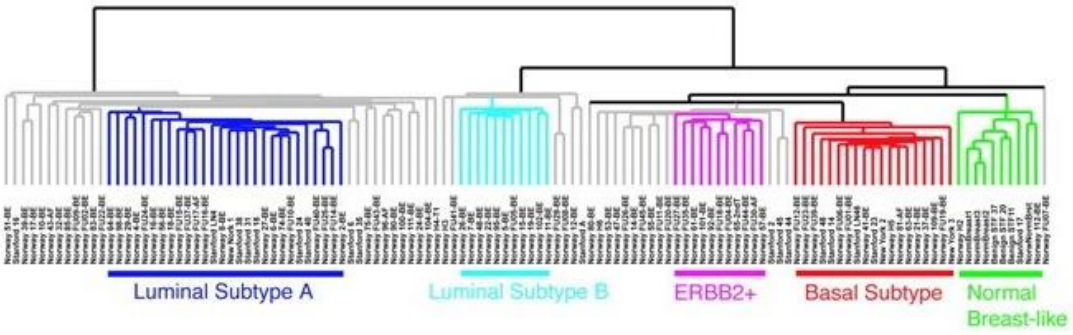

Figure 1.1. Molecular classification of breast cancer according to gene expression profiling [5].

1.2. Subtype-specific first-line treatments for breast cancer

Most of the breast cancer patients (around 70%) are HR+ subtype. Due to the overexpression of ER-α, patients in this subtype are mainly treated with hormone-targeted therapies such as tamoxifen and aromatase inhibitors in clinics [6]. On the other hand, HER2+ group, in which HER2 gene is amplified/overexpressed, encompasses around 20% of all the breast cancer cases. HER2 targeting monoclonal antibodies such as trastuzumab (Herceptin) or pertuzumab (Perjeta) are in clinical use to treat HER2+ breast cancers. These antibodies have shown efficiency towards blocking tumor growth as well as to enhance chemotherapy response [7, 8]. In addition, a dual inhibitor of EGFR and HER2 called lapatinib has been approved since 2007 to be used in combination with chemotherapy in clinics to treat HER2 overexpressing metastatic breast cancers [9]. Lastly, TNBCs are the most aggressive subtype of breast cancer which accounts for nearly 10-15% breast cancer diagnosed worldwide. Targeted-therapies are not available for TNBCs due to lack of druggable receptors e.g. ER-α or HER2; therefore, chemotherapy is the only treatment option for patients diagnosed with both early-stage and advanced-stage TNBCs [10]. Among chemotherapy agents, anthracycline and taxane-based chemotherapy agents are mainly used in both neo-adjuvant and adjuvant settings to treat TNBC [11].

1.3. Therapy resistance in breast cancer

Despite the availability of large number and various types of therapy agents (both chemo and targeted therapy) which are effective in limiting tumor burden at initial stages, cancer cells still manage to evade and exhibit re-growth of existing tumor or metastasize to distant organs. Currently, one of the major obstacles in achieving an effective cancer treatment is the emergence of therapy resistance: both "*de novo*" and "acquired" [12]. *De novo* resistance occur at the very beginning of treatment where tumor mass does not respond to treatment due to pre-existing molecular signature which interferes with the anti-cancer mechanisms of given treatment. In contrary, acquired resistance occurs in response to long-term treatments where cancer cells manage to survive under given anti-cancer treatment after initial response and become resistant. This kind of resistance is mostly associated with genomic, transcriptomic and epigenetic changes in tumor in response to prolonged treatments.

1.3.1. Targeted therapy resistance mechanisms in hormone-positive and HER2-amplified breast cancers

Cross-talk between ER-α and HER2 is one of the well-studied mechanisms of tamoxifen resistance. In the presence of HER2, tamoxifen can serve agonistically to ER-α by bringing transcription co-activators rather than repressors to ER-α transcription complex; thus, promoting transcription of ER-α target genes [13-15]. In addition to HER2 signaling, other growth factor receptors (i.e., insulin-like growth factor receptor or fibroblast growth factor receptor) can confer tamoxifen resistance by activating MAPK and PI3K/AKT/mTOR signaling cascades [16, 17]. Other resistance mechanisms include lack of ER-α expression due to hypermethylation of ER-α promoter [18] and dysregulated drug metabolisms [19, 20]. Constitutively active ligand-independent mutant ER-α can

confer resistance to aromatase inhibitors by altered transcriptional regulation at downstream [21, 22]. Other mechanisms of resistance to aromatase inhibitors include hyperactive interferon signaling [23] and disturbance in the balance of pro- and anti-apoptotic genes [24]. In order to overcome resistance, mTOR and CDK4/6 inhibitors have shown promising results in combination with other therapy agents in clinical trials and have been commercialized. For instance, everolimus, an allosteric inhibitor of mTOR, has been approved for use in post-menopausal woman with HR+ breast cancer as well as in other cancer types [25]. Recently, FDA has approved two different CDK4/6 inhibitors, palbociclib and ribociclib, to treat HR+ and HER2-negative advanced therapy resistant or metastatic tumors based on results of clinical trials where significant improvement in clinical outcome was observed when these inhibitors were combined with chemotherapy agents, letrozole or fulvestrant [26].

Multiple mechanisms responsible for trastuzumab resistance have been identified. In order to inhibit binding of antibody to HER2, cells often adapt to cleavage of the extracellular domain of the HER2 receptor [27-29]. Overexpression of other members of ErbB family such as HER3 or other tyrosine kinase receptors like IGF1R to promote downstream signaling have also been reported in the context of trastuzumab resistance [30, 31]. Other well-studied resistance mechanisms include loss of phosphatase and tensin homolog (PTEN) tumor suppressor or activation of oncogenes like SRC to activate HER2 signaling pathway even in the presence of trastuzumab [32-35]. Due to identification of proteins responsible for developing resistance, combination therapies have been tested to treat advanced stage therapy resistant HER2-amplified breast cancer [36]. For instance, combining trastuzumab with small molecule tyrosine kinase inhibitor, lapatinib, followed by PI3K/mTOR inhibition has shown to improve the survival outcome [37]. Furthermore, combination of mTOR inhibitor, evorolimus, with

trastuzmab has benefitted the patients in clinical trials [38]. In addition, antibody drug conjugate TDM1 (trastuzumab + emtansin) has been approved for metastatic HER2-amplified breast cancer patients after superior effect of T-DM1 over lapatinib and capecitabine combination in patients pretreated with trastuzumab and taxane therapies [39].

1.3.2. Chemotherapy resistance mechanisms in TNBCs

The extent of pathological response to neo-adjuvant treatment at surgery has been established as a prognostic marker for disease recurrence in breast cancer [40]. As compared to other subtypes, TNBC patients show low risk of recurrence if pathological complete response (pCR) is achieved [41]. While only 30-40% of TNBC patients show pCR towards treatment, others have less than 60% 5-year survival due to aggressive relapse as a response of chemotherapy resistance [42]. Recently, PTEN deletions/mutations and copy number amplifications of proto-oncogenes MYC, JAK2, PIM1 have been frequently observed in residual disease after neo-adjuvant chemotherapy treatment of TNBCs, thus, suggesting high rate of chromosomal instability as a driving force to develop chemotherapy resistance in TNBCs. However, due to subclonal nature of driver mutations in TNBCs, single agent targeted therapy is unlikely to be successful [43]. Aberrant NFKB signaling has also been associated with chemotherapy resistance in cancer, in general, but found difficult to be targeted because of the off- target effects and toxicities as a large spectrum of cellular processes revolve around NFKB [44]. Bortezomib, a ubiquitin-proteasome inhibitor known to suppress NFKB signaling by inhibiting IKB degradation [45] showed promising results in myeloma and lymphoma, but failed to prove its efficacy in combination with chemotherapy agents in solid tumors [46]. Interestingly, loss of proto-oncogene MYC has been shown to confer chemotherapy

resistance in breast cancer by misbalancing the expression of genes regulating apoptosis [47]. Other reported mechanisms of chemotherapy resistance in breast cancer include mutations in DNA repair enzymes [48], altered expression of drug transporter proteins [49], greater drug detoxification [50].

1.4. Tumor microenvironment and drug resistance

Other than malignant cells, tumor microenvironment comprises of immune cells, fibroblasts, tumor vasculature, signaling molecules and extracellular matrix (ECM) which also play pivitol roles in tumor cell maintainence and survival. Although, ECM has been proposed as safegaurd preventing cancer initiation in early life stages, it has been shown playing active roles in pathological incidences like tumorigenesis [51]. Tumor microenvironment associated ECM largely differs from that of the normal tissue and has been shown to serve as a basic scaffold for chemotaxis driven cancer cell invasion and metastasis [52]. Interplay between cancer cells and ECM elements (ECM modulating enzymes, collagens, laminin etc) is dynamic. Attachment to ECM has shown to alter polarization of malignant cells and cause resistance to etoposide-induced apoptosis in breast cancer [53]. Specifically, cell adhesion molecules-mediated drug resistance depends on association of integrin to ECM components including fibronectin, collagen and laminin [54]. Accumulating evidence has shown that changes in composition and topography of ECM upon therapy are directly sensed by multiple cell adhesion molecules including integrins which activate downstream pro-survival signaling to resist the given therapy [15]. ECM remodelling and integrin signaling mediated resistance has also been implicated to radiation and targeted therapies by attenuating activities of receptor tyrosine kinases (RTKs) such as EGFR [55, 56]. Desmoplastic stroma in tumor microenvironment

also poses a physical barrier for efficient delivery of therapy agents, thus rendering treatment options ineffecient and/or unsucessful [57].

As solid tumors grow in size, the inner core of the tumor mass gets deprived of oxygen. Tumor cells usually counteract this by adapting to hypoxia *via* upregulating transcription factors known as hypoxia-inducible factors (HIFs) [16]. Although human genome express three HIF-α isoforms, hypoxia-driven phenotypes and mechanisms have been mainly associated with HIF1-α which is widely expressed in tissues as compared to other family members [17] and transactivates distinct set of genes [18]. Patches of hypoxic tumor microenvironment has been well-established as significant contributor to chemotherapy failure and drug resistance due to fact that hypoxia is being causally involved in regulating multiple aspects of tumor biology such as resistance to apoptosis, metabolic reprogramming, angiogenesis and pH homeostasis [19, 20]. Therefore, studying drug resistance in settings where the hypoxic tumor microenvironment taken into account is critical towards the identification of true driving factors with high potential for successful translation in the clinic.

1.5. Metastasis in breast cancer

The majority of cancer deaths are not caused by primary tumors, but rather by the dissemination of the disease, i.e. the development of distant metastases. Metastasis is accomplished in two major steps: dissemination and colonization. Dissemination phase includes local invasion, intravasation into the systemic circulation, survival in the circulatory system and extravasation. Colonization phase includes the adaptation of these cells to a foreign microenvironment where the microscopic cells turn into macroscopic tumors. The whole process is outcome of the interplay between genetic and epigenetic modifications in tumor as well as in the tumor microenvironment [58].

Nearly 15% of all breast cancer patients experience an agressive disease and develop distant metastasis within 3 years of diagnosis of primary tumors, but it can also take 10 or more years after the intial detection of primary tumor to establish metastatic growth at distant organs [59]. Once disseminated, breast carcinoma can metastasize to various organs. The most preferential sites of breast cancer metastasis include bone, lungs and liver (Figure 1.2). Analysis of advanced stage breast cancer patients has shown subtype-specific tendency of breast cancer to metastasize. While HR+ patients show more bone metastasis, HER2-amplified patients exhibit increased incidence rate of liver metastasis, and TNBCs preferentially metastasized to brain and lungs [60]. In addition, breast cancer recurrence and mortality rate have also been associted with its subtypes. ER negative patients, in general, and TNBCs, in particular, usually develop metastasis within first 5 year of diagnosis. On the other hand, more than 50% of recurrence incidences in ER positive patients appear after 5 years of first diagnosis [61].

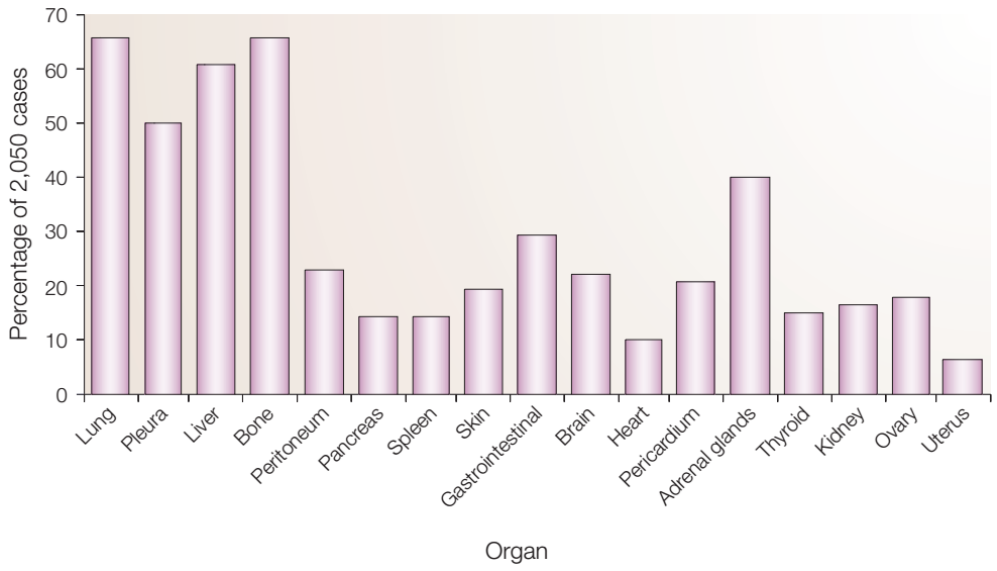

Figure 1.2: Most common metastasis sites of breast cancer [59]. See Appendix for the copyright permission.

Established prognostic markers of breast cancer metastasis include presence of lymph-node metastasis, larger-sized primary tumors and loss of histopathological differentiation. However, these traditional markers are only able to predict the course of disease confidently in very small population of patients. Therefore, additional prognostic markers, especially molecular markers, are needed to better predict the course of disease and metastasis incidence [59]. In this regard, there have been few studies which determined a set of protein-coding genes mediating organ-tropic metastasis in breast cancer. It has been shown that there are two sets of genes, one of which regulates both primary breast tumor growth (in case of ID1, CXCL1, PTGS2 and MMP1) and lung metastasis capacity while the other set involves gene e.g. SPARC and MMP2 which regulate lung metastatic virulence specifically [62]. Gene expression analysis of brain-tropic cancer cells and of clinical samples, coupled with functional analysis, identified the cyclooxygenase COX2, the epidermal growth factor receptor (EGFR) ligand HB-EGF, and the alpha2,6-sialyltransferase ST6GALNAC5 as mediators of cancer cell passage through the blood-brain barrier [63]. Set of genes including VCAM-1, NF-kB, JAGGED1, Src, matrix metallopeptidase 1 (MMP1), lysyl oxidase (LOX) and certain cytokines (CXCR4, CXCL12, TGFβ) have been associated with metastatic spread of breast cancer to bones [61].

1.6. MicroRNAs and their dysregulation in cancer

MicroRNAs (miRNAs) are a large family of small regulatory RNAs, acting in post-transcriptional gene regulation. They are 20-22 nucleotides long and recognize their target mRNAs by complementary base pairing. They control gene expression by mRNA cleavage, mRNA destabilization or inhibition of translation [64]. Almost half of miRNAs reside in clusters and transcribed as polycistronic precursor miRNAs [65]. Other

miRNAs, located in intergenic regions, are transcribed by their own promoters while those present in intronic regions are likely under the control of the host genes' promoters [66]. Currently, it has been reported that there are more than 2600 unique mature miRNAs in human (miRBase version 21) [67]. Most miRNAs are transcribed by RNA polymerase II as primary transcripts (pri-miRNAs), usually several kilobases long, which fold into hairpin structures containing imperfectly base-paired stem-loop structures [68]. RNase III endonuclease Drosha then cleaves primary miRNAs (pri-miRNAs) into ~70 nt long precursor miRNAs (pre-miRNAs) which are later transported to cytoplasm by RanGTP-dependent dsRNA-binding protein exportin-5 (XPO5) [69]. In cytoplasm, RNase III endonuclease Dicer cleaves pre-miRNAs into mature miRNAs which are loaded to RNA-induced silencing complexes. Along with Argonaute (Ago) proteins (mainly Ago1 and Ago2 in mammals) of the complex, miRNAs downregulate gene expression by binding to target mRNAs (Figure 1.2).

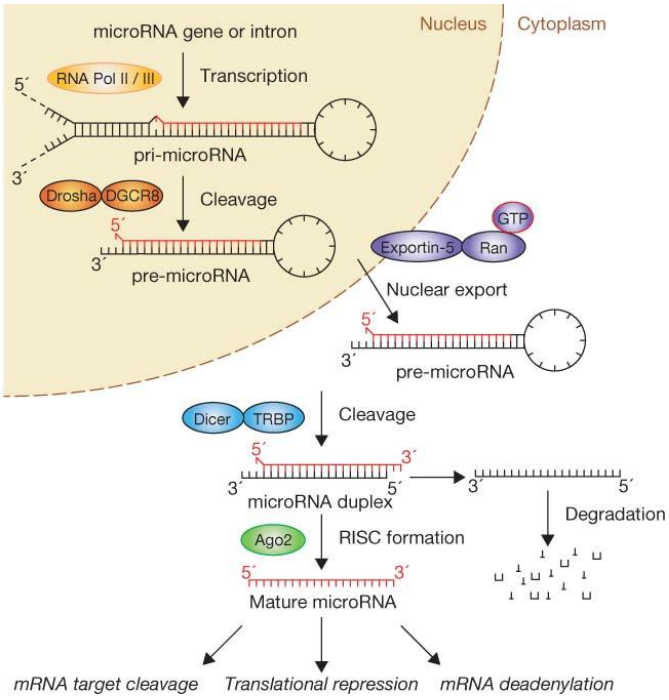

Figure 1.3: Schematic demonstration of miRNA biogenesis [70]. See Appendix for the copyright permission.

Although miRNA binding sites have also been found in 5'-UTR [71] and open reading frames (ORFs) [72] of the genes, they preferentially interact with seed-matching sequences in the 3'-UTR of mRNA. One miRNA can downregulate multiple genes due to the short sequence required for mRNA recognition, which is known as the 'seed region' spanning between the 2^{nd} and the 7^{th} (or 8^{th}) nucleotide of mature miRNAs. Taking both direct and indirect regulations together, it is not rare that a single miRNA can regulate the expression of tens or hundreds of genes. Out of all the identified human miRNAs, almost 50% are located at fragile sites on chromosomes known for having common alterations (i.e. amplification, deletion and rearrangements) in cancer [73]. Roles of miRNAs in cellular processes like cell cycle progression, proliferation, metabolism, apoptosis, and stress resistance [74] cannot be overlooked as more than 60% of human protein coding genes are predicted to be under selective pressure to be regulated by miRNAs [75].

1.7. MicroRNAs and tumor progression, metastasis and drug resistance

Considering the enormous regulatory potential of miRNAs, it is not surprising that they play crucial roles in cancer development, progression, metastasis and drug resistance [76]. For instance, elevated expression of oncogenic miR-17∽92 cluster (comprising of 6 miRNAs) has been reported during lymphomagenesis which allows continuous activation of oncogenic PI3K and NF-kB signaling by suppressing negative regulators of these pathways [77]. Another oncogenic miRNA, miR-21, is upregulated in lung, prostate, breast and pancreatic cancers compared to normal tissues [78]. In line with this, knockdown of miR-21 in breast cancer inhibited tumor growth and enhanced apoptosis by downregulating anti-apoptotic protein Bcl-2 [79]. miR-155 is overexpressed in pancreatic cancer where it promotes tumor development by repressing the expression of tumor suppressor Tp53INP1, and oligonucleotide-mediated inhibition of miR-155

restored Tp53INP1 levels along with significant increase in apoptotic cell death [80]. Tumor suppressor let-7 family miRNAs have shown to target a network of cell cycle-associated genes including E2F5, CCNA2, CDK8, hence playing important roles in regulating multiple proliferation pathways and controlling tumor growth [81]. miR-34 is another well-studied tumor-suppressor miRNA which is directly regulated by p53 and controls p53-mediated cell death. Low miR-34 expression attenuates p53-mediated apoptosis and contributes to tumor development [82]. Taken together, their function as negative regulators of multiple targets in biological networks and their common dysregulation in cancer make miRNAs attractive targets for cancer therapy.

miRNAs have been associated with drug resistance to both chemo- and targeted-therapies. Inhibition of miR-21 has been reported to increase gemcitabine sensitivity in cholangiocarcinoma and to inhibit the growth of topotecan-treated MCF7 cells [83]. In medulloblastoma, miR-34a has been demonstrated to sensitize cancer cells to mitomycin C and cisplatin by directly targeting the oncogenic gene MAGE-A, and to induce apoptotic cell death by modulating tumor suppressor p53 levels in a positive feedback loop [84]. In another study, miR-137 has been shown to target constitutive androstane receptor (CAR), which is an important regulator of multi-drug resistance (MDR), and its overexpression sensitized neuroblastoma, hepatocellular carcinoma (HCC) and colon cancer cells to doxorubicin [85]. Similarly, miRNAs have also been shown to regulate resistance to targeted therapies. Two independent studies have associated miR-221/222 with resistance to tamoxifen, by establishing miR-221/222 downregulating the expression of ER alpha [86] and p27/Kip1 [87]. Furthermore, it has been shown that miR-221/222 also confers resistance to fulvestrant, a selective ER downregulator (SERD), by modulating both Wnt/β-catenin and TGF-β pathways [88]. We have recently demonstrated that miR-375 is downregulated in tamoxifen resistant MCF-7 cells

compared with parental ones and re-expression of miR-375 sensitized resistant cells to tamoxifen partially by downregulating the oncogene metadherin (MTDH) [89]. Altogether, these reports clearly indicate the involvement of miRNAs in resistance to both chemotherapy and targeted therapy, and these miRNAs may be therapeutically modulated to sensitize tumor cells again to the drugs.

miRNAs have also been implicated in regulation of metastatic cascade. For instance, the miR-200 family has been found downregulated in metastases compared to primary tumors [48, 49] and plays a central role in the inhibition of EMT by forming a double-negative feedback loop with ZEB1 and ZEB2, both of which are the transcriptional repressors of cell-cell contact protein E-Cadherin [50, 51]. miR-31 has been demonstrated to regulate several post-intravasation steps including intraluminal viability, extravasation and survival at distal tissue in addition to the invasion and metastatic colonization steps by simultaneous targeting of three key genes: integrin α5 (ITGA5), radixin (RDX) and Ras homolog gene family , member A (RHOA) [90]. Recently, it was shown that miR-520/373 family inhibits both *in vitro* cell invasion and *in vivo* intravasation of highly invasive ER (-) breast cancer cells. Decreased expression of miR-520c was found to be correlated with the lymph node metastasis of ER (-) breast cancer patients [91]. miR-200 has been shown to promote the colonization of breast cancer cells by directly targeting the Sec23a gene which is involved in the secretion of metastasis-suppressive proteins [92]. Recently, miR-612 is suggested to suppress the colonization of HCC cells to the lungs [93]. Altogether, these findings suggest that miRNAs regulate metastasis at multiple steps by modulating different components of the cellular networks.

1.8. Modulation of microRNAs as drug candidates

With the discovery of microRNAs as crucial regulators of biological processes and their dysregulation in various human diseases, in general, but in cancer, in particular, therapeutic targeting of miRNAs is very attractive for scientists for novel therapy development in human pathologies [94]. There are several strategies being evaluated to target miRNAs or use them as targeting agents in cancer, such as i) inhibition of oncogenic miRNAs by antisense DNA oligonucleotides, antagomirs, locked nucleic acids (LNAs), RNA sponges or miR-masking; ii) exogenous expression of tumor suppressor miRNAs; and iii) targeting miRNAs by using small molecules [95]. Recently, an antisense nucleotide, Miravirsen, has been introduced as a potential drug to treat hepatitis C virus (HCV) infection. In principle, HCV requires liver specific miR-122 expression for replication. Miravirsen binds to miR-122 and inhibits its biogenesis in liver; thus, inhibiting HCV to replicate and multiply. After showing its success in treating HCV in chimpanzees, Miravirsen is now being tested in human clinical trials and has been found safe in term of toxicity [96]. MRX34, a liposomal encapsulated nanoparticle formulation, is the first miRNA-based cancer therapy agent. It is a double-stranded mimic of miR-34, a well-established tumor suppressor miRNA known for inhibiting oncogenicity and for inducing cancer cell death [97]. MRX34 has shown promising results in the Phase 1 clinical trial of different cancer types including renal cell carcinoma, melanoma and hepatocellular carcinoma [98]. Combination of miRNA delivery system with therapy agents has also shown promising results. For instance, delivery of LNAs encapsulated miR-10b in combination with a low dose of doxorubicin was enough to achieve a significantly greater decrease in tumor burden compared with doxorubicin monotherapy without any evidence of damage to normal tissues [99]. These studies clearly suggest that miRNAs have high potential to be used as the therapeutic drugs without toxicity in future.

1.9. The rationale and the aims of the dissertation

Therapy resistance and metastasis are two major hallmarks of cancer. Despite the huge advances in the field of drug design, cancer cells still manage to evade therapy, exhibit regrowth of tumor and/or metastasize to distant organs. Not only coding, but also non-coding genome (long non-coding RNAs, miRNAs, circular RNAs) is being extensively studied to understand the underlying mechanisms of therapy resistance and metastasis. Notably, treatment options are restricted to chemotherapy in TNBC due to lack of available druggable targets. This dissertation starts from the view to utilize unbiased genome-wide approaches to identify novel hubs of therapy resistance and metastasis in breast cancer, then to apply appropriate *in vitro* approaches to explore molecular mechanisms regulated by these hubs, and to validate findings using *in vivo* models in combination with *in silico* cross validation using online available patient data.

In this dissertation, the aims are as following:

- To identify novel coding/non-coding molecular switches regulating tumor progression, metastasis and chemo-response in breast cancer
- To identify novel drug targets overcoming chemotherapy resistance specifically in TNBCs

Chapter 2

Materials

2.1. Buffers

1X Anode Buffer I	300 mM Tris, 20% (v/v) methanol
1X Anode Buffer II	25 mM Tris, 20% (v/v) methanol
1X Cathode Buffer	40 mM 6-aminocaparoic acid, 20% (v/v) methanol
1X PBS	137 mM NaCl, 2.7 mM KCl, 10 mM Na_2HPO_4, 2 mM KH_2PO_4 (pH: 7.4)
1X SDS-PAGE Running Buffer	25 mM Tris, 14.41 g/l glycine, 1% (v/v) SDS
1X TAE	40 mM Tris, 20 mM acetic acid, 1 mM EDTA
1X TBST	20 nM Tris, 137 mM NaCl, 0.2% (v/v) Tween20
RIPA Lysis Buffer	150 mM NaCl, 1% (v/v) NP-40, 0.5% (v/v) Sodium DOC, 50 mM Tris-HCl (pH:8.0), 50 mM NAF, 1 mM $NaVO_4$, 4% (v/v) Protease inhibitor, 4% (v/v) Phospatase inhibitor

2.2. Chemicals and Reagents

4X Protein Loading Dye	250 mM Tris HCl (pH: 6.8), 10% (w/v) SDS, 0.1% (w/v) Bromophenol blue, 50% Glycerol (v/v), 25% (v/v) β-mercaptoethanol
6-aminocaparoic acid	Sigma Aldrich, St Louis, MO, USA
X DNA loading Dye	New England Biolabs, Ipswich, MA, USA

7-AAD	BD Biosciences, San Diego, CA, USA
Acetic acid	Sigma Aldrich, St Louis, MO, USA
Acrylamide/bisacrylamide	Applichem, Darmstadt, Germany
Agar	Sigma Aldrich, St Louis, MO, USA
Agarose	Promega, Madison, WI, USA
Ammonium peroxisulfate	Carlo Erba, Cornaredu, Italy
Bouin's solution	Sigma Aldrich, St Louis, MO, USA
Bovine Serum Albumin	Santa Cruz, Dallas, TX, USA
Protease inhibitor cocktail	Roche Applied Science, Mannheim, Germany
D-Luciferin Potassium salt	Sigma Aldrich, St Louis, MO, USA
DAPI	Sigma Aldrich, St Louis, MO, USA
dNTPs	Thermo Fisher Scientific, Waltham, MA, USA
ECL	Amersham Pharmacia Biotech, Amersham, UK
	Thermo Fisher Scientific, Waltham, MA, USA
Ethanol	Sigma Aldrich, St Louis, MO, USA
Isopronapol	Sigma Aldrich, St Louis, MO, USA
Ethidium Bromide	Thermo Fisher Scientific, Waltham, MA, USA
Gene Ruler 100bp DNA Ladder	New England Biolabs, Ipswich, MA, USA
Gene Ruler 1kb DNA Ladder	New England Biolabs, Ipswich, MA, USA
Isopronapol	Sigma Aldrich, St Louis, MO, USA
LightCycler 480 SYBR Green I Master	Roche Applied Science, Mannheim, Germany
Lipofectamine 2000	Invitrogen, Carlsbad, CA, USA
Methanol	Sigma Aldrich, St Louis, MO, USA

Milk powder	Sigma Aldrich, St Louis, MO, USA
Nuclease free water	Applied Biosystems/Ambion, Austin, TX, USA
Page Ruler Protein Ladder	Thermo Fisher Scientific, Waltham, MA, USA
Phosstop	Roche Applied Science, Mannheim, Germany
Ponceu S	Sigma Aldrich, St Louis, MO, USA
Shandon Immu-mount	Thermo Fisher Scientific, Waltham, MA, USA
Sodium Chloride	Merck, Darmstandt, Germany
Sodium Dodecyl Sulfate (SDS)	Merck, Darmstandt, Germany
TEMED	Serva, Heidelberg, Germany
TRIsure	Bioline, Luckenwalde, Germany
Triton X-100	Sigma Aldrich, St Louis, MO, USA
Trizma base	Sigma Aldrich, St Louis, MO, USA
Trypton	Sigma Aldrich, St Louis, MO, USA
Tween-20	VWR, Radnor, PA, USA
WST-1	Roche Applied Science, Mannheim, Germany
Yeast Extract	Sigma Aldrich, St Louis, MO, USA

2.3. Enzymes and Enzyme Buffers

10X Cut Smart Buffer	New England Biolabs, Ipswich, MA, USA
10X T4 DNA ligase Buffer	Thermo Fisher Scientific, Waltham, MA, USA
BsmBI Restriction enzyme	New England Biolabs, Ipswich, MA, USA
NotI Restriction enzyme	New England Biolabs, Ipswich, MA, USA
Phusion Polymerase	New England Biolabs, Ipswich, MA, USA

T4 DNA Ligase	Thermo Fisher Scientific, Waltham, MA, USA
T4 Kinase	Thermo Fisher Scientific, Waltham, MA, USA
Taqman universal mix	Thermo Fisher Scientific, Waltham, MA, USA
XhoI Restriction enzyme	New England Biolabs, Ipswich, MA, USA

2.4. Media and Supplements

DMEM	Lonza, Basel, Switzerland
Fetal Bovine Serum (FBS)	Biowest, Nuaille, France
LB Agar	1.5% (w/v) agar, 10 g/l trypton, 5 g/l yeast extract, 10 g/l NaCl
LB Broth	10 g/l trypton, 5 g/l yeast extract, 10 g/l NaCl
Matrigel	BD, Flanklin Lakes, NJ, USA
Non-essential amino acids	Lonza, Basel, Switzerland
optiMEM	Invitrogen, Carlsbad, CA, USA
Penicillin/Streptomycin	Lonza, Basel, Switzerland

2.5. Kits

BCA Protein Assay kit	Pierce, Rockford, IL, USA
BrdU FITC Flow kit	BD, Flanklin Lakes, NJ, USA
Caspase-Glo® 3/7 Assay kit	Promega, Madison, WI, USA
Cell Titer-Glo and 3D cell Titer-Glo Luminescent Cell Viability Assay kit	Promega, Madison, WI, USA

Trans-lentiviral Packaging kit	Dharmacon, Lafayette, Colorado, United States
Dual Luciferase Reporter kit	Promega, Madison, WI, USA
First strand cDNA synthesis kit	Fermantas, St. Leon-Roth, Germany
Gel and PCR clean up kit	MN, Duren, Germany
Lysyl Oxidase (LOX) Activity Assay kit (Fluorometric)	Abcam, Cambridge, United Kingdom
MycoAlert detection kit	Lonza, Basel, Switzerland
Plasmid isolation kit	MN, Duren, Germany
Plasmid Maxi kit	Qiagen, Hilden, Germany
Taqman miRNA Assays	Applied Biosystems, Foster City, CA, USA

2.6. Equipments

Accuri FACS	BD Biosciences, San Diego, CA, USA
Axiovision 4.3 microscopy	Carl Zeiss, Munich, Germany
Centrifuges	Thermo Fisher Scientific, Waltham, MA, USA
	Beckman, Pasadena, CA, USA
Cell culture hood	Nüve, Ankara, Turkey
Cell culture incubator	Nüve, Ankara, Turkey
Counting chamber	Marienfeld, Königshofen, Germany
Freezer (-80^{o}C)	Hettich, Geldermansen, Holland
Freezer (-20^{o}C) and Fridge (4^{o}C)	Bosch, Stuttgart, Germany
Horizontal Shakers	Bellco, Vineland, NJ, USA
Hypoxia Chamber	StemCell Technologies, Vancouver, Canada

LightCycler 96	Roche Applied Science, Mannheim, Germany
Mini-PROTEAN Gel casting module	Biorad, Hercules, CA, USA
Mini-PROTEAN Tetra Cell	Biorad, Hercules, CA, USA
Multichannel Pipette	Thermo Fisher Scientific, Waltham, MA, USA
Nanodrop 1000	Thermo Fisher Scientific, Waltham, MA, USA
Nikon TS300 Inverted microscope	Nikon, Tokyo, Japan
Thermocycler	Thermo Fisher Scientific, Waltham, MA, USA
Power supplies for electrophoresis	Biorad, Hercules, CA, USA
Semidry Western Blot transfer unit	Biorad, Hercules, CA, USA
Synergy HT microplate reader	Biotek, Winooski, VT, USA
UV-Reader	Vilber Lourmat, Eberhardzell, Germany
Vortex	Isolab, Wertheim, Germany
Water bath	Nüve, Ankara, Turkey
X-ray cassette	Amersham Pharmacia Biotech, Amersham, UK
X-ray hyper processor	Amersham Pharmacia Biotech, Amersham, UK

2.7. Consumables

100 mm dishes	Greiner bio-one, Frickenhausen, Germany
145 mm dishes	Greiner bio-one, Frickenhausen, Germany
96-well plates	Greiner bio-one, Frickenhausen, Germany
6-well plates	Greiner bio-one, Frickenhausen, Germany
Filtered pipette tips (10 ul, 20 ul, 200 ul, 1000 ul)	Greiner bio-one, Frickenhausen, Germany

Cell scrapers	Greiner bio-one, Frickenhausen, Germany
Coverslips	Marienfeld, Königshofen, Germany
Cryovials	Greiner bio-one, Frickenhausen, Germany
Microscope slides	Marienfeld, Königshofen, Germany
Parafilm	VWR, Radnor, PA, USA
PCR tubes	Axygen, Corning, NY, USA
Plastic pipettes (10 ml, 25 ml)	Corning Incorporated, Corning, NY, USA
PVDF Membrane	Biorad, Hercules, CA, USA
Reaction tubes (500 ul, 1.5 ml, 2 ml)	Axygen, Corning, NY, USA
Storage bottles (250 ml, 500 ml, 1 L)	Corning Incorporated, Corning, NY, USA
Whatmann paper	GE Healthcare, Little Chalfont, UK
X-ray films	Kodak, Rochester, NY, USA
Cuvettes	VWR, Radnor,PA, USA
qPCR Plates	Roche Applied Science, Mannheim, Germany
White plates	Costar, Corning, NY, USA

Chapter 3

Methods

3.1. Culturing Human Breast Cancer Cell lines

Human breast cancer cell lines MDA-MB-157, MDA-MB-231, MCF-7, BT474, SK-BR-3, ZR-75-1 together with normal breast epithelial cell lines MCF-10A and MCF-12A and mouse mammary cancer cell line 4T1 were obtained from ATCC (Manassas, VA, USA). 231.Luc.GFP was a kind gift from Dr. Dihua Yu (MD Anderson Cancer Center, Houston, TX, United States). MDA-MB-231 and SK-BR-3 cell lines were cultured with Dulbecco Modified Eagle Medium while MCF-7, BT474 and ZR-75-1 cell lines were cultured with DMEM supplemented with 0.1% insulin. MCF10A and MCF-12A cell line was cultured with DMEM supplemented with 0.1% insulin (0.01 mg/ml), 0.002% EGF (20 ng/ml). All media were supplemented with 50 U/ml penicillin/streptomycin, 1% non-essential amino acids and 10% fetal bovine serum. All cell lines were tested for mycoplasma contamination regularly using MycoAlert mycoplasma detection kit (Lonza, Basel, Switzerland).

3.2. Transient transfection with miRNA mimics, hairpin inhibitors, siRNAs and expression and reporter constructs

Transient transfection was performed 24 hours after cell seeding using Lipofectamine 2000 (Invitrogen, Carlsbad, CA, USA) and OptiMEM. Briefly, 4000-6000 cells/well of 96-well plate or 150,000-200,000 cells/well of 6-well plate were seeded in 100 µl or 1.5 ml Penicillin/Streptomycin free (P/S-free) media, respectively. For one well of 6-well transfection, 2-3 µl of lipofectamine (2 µl in case of miRNA mimics, siRNAs, hairpin inhibitors whereas 3 µl in case of expression or reporter constructs) was diluted in 250 µl

optiMEM (mix A) and vortexed for 20 seconds. Simultaneously, miRNA mimics, siRNAs, hairpin inhibitors, expression or reporter constructs were separately diluted in 250 µl optiMEM (mix B) and vortexed for 20 seconds. Both vials (mix A and mix B) were incubated at room temperature for 5 minutes, then mixed in 1:1 (v/v) ratio and vortexed for 20 seconds followed by incubation at room temperature for 20 minutes. Media was aspirated from cells and replaced with 1 ml fresh P/S-free media. 500 µl of transfection mixture was added on top of the cells resulting final volume of 1.5ml transfection medium. Cells were incubated at 37ºC, 5% CO_2 for further experiments. For one well of 96-well format, transfection mixture was prepared 10 times less as compared to that used for transfection in one well of 6-well plate.

For miRNA mimic viability screen, miRNA mimics were transfected at a concentration of 20nM for 48 hours. For other experiments, miR-644a mimic and siCTBP1s were transfected at a concentration of 40 nM whereas miR-142-3p and siLOX were transfected at a concentration of 20 nM for either 48 or 72 hours. Hairpin inhibitors were transfected at a concentration of 100nM for either 48 hours or 72 hours. Transfection of GFP-tagged CTBP1 human ORF clone (NM_001012614; Cat. No. RG208594), and Myc-DDK tagged TP53 human mutant ORF clone (NM_000546; Cat. No. RC200003, expressing transcript variant 1 of Homo sapiens protein p53 having an R175H mutation) and reported constructs carrying 3'-UTRs of human CTBP1, HIF1A, LOX and ITGA5 were carried out at 50 ng (for 96-well plate) or 500 ng (for 6-well plate) per well.

3.3. Plasmid construction and site-directed mutagenesis

The 3'-UTR sequence of CTBP1 containing binding site for miR-644a and the 3′-UTRs of HIF1A, LOX and ITGA5 containing binding sites for miR-142-3p were amplified from genomic DNA of MDA-MB-231 cells using primers listed in Table 3.1.

Table 3.1. Sequences of forward and reverse primers used for 3'UTR cloning.

Gene Symbol	Gene ID	Direction	Primer
CTBP1	1487	Forward	5'-ccgctcgagcatgtagactgctggggc-3'
		Reverse	5'-atttgcggccgcccacagaagatgtttatttgatgtaac -3'
HIF1A	3091	Forward	5'-ccgctcgagcatgtagactgctggggc-3'
		Reverse	5'-atttgcggccgcccacagaagatgtttatttgatgtaac -3'
LOX	4015	Forward	5'-ccgctcgagttcaatccctgaaatgtctgc-3'
		Reverse	5'-atttgcggccgccataaagccaatgtctgagca-3'
ITGA5	3678	Forward	5'-ccgctcgagcccaatttcagactcccattcctg-3'
		Reverse	5'-atttgcggccgcgttctggtcagtgggggcac-3'

Both 3'-UTR amplicons and psiCHECK™-2 reporter vector were double digested with XhoI and NotI restriction enzymes using protocol described in Table 3.2. Double digestion reaction was carried out at 37^{o}C for 90 minutes followed by enzyme inactivation at 65^{o}C for 10 minutes.

Table 3.2. Protocol for double restriction digestion.

Name	Concentration/Volume
DNA	2 µg (X µl)
NotI	1.25 µl
XhoI	1.25 µl
Cut Smart Buffer	10 µl
Nuclease-free H_2O	(37.5-X) µl

Ligation of restricted vector and insert was carried out using protocol provided in Table 3.3 at 22^{o}C for 60 minutes. Following formula was used to calculate vector and insert concentrations for ligation reaction.

Insert (ng) = Vector (ng) x 5 x (Insert (bp) / Vector (bp))

Table 3.3. Protocol for ligation reaction.

Name	Concentration/Volume
T4 DNA Ligase	1 µl
T4 DNA Ligase Buffer (10X)	2 µl
psiCHECK™-2 (double digested vector)	50 ng
Insert DNA (double digested 3'UTR amplicon)	200 ng
Nuclease-free H_2O	To 20 µl

After ligation, 10 µl product was transformed into DH5α bacteria strain by providing 42 ^oC heat shock for 45 seconds. One ml of fresh LB media was added to transformed DH5α and incubated at 37^oC shaker for 1 hour. Transformed DH5α containing LB media was then spread on 500 µg/ml Ampicillin containing agar plates and incubated at 37^oC overnight. Next day, 5 colonies from each transformation were selected and amplified in 10 ml LB on 37^oC shaker overnight. In order to verify the sequence of constructs, restriction digestion was performed using protocol described in the beginning. Vectors were then amplified in 100-200 ml LB culture, isolated using Maxi prep isolation kit and sent to sequencing with universal sequencing primers of psiCHECK™-2 vector. psiCHECK™-2_Rluc_Forward: 5'-CGCTCCAGATGAAATGGGTAAG-3', psiCHECK™-2_Reverse: 5'-CGAGGTCCGAAGACTCATTT-3. For site-directed mutagenesis, the predicted hsa-miR-644a target site of the previously described psiCheck2/CTBP1-3'-UTRwt construct were disrupted by four point mutations in the seed region using following primers. Forward: 5'-TCAGGACAATGAATCCTTCCCGTTTTTCTTTTTATACTAGATAGTGCATTGTTTTTTCTACCT-3'. Reverse: 5'-AGGTAGAAAAAACAATGCACTATCTAGTATAAAAAGAAAAACGGGAAGGATTCATTGTCCTGA-3'.

3.4. Dual luciferase assay

MDA-MB-231 and MCF-7 cells were seeded in P/S-free media into the 96-well plates with the concentration of 4,000 and 8,000 cells/well, respectively followed by transfections as previously described in Section 3.2. Cells were lysed with 60 μl of 1X passive lysis buffer and shaken at room temperature for 15 minutes to ease cell lysis. Forty μl of cell lysate from each well was transferred to 96-well opaque flat bottom white plates. Forty μl of reagent I and 40 μl of reagent II were added on top of the cells. After adding each substrate, luminescence was measured with Synergy HT microplate reader (Biotek, Winooski, VT, USA) and *renilla luciferase* activity was normalized to *firefly luciferase* activity of psiCHECK™-2 vector. At least 5 biological replicated were used for each condition.

3.5. *In vitro* sensitization and cell viability assay

For 2D culture drug sensitization assays, drug treatments were done one day after miRNA mimic, siRNA or expression vector transfections with doxorubicin (0.05-10 μM), cisplatin (0.001-30 μM), tamoxifen (2.5-40 μM) or gefitinib (0.1-20 μM). The drugs were given in 40 μl and 500 μl volumes per well of 96-well and 6-well plate, respectively. Cell viability was assessed by Cell Titer-Glo cell viability assay kit (Promega, Madison, WI, USA) after 3 days of drug treatment or 3 days after miRNA mimic, siRNA or expression vector transfection. Briefly, both reagents and cells in 96-well format were incubated at room temperature for 30 minutes. Then, thirty μl of Cell Titer-Glo reagent was added to each well and plate was shaken at high speed for 10 minutes to ease cell lysis. Lysed product from each 96-well was transferred to corresponding wells of 96-well opaque, flat bottom white plates, and luminescence signal was measured with Synergy HT microplate reader (Biotek, Winooski, VT, USA). For drug sensitization assays, drug treatment was

done 24 hours after transfection with miRNAs or siRNAs. At least 4 biological replicated were used for each condition.

3.6. Apoptosis assay

Apoptosis index was assessed by Caspase-Glo 3/7 assay kit (Promega, Madison, WI, USA). Briefly, both reagents and cells in 96-well format were incubated at room temperature for 30 minutes. Then, thirty µl of Caspase-Glo 3/7 reagent was added to each well, and plate was shaken at high speed for 10 minutes to ease cell lysis. Lysed products from each 96-well were transferred into the corresponding wells of 96-well opaque, flat bottom white plates, and luminescence signal was measured with Synergy HT microplate reader (Biotek, Winooski, VT, USA). At least 4 biological replicated were used for each condition.

3.7. Poly-hydroxyethylmethacrylate (poly-HEMA) assay

96-well plates were coated with 50 µl/well of poly-HEMA (120 mg/ml in 95% ethanol), and cells were cultured in coated plates to measure anchorage-independent growth. Cells were seeded at a density of 8,000 cells/well, and changes in the growth of cells were examined by taking images at 1^{st}, 3^{rd}, 5^{th} and 7^{th} day after seeding with 5X magnification using Nikon Eclipse inverted microscope (Nikon, Japan). At the end of experiment, 10 µl of WST-1 reagent (Roche Applied Science, Mannheim, Germany) was added to each well. Four hours later, cell viability was quantified by measuring absorbance at 450nm using SynergyHT microplate reader (Biotek, Winooski, VT, USA). At least 3 biological replicates were used for each condition.

3.8. 3D matrigel assay

The 3D matrigel assay was performed in matrigel (BD, Flanklin Lakes, NJ, USA) coated 96-well plates. The surface of 96-well plates was coated with 15 µl/well matrigel and incubated at 37 °C for 20 minutes to solidify. 231.Luc.GFP cells were seeded and transfected (if needed) in 6-well plate as previously described in Section 3.2. Twenty-four hours post-transfection, cells were collected, counted and seeded in matrigel coated plates at a density of 5,000 cells/well in normal media and incubated at 37 °C for 30 minutes to adhere. Drug solutions were prepared in 10% matrigel media and added on top of the cells. 72 hours later, the viability was assessed by 3D Cell Titer Glo (Promega, Madison, WI, USA). Briefly, both reagents and cells in 96-well format were incubated at room temperature for 30 minutes. Then, thirty µl of 3D cell titer Glo reagent was added to each well, and plate was shaken at high speed for 20 minutes to ease cell lysis. Lysed product from each 96-well was transferred to corresponding wells of 96-well opaque, flat bottom white plates, and luminescence signal was measured with Synergy HT microplate reader (Biotek, Winooski, VT, USA). Microscopy images were taken just before the viability measurements with Leica DMi8 microscope. At least 3 biological replicated were used for each condition.

3.9. Real-Time Cell Analyzer (RTCA) assays

3.9.1. Real-time cell viability assay

Real-time cell viability assay was performed in 16-well E-plates (Acea Biosciences, San Diego, CA, USA). Briefly, plates were normalized in the RTCA instrument after adding 75 µl of P/S-free media in each well before cell seeding. MDA-MB-231, MCF-7 and MDA-MB-436 cells were seeded at a rate of 8,000cells/well of E-plates in 75 µl media. E-plates were incubated at room temperature for 30 minutes to settle down the cells

before placing in RTCA instrument. Program was set to read cell index every 30 minutes for 120 hours. For transfection, E-plates were removed from RTCA instrument, and 50 µl transfection mixture was added in each well, and plates were placed back into the instrument. Cell index was normalized to transfection time. At least 3 biological replicated were used for each condition.

3.9.2. Real-time migration and invasion assay

Real-time migration and invasion assays were performed in 16 well CIM-plates (Acea Biosciences, San Diego, CA, USA). Cell were seeded and transfected in 6-well plate format beforehand. For invasion assay, top chamber was coated with 800 µg/ml matrigel diluted in serum-free media was and incubated at 37ºC for 4 hours. In the meantime, 160 µl complete media (containing 10% FBS) was added to bottom chamber, and top chamber was placed tightly on it. After adding 50 µl starvation media (containing 1% FBS) on top chamber, CIM-plate was incubated at 37ºC for 1 hour and then placed into RTCA instrument for normalization. 24 hours post transfection, cells were collected from 6-well plate, counted and seeded on CIM-plates at a density of 30,000 cells/well. CIM-plates were incubated at room temperature for 30 minutes to settle the cells down, and then plates were placed into RTCA instrument. Program was set to read cell index every 15 minutes for 72 hours. Migration assay was performed in the same manner without coating top chamber with matrigel. At least 3 biological replicated were used for each condition.

3.10. Migration (wound healing) assay

Cells were seeded and transfected in 6-well plates as described previously in Section 3.2. Forty-eight hours post-transfection, a scratch was made in the middle of each well with a

20 µl pipette tip. Cells were then observed at varying time points with 4X magnification using Nikon Eclipse inverted microscope (Nikon, Japan) for a total of 48 hours. Distance between the cells was measured using ImageJ software (NIH, MD, USA). At least 3 biological replicated were used for each condition.

3.11. Cell cycle analysis

Cells were seeded and transfected in 6-well plates as previously described in Section 3.2. Culture media was refreshed 24 hours after transfection, and 10 µl of BrdU solution (containing 1 mM of BrdU diluted in 1X PBS) was carefully added. Cells were incubated for 45 minutes at 37 ^{o}C, 5% CO_2. After incubation, cells were collected in FAC tubes and pulled down by centrifugation at 1500 rpm for 5 minutes. Cells were then washed with 1 ml wash buffer (1X PBS) and incubated with 100 µl/tube Cytoperm buffer for 30 minutes on ice to permeabilize. After incubation, cells were washed with 1 ml of wash buffer and incubated with 100 µl/tube of DNase solution (30 µl DNase diluted in 70 µl PBS) at 37 ^{o}C for 1 hour. Cells were again washed with wash buffer and re-suspended in 100 µl of staining solution (3% FBS in 1X PBS). A hundred µl of staining solution containing 5 µl of 7-AAD was added to cells and incubated at 4^{o}C for 1 hour. Cells were then washed with 1 ml wash buffer and re-suspended in 300 µl 1X PBS. Stainings were measured by Accuri FACS instrument (BD Biosciences, San Diego, CA, USA). At least 3 biological replicated were used for each condition.

3.12. Immunofluorescence

Cells were seeded on square cover slips in 6-well plates and transfected as described previously in Section 3.2. Twenty-four hours post-transfection, cells were fixed with 2%

paraformaldehyde for 15 minutes and permeabilized with 0.2% Triton X-100 solution in PBS for 5 minutes. Samples were blocked with 3% BSA/PBS for 30 minutes. For F-actin staining, cells were incubated in Alexa Fluor 488 phalloidin (1:40 diluted in 3% BSA/PBS) for 30 minutes at room temperature; and for nuclear staining, cells were incubated in 1 µg/µl 4',6-Diamidin-2-phenylindol (DAPI, diluted in 3% BSA/PBS) for 10 minutes. Cover slips were mounted with Shandon Immu-Mount reagent, and images were taken with 20X and 40X focus on Axiovision 4.3 Florescent microscope (Zeiss, Munich, Germany).

3.13. Hypoxia assay

Cells were seeded into 6-well plate and incubated overnight at 37^{o}C in normoxic conditions. Twenty-four hours later, plates were placed in Hypoxia Incubator Chamber (StemCell Technologies, Vancouver, Canada) in 1% Oxygen (5% CO_2 and 94% Nitrogen) at 37 °C for 0-48 hours. After each time point, cells were collected after trypsinization and preserved for RNA and protein isolation.

3.14. Quantitative Real-Time Polymerase Chain Reaction (qRT-PCR)

3.14.1. RNA isolation

Cells were seeded, transfected and/or treated (where indicated) in 6-well plates as mentioned previously in Sections 3.2 and 3.5. After indicated times, cells were washed with 1X PBS, trypsinized and pelleted. RNA isolation was performed using TRIsure reagent according to manufacturer's instructions.

3.14.2. cDNA synthesis

Two µg of total RNA from each sample was reverse-transcribed to cDNA using RevertAid RT Reverse Transcription kit (Fermantas, St. Leon-Roth, Germany) according to the protocol provided as Table 3.4, and the reaction was incubated in thermocycler using the program described in Table 3.5. All samples were diluted to 1:10 after cDNA synthesis for qRT-PCR experiments.

Table 3.4. Components of reverse transcription reaction.

Reagent	**Concentration/Volume**
RNA	2 µg (X µL)
oligoDT	1 µL
x Revert Aid reaction buffer	4 µL
Ribolock Ribonuclease Inhibitor	1 µL
dNTPs (10mM)	2 µL
Revert Aid H Minus M-MuLV RT	1 µL
Nuclease-free H_2O	(20-X) µL

Table 3.5. Thermocycler program for cDNA synthesis.

Temperature	**Time**
37º	5 minutes
42ºC	60 minutes
70ºC	10 minutes
4ºC	∞

3.14.3. qRT-PCR for mRNA expression

For qRT-PCR, reaction mix was prepared for each primer pair as listed in Table 3.6 according to the protocol provided in Table 3.7.

Table 3.6. Sequences of forward and reverse primers used in qRT-PCR analysis.

Gene Symbol	Gene ID	Forward Primer	Reverse Primer
ACTB	60	5'-ccaaccgcgagaagatga-3'	5'-ccagaggcgtacagggatag-3'
BAX	581	5'-gggtggttgggtgagactc-3'	5'-agacacgtaaggaaaacgcatta-3'
CDH1	999	5'-cccgggacaacgtttattac-3'	5'-gctggctcaagtcaaagtcc-3'
CTBP1	1487	5'-acccttacttgtcggatggc-3'	5'-atgaggtggtggttgtgct-3'
FN	2335	5'-ctggccgaaaatacattgtaaa-3'	5'-ccacagtcgggtcaggag-3'
GAPDH	2597	5'-gcccaatacgaccaaatcc-3'	5'-agccacatcgctcagacac-3'
HIF1A	3091	5'-ccacaggacagtacaggatg-3'	5'-tcaagtcgtgctgaataatacc-3'
HPRT	3251	5'-tgaccttgatttattttgcatacc-3'	5'-cgagcaagacgttcagtcct-3'
ITGA10	8515	5'-gtgtggatgcttcattccag-3'	5'- gccatccaagacaatgacaa-3'
ITGA5	3678	5'-gtcgggggcttcaacttagac-3'	5'-cctggctggctggtattagc-3'
ITGB5	3693	5'-gggagtttgcaaagtttcagag-3'	5'-tgtgcgtggagataggcttt-3'
KRT18	3875	5'-tgatgacaccaatatcacacga-3'	5'-ggcttgtaggccttttacttcc-3'
LOX	4015	5'-ggatacggcactggctactt-3'	5'-gacgcctggatgtagtaggg-3'
MMP9	4318	5'-gaaccaatctcaccgacagg-3'	5'-gccacccgagtgtaaccata-3'
MYC	4609	5’-cagctgcttagacgctggatttt-3’	5’-accgagtcgtagtcgaggtcat-3’
NOXA	5366	5'-atgaatgcaccttcacattcctct-3'	5'-tccagcagagctggaagtcgagtgt-3'
p21	1026	5'-tgagccgcgactgtgatg-3'	5'-gtctcggtgacaaagtcgaagtt-3'
p53	7157	5’-cccaagcaatggatgatttga-3’	5’-ggcattctgggagcttcatct-3’
PUMA	27113	5’-ccagggctgcttccacgacg-3’	5’-acactgccgagggcaccagg-3’
SNAI2	6591	5'-tggttgcttcaaggacacat-3'	5'-gttgcagtgagggcaagaa-3'
ZEB1	6935	5'-gggaggagcagtgaaagaga-3'	5'-tttcttgcccttcctttctg-3'
ZEB2	9839	5'-aagccagggacagatcagc-3'	5'-ccacactctgtgcatttgaact-3'
ZO1	7082	5'-cagagccttctgatcattcca-3'	5'-catctctactccggagactgc-3'

Table 3.7. Master mix for qRT-PCR reaction.

Reagent	Volume
SYBR Green	5 µL
Forward Primer (20 µM)	0.25 µL
Reverse Primer (20 µM)	0.25 µL
Nuclease-free H_2O	2.5 µL

qRT-PCR reaction was carried out in 96-well plate. After adding 8 µl of master mix in each well, 2 µl of cDNA (20 ng) was added and carefully mixed by pipetting. Plate was tightly sealed, centrifuged at 1000 rpm for 1 minute at 4ºC and ran on LightCycler 96 qRT-PCR Thermocycler (Roche Applied Science, Mannheim, Germany) with thermocycler program shown in Table 3.8.

Table 3.8. qRT-PCR program.

Pre-incubation

Target (°C)	Acquisition Mode	Hold (hh:mm:ss)	Ramp Rate (°C/s)	Acquisitions (per °C)	Sec Target (°C)	Step Size (°C)	Step Delay (cycles)
95	None	00:05:00	4.4	5	0	0	0

Amplification

Target (°C)	Acquisition Mode	Hold (hh:mm:ss)	Ramp Rate (°C/s)	Acquisitions (per °C)	Sec Target (°C)	Step Size (°C)	Step Delay (cycles)
95	None	00:00:10	4.4	5	0	0	0
58	Single	00:00:20	2.2	5	0	0	0

72	None	00:00:20	4.4	5	0	0	0

Melting Curve

Target (°C)	Acquisition Mode	Hold (hh:mm:ss)	Ramp Rate (°C/s)	Acquisitions (per °C)	Sec Target (°C)	Step Size (°C)	Step Delay (cycles)
95	None	00:00:05	4.4	5	0	0	0
55	None	00:01:00	2.2	5	0	0	0
95	Continuous	00:00:00	0.11	5	0	0	0

Cooling

Target (°C)	Acquisition Mode	Hold (hh:mm:ss)	Ramp Rate (°C/s)	Acquisitions (per °C)	Sec Target (°C)	Step Size (°C)	Step Delay (cycles)
40	None	00:00:30	2.2	5	0	0	0

3.14.4. Reverse transcription for miRNA expression

Taqman miRNA Assays (Foster City, CA, USA) were used for miRNA cDNA synthesis and qPCR. miRNA reverse transcription reaction was carried out using protocol described in Table 3.9 with master mix prepared using protocol shown in Table 3.10.

Table 3.9. Thermocycler protocol for Taqman miRNA reverse transcription.

Temperature	Time
16ºC	30 minutes
42ºC	30 minutes
85ºC	5 minutes
4ºC	∞

Table 3.10. Components of Taqman miRNA reverse transcription reaction.

Reagent	**Volume (µL)**
RNA	5 (10 ng)
dNTPs (100nM)	0.15
MultiScribe TM Reverse Transcriptase (50U/µL)	1
10x RT Buffer	1.5
RNase Inhibitor (20U/µL)	0.19
5X Taqman RT primer	3
Nuclease-free H_2O	4.16
Total	15 µL

3.14.5. qRT-PCR for miRNA expression

For qRT-PCR, reaction mix was prepared for each miRNA primer according to the protocol provided in Table 3.11. qRT-PCR reaction was carried out in 96-well plate. After adding 8.67 µl of master mix in each well, 1.33 µl of cDNA was added and carefully mixed by pipetting. Plate was tightly sealed, centrifuged at 1000 rpm for 1 minute at 4^{o}C and ran on LightCycler 96 qRT-PCR Thermocycler (Roche Applied Science, Mannheim, Germany) with program shown in Table 3.12.

Table 3.11. Mastermix for Taqman miRNA PCR amplification.

Reagent	**Volume (µL)**
Taqman 2X Universal PCR Master Mix	5
20X Taqman microRNA assay mix	0.5
Nuclease-free H_2O	3.17
Total	8.67

Table 3.12. qPCR protocol for Taqman miRNA amplification.

Parameter	Value			
Run mode	9600 emulation (Default)			
Sample volume	20 µL			
Thermal cycling parameters	Step	Type	PCR	
		Hold	40 cycles	
			Denature	Anneal
	Time	10 min	15 sec	60 sec
	Temp (°C)	95	95	60
Auto Increment Settings	Accept default. (Default is 0)			
Ramp Rate Settings	Accept default. (Default is Standard)			
Data Collection	Accept default. (Default is 60°C)			

3.15. Protein Biochemistry

3.15.1. Protein Isolation

Cells were seeded, transfected (where indicated) and/or treated in 6-well plates as mentioned previously in Sections 3.2 and 3.5. After indicated times, culture media was collected and centrifuged at 5000 rpm for 5 minutes to collect the apoptotic bodies (in case of drug treatments). Cells were then trypsinized and collected. Depending on cell pellet size, 50-100 µL RIPA lysis buffer (Table 3.13) was added to the cells and mixed thoroughly by pipetting up and down. Suspension was then transferred to 1.5 ml Eppendorf tubes and vortexed for 5-10 seconds every 5 minutes for a total of 30 minutes. Later, this suspension was centrifuged at 13,000 rpm 4°C for 30 minutes. Supernatant was collected as protein and stored at -20°C for further experiments.

Table 3.13. Components of the RIPA buffer.

Ingredients	Stock Conc.	Final Conc.	For 1 ml
NaCl	2 M	150 mM	75 µl
NP-40	10%	1%	100 µl
Sodium DOC	10%	0.5%	50 µl
SDS	10%	0.1%	10 µl
Tris HCl (pH 8.0)	2 M	50 mM	25 µl
NAF	1 M	50 mM	50 µl
$NaVO_4$	100 mM	1mM	10 µl
Protease Inhibitor	25X	4%	40 µl
Phosphatase Inhibitor	10X	4%	40 µl
ddH_2O			600 µl

3.15.2. Protein Quantification

BCA protein assay kit (Pierce, Rockford, IL, USA) was used for protein quantification. Briefly, range of 0-2 µg/µL BSA standard solutions were prepared according to manufacturer's instructions. Solution A and B were mixed in 50:1 ration to prepare working solution which was pipetted into 96-well plate at an amount of 200 µl/well. Dilution factor of 5 was used between standard and protein samples. Twenty-five µl of each standard and 5 µl of each protein sample were pipetted in working solution in duplicates. Plate was incubated at 37^{o}C for 30 minutes. Later, absorbance was measured on SynergyHT microplate reader (Biotek, Winooski, VT, USA) at 562nm. A standard calibration curve was drawn depending on absorbance readings from BSA standards, and sample concentrations were quantified from line graph of the curve.

3.15.3. Sodium dodecyl sulfate polyacrylamide gel electrophoresis (SDS-PAGE)

Protein samples were mixed with 4X protein loading dye, and heated to 95^{o}C for 3-5 minutes. Polyacrylamide gels were prepared according to Table 3.14.

Table 3.14. Mixture for stacking and resolving gels in different concentrations.

Reagent	**Resolving gel**			**Stacking gel**
	8%	**10%**	**12%**	**5%**
ddH_2O	2.3 ml	1.9 ml	1.6 ml	1.36 ml
30% acrylamide mix	1.3 ml	1.7 ml	2 ml	340 µl
1 M Tris	(pH=8.8) 1.3 ml	(pH=8.8) 1.3 ml	(pH=8.8) 1.3 ml	(pH=6.8) 260 µl
10% SDS	50 µl	50 µl	50 µl	20 µl
10% APS	50 µl	50 µl	50 µl	20 µl
TEMED	5 µl	5 µl	5 µl	2 µl
Total volume	5 ml	5 ml	5 ml	2 ml

Using Mini-PROTEAN Gel casting module (Biorad, Hercules, CA, USA), resolving gel solution was poured initially and overlaid with isopropanol until gel polymerized. After removing isopropanol from gel casting system, stacking gel solution was poured on top of resolving gel, and 10 or 15 well comb was placed in it. 10-20 µg protein samples were loaded per well, and empty wells were filled with diluted protein loading dye. Electrophoresis was performed at 90V in the beginning for 20 minutes and later at 110-120V for 90-120 minutes.

3.15.4. Western blotting

For semi-dry transfer, four of 3 mm thick Whatmann papers (7x9 cm^2) were moistened in anode buffer-I, two in anode buffer-II and six in cathode buffer. PVDF membrane was first dipped in 100% methanol for 3 minutes, and then in anode buffer II for 1 minute. Whatmann papers, gel and membrane were stacked in Biorad Semi-Dry Turbo Blot machine (Biorad, Hercules, CA, USA) from anode to cathode in the following order: 4 anode I, 2 anode II, PVDF membrane, stacking gel, 6 cathode moistened Whatmann papers. Transfer was performed at 25V for 30-60 minutes. After transfer, Ponceu S staining was performed for 3 minutes to visualize the protein samples on PVDF membrane. Membranes were then washed with ddH_2O until Ponceu stain was completely removed and cut at specific molecular weight (kDa) of interest. Cut membranes were blocked with 5% (w/v) milk:1X TBS-T or 5% (w/v) BSA:1X TBS-T for 1 hour at room temperature on slow shaking. Later, blocking solution was removed, and membranes were incubated with primary antibody (Table 3.15) either for 1-hour at room temperature or overnight at 4^oC.

After primary antibody incubation, membranes were washed with 1X TBS-T three times for 10 minutes on shaker followed by secondary antibody incubation either for 1-hour at room temperature or overnight at 4^oC. Later, membranes were again washed with 1X TBS-T three times for 10 minutes on shaker. After washing, Amersham ECL reagent (Amersham Pharmacia Biotech, Amersham, UK) or Pierce ECL Western Blotting Substrate (Thermo Fisher Scientific, Waltham, MA, USA) was applied on membranes, and X-ray films were exposed to membranes for different time points ranging from 3 seconds to 30 minutes and then membranes were developed.

Table 3.15. List of antibodies used in Western blot.

Antibody	Provider	Catalog number	Dilution
Beta-actin	MP Biomedicals	691001	1:10000
CDK2	Sigma	C5223	1:1000
CDK4	Epitomics	2341-1	1:1000
Cleaved Caspase 3	CST	9661	1:1000
CTBP1	BD	612042	1:1000
Cyclin D1	CST	2922	1:1000
Fibronectin	Santa Cruz Biotechnology	81767	1:1000
HIF1-a	Abcam	51608	1:1000
ITGA5	Sigma	HPA002642	1:1000
LOX	Abcam	174316	1:2000
Noxa	Santa Cruz Biotechnology	30209	1:1000
p21	BD Biosciences	554228	1:1000
p53	CST	2527	1:1000
p-Cdc2	CST	2543S	1:1000
p-Cdc25C	CST	4901S	1:1000
phospho-FAK (Y397)	Abcam	39967	1:5000
Phospho-Rb (S807/811)	CST	8516	1:1000
Phospho-Src (Y416)	CST	2101	1:1000
Vimentin	CST	5741	1:1000
ZEB-1	CST	3396	1:1000
ZO1	CST	13663	1:1000

3.16. LOX activity assay

LOX activity within cells and within tumors was measured using fluorometric LOX Activity Assay Kit (Abcam, Cambridge, UK). Briefly, cell culture media was collected from control and BAPN (LOX inhibitor) treated cells. Collected media was then centrifuged at 5,000 rpm for 5 min at 4^{o}C. Supernatant was collected, and multiple dilutions were made in 1X PBS + 0.1% BSA. For tumors, 1-2 mg tissue samples were sonicated in extraction buffer (6 M urea, 10 mM Tris pH 7.4 and protease inhibitor) for 5

cycles (10 sec on/off). Samples were then centrifuged at 13,000 rpm at 4ºC for 30 minutes. Supernatant was collected, protein concentrations were measured using BCA kit as described in Section 3.15, and multiple dilutions were made in 1X PBS + 0.1% BSA. Reaction mix (1X HRP substrate and 50 U/ml HRP in assay buffer) was added to 96-well opaque, flat bottom white plates at a density of 50 µl/well. Fifty ul of and diluted supernatant or tissue lysate was added in each well and mixed. Plate was then incubated at 37ºC for 10-40 minutes protected from light. Fluorescence was measured at Excitation/Emission = 540/590 nm wavelength using SynergyHT microplate reader (Biotek, Winooski, VT, USA).

3.17. Lentiviral vector-based stable transfections

SMARTchoice human lentiviral hsa-miR-644a shMIMIC hCMV-turboGFP, GIPZ non-silencing lentiviral shRNA control, GIPZ human CTBP1 shRNA vectors with clone IDs V3LHS_380132, V3LHS_398420 and V3LHS_113279 encoding different shRNA sequences, TRIPZ inducible lentiviral non-silencing shRNA Control and TRIPZ human LOX shRNA vector with clone ID V3THS_348882 were purchased from Dharmacon (Lafayette, CO, USA). MDA-MB-231.luc cells were transduced with miR-644a viral particles in 24-wells plate, and 96 hours post-transduction, selection with 1 µg/ml of puromycin was started. To produce viral particles with shRNA vectors, 6 µg of each of these vectors and 4.3 µl of trans-lentiviral packaging mix were used to co-transfect HEK293FT cells in 6-wells plate with $CaCl_2$ reagent. 48 hours post-transfection, first viral particles were harvested and transduced into 231.Luc.GFP cells. 96 hours post-transduction, selection with 1 µg/ml of puromycin was started. LentiCRISPRv2 vector was [100] was purchased from Addgene (Cambridge, MA, USA). For sgRNA design, candidate target sequences were determined using E-CRISPR tool [101]. For the

packaging of pLentiCRISPR/CTBP1 sgRNA1 and pLentiCRISPR/CTBP1 sgRNA2 vectors, 30% confluent HEK293FT cells in 100 mm plates have been co-transfected using 42 μg of these vectors, 31.5 μg of pMD2.G (Addgene, Cambridge, MA, USA) and 21 μg psPAX2 (Addgene, Cambridge, MA, USA). Transfection, transduction and selection were performed as described previously for shRNA vectors.

3.18. *In vivo* animal experiments

3.18.1. Primary xenografts

All animal experiments have been approved by the Animal Ethics Committee of Bilkent University (Protocol numbers: 2013/45, 2014/39, 2015/30, 2016/3). For primary tumors, 6–8 weeks old female athymic nu/nu mice and Balb/c mice were subcutaneously injected without incision, with 2×10^6 MDA-MB-231 (or 231.Luc.GFP) cells and 2×10^5 4T1 cells, respectively, into both left and right mammary fat pads (MFP). Primary tumor growth was monitored by measuring the tumor volume twice a week with a caliper after tumors became palpable. Tumor volumes were calculated as (length × width^2)/2.

3.18.2. Development of doxorubicin resistance

For development of doxorubicin resistant xenografts, primary tumors were developed using the abovementioned protocol, and doxorubicin treatment was started after tumors became palpable. Mice were treated with a dose of 5 mg/kg body weight weekly through intravenous injection. In the beginning, all tumors showed sensitivity towards treatment and showed decrease in volume. Some of these sensitive tumors were collected after 8-10 weeks of treatment. Later, remaining tumors started to increase in size, and showed resistance towards treatment, and these resistant tumors were collected after 12-15 weeks

of treatment. For shLOX induction experiments, doxycycline was given at 100 μg/ml in drinking water. For LOX inhibitor experiments, BAPN was administered intraperitoneally at a dose of 100 mg/kg body weight twice a week. In both experiments, doxorubicin was administered intravenously at 2.5 mg/kg body weight weekly.

3.18.3. Tail-vain metastasis

For tail-vein metastasis assay, $1.5x10^6$ cells were injected into tail vein of each 6-8 weeks old female athymic Nu/nu mice, with 3-5 mice per group. The mice were sacrificed, and lung metastasis was evaluated once one of the mice became moribund with a luciferase assay. Due to heterogeneous distribution of nodules, three different parts were randomly collected from each lung to make a tissue pool and weighed for normalization. Lung tissues were ground in cold PBS by tissue homogenizer and treated with lysis buffer (Promega, Madison, WI, USA). 500 ul lysis buffer was added to 140-180 mg weight. After 15 min incubation, 100 μl of luciferase substrate (Promega, Madison, WI, USA) was added to 20 μl of the lysed sample, and luminescence was measured with Synergy HT microplate reader (Biotek, Winooski, VT, USA). For Bouin's fixation, harvested lungs were cleaned with PBS and placed into Bouin's solution on a shaker overnight. After fixation they were kept in 70% alcohol. The lung samples used for Bouin's fixation were excluded from luciferase assay and H&E stainings.

3.18.4. IVIS-imaging

All mice were sacrificed; tumors were collected and weighed when one of the tumors reached 1500 mm^3. Before sacrifice, primary tumors were monitored by bioluminescence imaging (BLI). Anesthetized mice were intraperitoneally injected with 150 mg/kg D-

luciferin (Perkin Elmer, Waltham, MA, USA). Bioluminescence images were acquired with Lumina III In Vivo Imaging System (Perkin Elmer, Waltham, MA, USA). Analysis was performed with live imaging software by measuring photon flux. All mice used were of the same age and similar body weight.

3.19. Immunohistochemistry (IHC)

IHC was performed on 3 μm cut sections using automated bond-max system (Leica microsystems GmbH, Wetzlar, Germany). Briefly, Paraffin-embedded specimens were de-paraffinized in Dewax solution and subjected to heat-mediated antigen-retrieval for 30 minutes at 90°C using Epitope Retrieval Solution 2 (EDTA-buffer pH 8.8) followed by peroxidase blocking for 5 minutes. Tissues were then incubated with the primary antibodies listed in Table 3.16 for 15 minutes and with Post Primary Reagent for 8 minutes followed by washing with Bond Wash solution for 6 minutes. Subsequently, tissues were incubated with Bond Polymer for 8 minutes and developed with DAB-Chromogen for 8 minutes followed by hematoxylin counterstaining. Images were acquired using Olympus BX50 microscope (Shinjuku, Tokyo, Japan). Immunoreactive scores were calculated as described in [102].

Table 3.16. List of antibodies used in Immunohistochemistry.

Antibody	Provider	Catalog number
ITGA5	Sigma	HPA002642
Phospho-Src (Y416)	CST	2101
Ki-67	ThermoFisher Scientific	MA5-14520
Cleaved Caspase 3	CST	9664

3.20. Bioinformatics and statistical analysis

3.20.1. miRNA target prediction

In order to identify miR-644a targets, Targetscan release 6.2 (http://www.targetscan.org), PITA miRNA target recognition from Segal Lab of Computational Biology (http://genie.weizmann.ac.il) and miRDB (http://mirdb.org/miRDB/index.html) were used as target prediction algorithms. Common predicted targets between all three databases and downregulated genes by miR-644a mimic (microarray results) were represented in a Venn diagram prepared using Venny 2.0. In order to find all the conserved miRNAs targeting HIF1A, LOX and ITGA5, Targetscan release 7.2 (http://www.targetscan.org) was used as a target prediction algorithm.

3.20.2. Microarray analysis

Expression profiling data were normalized with quantile normalization. Quality control and differential gene expression analysis was conducted using limma in Bioconductor [103]. Microarray data can be retrieved from NCBI Gene Expression Omnibus (GEO) database with the accession number GSE82058 [104].

3.20.3. Whole transcriptome sequencing (RNA-Seq) and data analysis

rRNA depleted stranded libraries for each condition (4 biological replicates for each of Doxorubicin sensitive and Doxorubicin resistant tumors) were generated, and multiplexed. Paired-end 100 bp sequencing was performed using the Illumina HiSeq 2000 platform at McGill University and Genome Quebec Innovation Centre. 60-70 million sequencing reads were obtained for each replicate. Raw sequence reads were aligned to the UCSC human reference genome (hg19) using TopHat v2.1.0 with default parameters. To count the mapped reads, HTSeq was used with the reference genome

annotation (USCS, hg19). In order to determine differentially expressed genes between doxorubicin sensitive and resistant groups, Bioconductor package, edgeR, was utilized.

3.20.4. GEO dataset analysis

Cell line and patient data were retrieved from the NCBI GEO database (GSE2603 [62], GSE4922 [105], GSE16446 [106], GSE19536 [107], GSE19783 [107], GSE22220 [108], GSE21653 [109], GSE22219 [108], GSE22226 [110], GSE25066 [111], GSE28425 [112], GSE35389 [113], GSE38167 [114], GSE40059 [115], GSE43816 [116], GSE45666 [117], GSE54088 [118], GSE58606 [119], GSE58644 [120], GSE58812 [121] and GSE62323 [122]) and from online survival analysis tool, KM-plotter [123], the Molecular Taxonomy of Breast Cancer International Consortium (METABRIC) [124] project data from EMBL European Genome–Phenome Archive (http://www.ebi.ac.uk/ega/) with an accession number EGAS00000000122 and The Cancer Genome Atlas (TCGA) data from Chipbase V2 (rna.sysu.edu.cn/chipbase/). Survival curves were generated using Kaplan-Meier method. Patients without any available survival time or event were excluded from the corresponding patient groups. All separations were done from the median.

3.20.5. DAVID/IPAs

Gene ontology (GO) analyses were done with DAVID bioinformatics tool [125]. For pathway enrichment, the core analysis was performed at Ingenuity Pathway Analysis (IPA) platform using top differentially expressed mRNA data (-0.59>Log2FC>0.59 and adjusted p-value of <0.05) from doxorubicin sensitive and resistant xenografts.

3.20.6. Generating gene signatures and GSEA

Significance scores of genes up and down-regulated by miR-644a mimic were calculated as previously described [126]. miR-644a Gene Signature (miR-644a-GS) score was defined as the ratio of the significance scores of genes up and down-regulated by miR-644a mimic. Doxorubicin resistant gene signature (DoxoR-GS) was generated comprising of top 441 differentially expressed mRNAs (-0.80>Log2FC>0.80 and p-value of 0.05) between sensitive and vs resistant xenografts. z-scores for DoxoR-GS were calculated for patients in GSE43816 and GSE58812. For the calculation of the DoxoR-GS score, the sum of z-scores of the downregulated genes in the DoxoR-GS was subtracted from the sum of z-scores of the upregulated genes for each patient [127]. Geneset enrichment analysis (GSEA) was performed using gene sets downloaded from the GSEA website: http://software.broadinstitute.org/gsea/index.jsp. To perform GSEA with GSE58644 dataset, patients were grouped based on their miR-644a-GS score. To perform GSEA with GSE22220 dataset, patients expressing high levels of miR-644a were separated into two groups as p53-*mut* and p53-*wt*. For the separation of patients as p53-*wt* or p53-*mut*, data provided by the publishers of the studies were utilized if available. In GSE58644 and GSE22220, the separation was done by clustering patients according to their expression levels of a gene signature associated with p53 status [128]. The accuracy of p53 status prediction with this gene signature was tested by using data from GSE19536 in which p53 status of the patients was provided. 85% and 77% of the p53-*mut* and p53-*wt* patients, respectively could be predicted from their expression levels of the p53 status signature. To perform GSEA with GSE43816 dataset, paired samples were separated based on time when samples were taken i.e., before and after chemotherapy treatment. To perform GSEA with GSE58812, patients were grouped either on the basis of DoxoR-GS score or LOX expression. For the microarray datasets

that contain negative expression values, a small number was added to all values such that all values became positive [129].

3.20.7. Statistical analysis

Significance of the differences in survival between two groups was calculated by Log-rank (Mantel-Cox) test. For correlation analysis, Pearson correlation co-efficients were calculated. Comparisons between two groups were made by 2-tailed Student's t-test. Box-plots depict median number and the 25th to 75th quartiles. Upper and lower whiskers represent the minimum and maximum values in the corresponding group. Graphs were prepared in GraphPad software (GraphPad software Inc., La Jolla, CA, USA). Significance cut-off were shown as *$P < 0.05$; **$P < 0.01$; ns, not significant.

Chapter 4

Results

PART I.

The miR-644a/CTBP1/p53 axis suppresses drug resistance by simultaneous inhibition of cell survival and epithelial-mesenchymal transition in breast cancer

4.1.1. miR-644a inhibits proliferation, promotes apoptosis, and its expression or gene signature correlates with tumor progression in breast cancer

To identify novel miRNAs regulating proliferation in breast cancer, we performed a small scale miRNA mimic cell viability screen entailing 35 miRNAs in MDA-MB-231 human breast cancer cell line (Figure 4.1A). As a positive control we used miR-200c, which was previously reported as a tumor suppressor miRNA [130-132]. Out of three most promising potential tumor suppressor miRNAs besides miR-200c, miR-299-3p and miR-127-5p have been reported as tumor suppressors in different cancer types [133, 134]. The other one, miR-644a, has not been characterized in the context of breast cancer. Therfore, I focussed on this miRNA for further studies. RTCA assay further confirmed inhibitory role of miR-644a mimic in viability of MDA-MB-231 cells (Figure 4.1B). Furthermore, miR-644a mimic reduced viability of other cell lines representing different breast cancer subtypes and two normal breast cell lines, MCF-10A and MCF-12A, (Figure 4.1C).

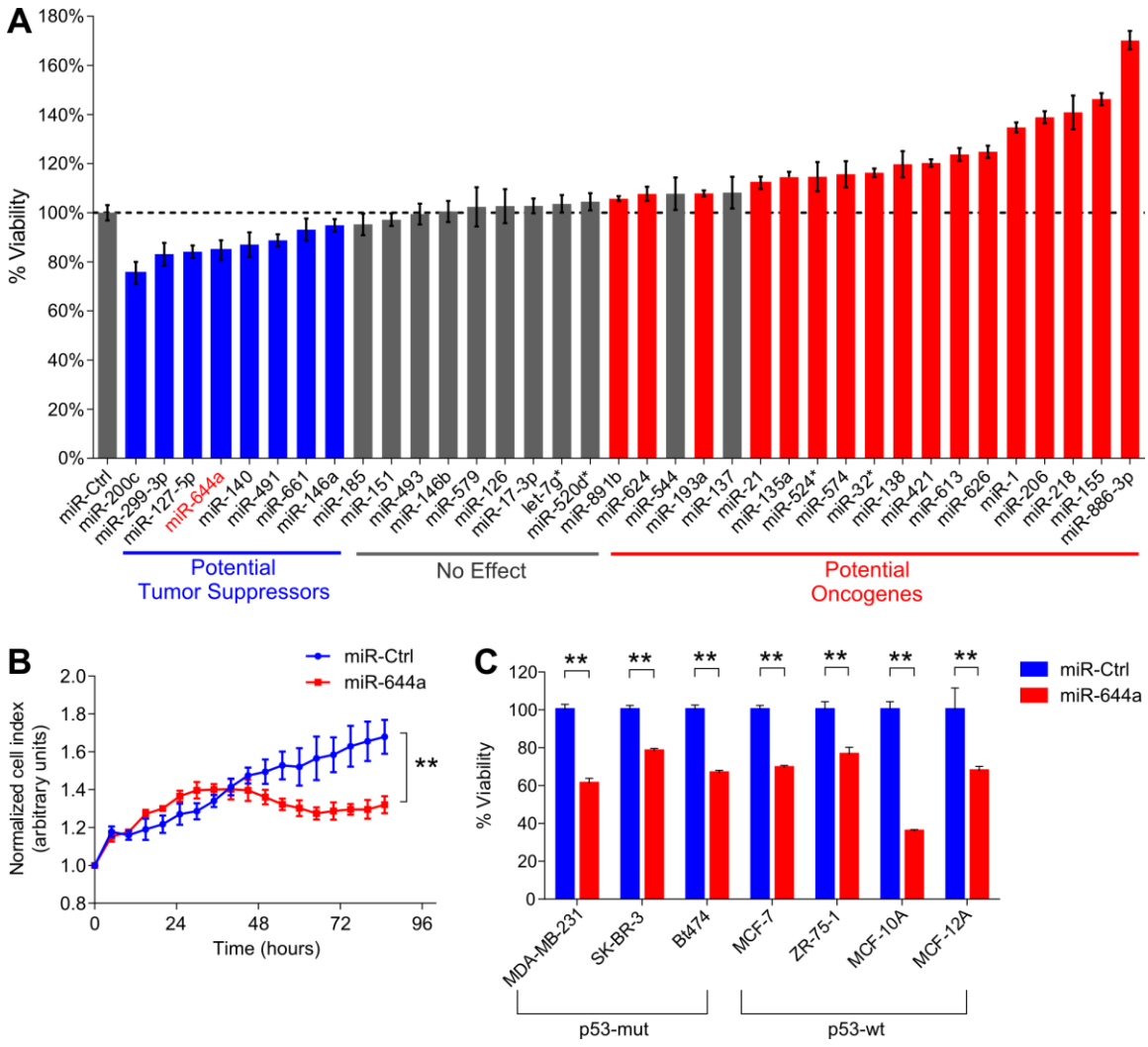

Figure 4.1. miR-644a inhibits proliferation of breast cancer cells *in vitro*. (**A)** miRNA mimic cell viability screen on MDA-MB-231 human breast cancer cell line comprising 35 different miRNAs, with miR-200c as a positive control. The cells were transfected with 20 nM of mimics for 48 hours, and viability was measured using Cell titer Glo. Color coding of the bars depicts the effect of each miRNA on cell viability (blue: decreasing viability, red: increasing viability, gray: no effect on viability). *n* = 4. **(B)** Real time growth of MDA-MB-231 cells transiently transfected with either a control miRNA (miR-Ctrl) or miR-644a mimic, monitored using an RTCA assay. *n* = 3. **(C)** Effect of miR-644a overexpression on the proliferation of 5 breast cancer cell lines and 2 normal breast cell lines transfected with either miR-Ctrl or miR-644a mimic for 48 hours. *n* = 4.

Upon miR-644a overexpression, only the breast cancer cell lines with p53 mutation (p53-*mut*) underwent apoptosis evidenced by increased cleaved caspase-3 (Figure 4.2A

and B) by inducing G2/M arrest characterized by increased phosphorylation of G2/M-arrest markers Cdc2 and Cdc25a (Figure 4.2C and E). In contrast, miR-644a overexpression in p53-*wt* MCF-7 cells resulted in G1 arrest with decreased expression of G1/S transition proteins and increased expression of CDK inhibitor p21, which leads to reduced phosphorylation of Rb protein (Figure 4.2D and E).

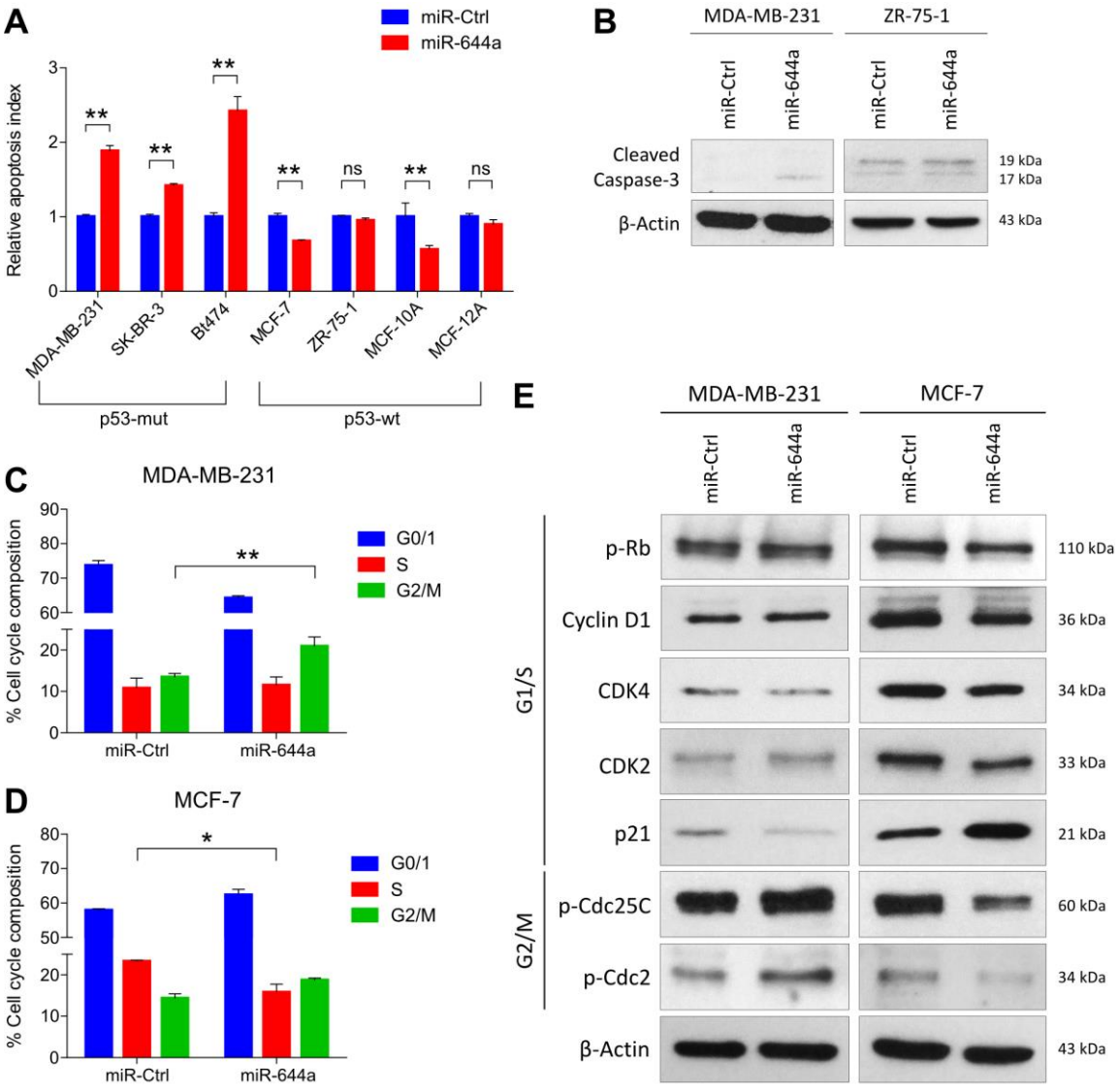

Figure 4.2. miR-644a promotes apoptosis in p53-*mut* but G1 cell cycle arrest in p53-*wt* breast cancer cells *in vitro*. (A) Changes in the apoptosis index based on Caspase-3/7 cleavage in 5 breast cancer and 2 normal breast cell line transfected with either miR-Ctrl or miR-644a mimic. *n* = 4. **(B)** Western Blot analysis showing the levels of cleaved Caspase-3 in p53-*mut*

MDA-MB-231 (left) and p53-*wt* ZR-75-1 cells (right) after 72 hours transfection with either miR-Ctrl or miR-644a mimic. Actin was used as a loading control. **(C and D)** Flow cytometric analysis of cell cycle in cells transfected with miR-Ctrl or miR-644a mimic showing G2/M arrest in MDA-MB-231 cells **(C)** and G1 arrest in MCF-7 cells **(D)** upon miR-644a mimic transfection. $n = 3$. **(E)** Western Blot analysis showing the levels of cell cycle proteins related to G1/S (pRb, Cyclin D1, CDK4, CDK2 and p21) and G2/M transition (p-Cdc25C and p-Cdc2) in p53-*mut* MDA-MB-231 (left) and p53-*wt* MCF7 cells (right) after 48 hours transfection with either miR-Ctrl or miR-644a mimic. Actin was used as a loading control.

To validate our findings *in vivo*, we engineered MDA-MB-231 cell line (referred to herein as 231.Ctrl) with lentiviral-transduced miR-644a mimic (referred to herein as 231.miR-644a) (Figure 4.3A), and observed a delayed and significantly decreased tumor growth (Figure 4.3B). Correspondingly, tumors collected from the 231.miR-644a group showed high levels of miR-644a expression (Figure 4.3E), were substantially smaller and weighed less (Figure 4.3C and D) further confirming the tumor suppressive role of miR-644a in breast cancer.

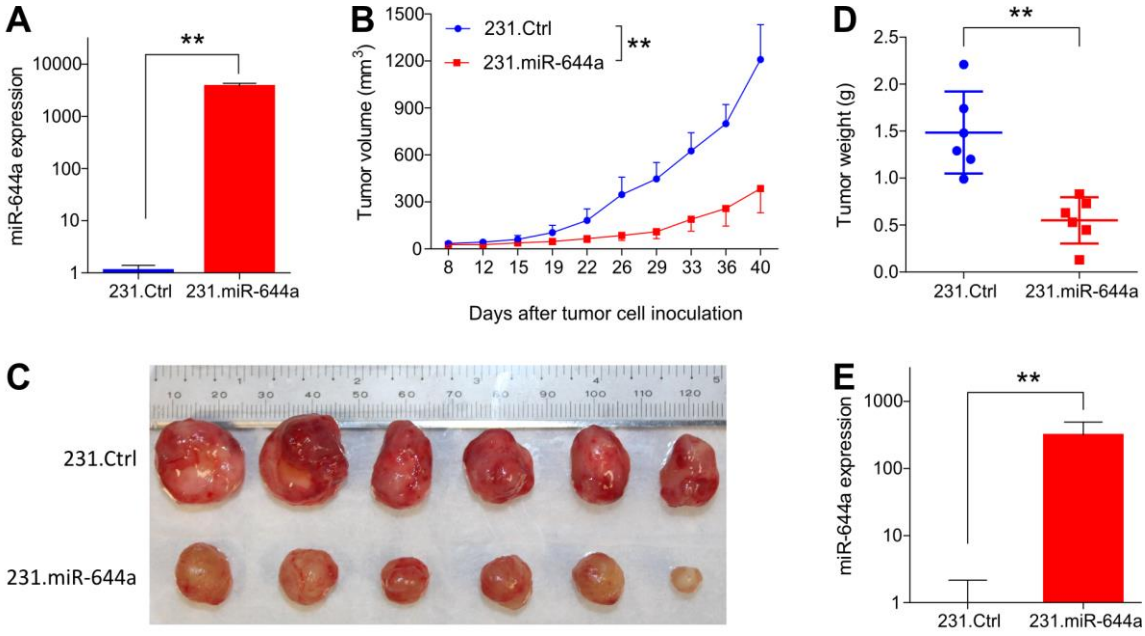

Figure 4.3. miR-644a inhibits breast cancer tumor progression *in vivo*. (A) qRT-PCR analysis of miR-644a in 231.miR-644a stable cells. **(B)** Tumor progression in xenografts generated with orthotopic subcutaneous injection of MDA-MB-231 cells stably expressing either a non-silencing control (231.Ctrl) or miR-644a (231.miR-644a) into nude mice. *n* = 6. **(C)** Representative images of tumors collected from xenografts of **(B)** on day 40. **(D)** Tumor weights of xenografts from **(C)** at day 40. **(E)** qRT-PCR analysis showing average miR-644a expression in 231.Ctrl and 231.miR-644a tumors collected from xenografts of **(C)** on day 40. *n* = 3.

To elucidate the pathological relevance of miR-644a, we examined the expression of miR-644a in publicly available expression datasets GSE45666 and GSE58606, and observed significantly lower miR-644a levels in breast tumors as compared to normal tissue (Figure 4.4A and B). Besides breast cancer, melanoma and osteosarcoma cell lines data from GSE35389 and GSE2845 respectively, also showed lower miR-644a levels in cancer cells as compared to their normal counterparts (Figure 4.4C and D) suggesting a potential tumor suppressor role for miR-644a.

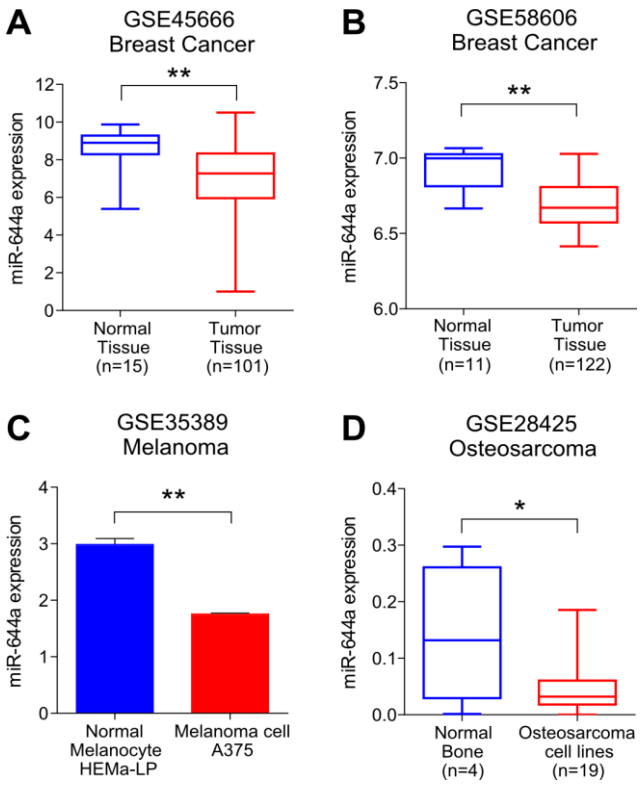

Figure 4.4. miR-644a is downregulated in multiple cancer types. (A) miR-644a expression in 101 breast tumor tissues and 15 normal tissues from GSE45666. **(B)** miR-644a expression in 122 breast tumor tissue and 11 normal tissue samples from GSE58606. **(C)** miR-644a expression in melanoma and as compared to a normal melanocyte cell line from GSE35389. **(D)** miR-644a expression in osteosarcoma cell lines as compared to a normal bone cell line from GSE28425.

In addition to gene-level analysis, we also performed gene expression profiling to derive a miR-644a signature, and used this signature to elucidate miR-644a-induced changes in a more global manner. To this end, we forced expression of miR-644a using mimics in three breast cancer cell lines representing different subtypes of breast cancer. We then collected commonly up- and down-regulated genes among these three cell lines to create a miR-644a gene signature (miR-644a-GS). GO term analysis revealed association of miR-644a-GS with biological processes contributing to tumor progression, such as cell cycle, apoptosis, actin cytoskeletal organization and cell adhesion (Figure 4.5).

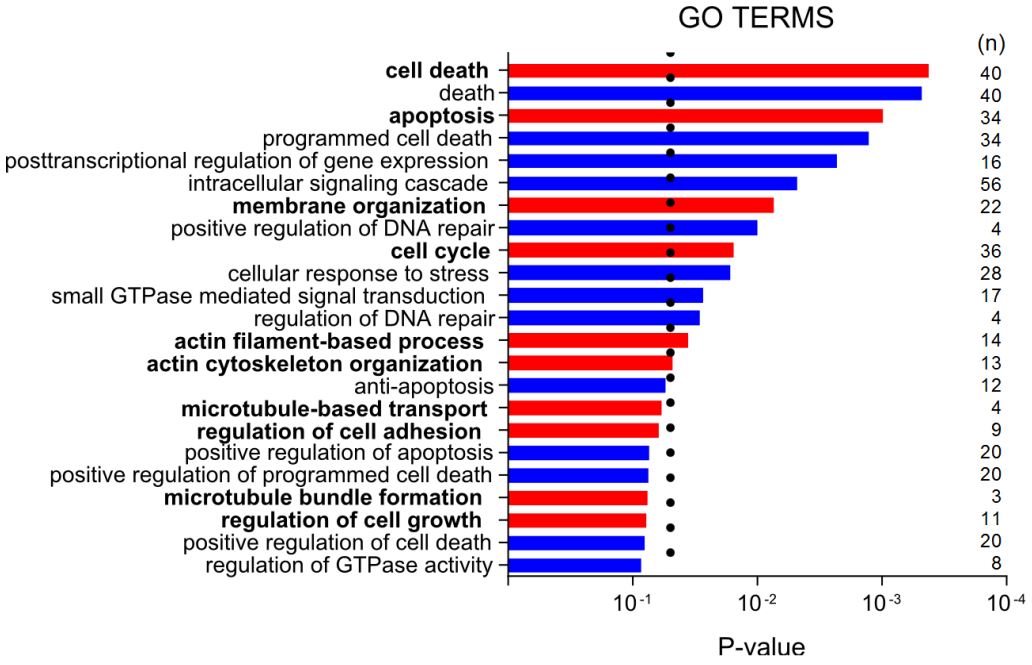

Figure 4.5. GO Terms associated with miR-644a-GS. n = number of genes.

GSEA of GSE58644 dataset showed a significant correlation between miR-644a-GS and tumor progression in breast cancer patients. Notably, a gene set containing genes downregulated in lobular carcinoma compared to normal lobular breast cells was enriched in patients with high miR-644a-GS scores (Figure 4.6A). Moreover, genes associated with histologic grade 1 and grade 3 in breast cancer patients were significantly enriched in high and low miR-644a-GS scorers, respectively (Figure 4.6B and C). Consistent with this observation, in the same dataset, miR-644a-GS score was lower in tumors with more aggressive disease state characterized by higher tumor grade and stage (Figure 4.6D and E).

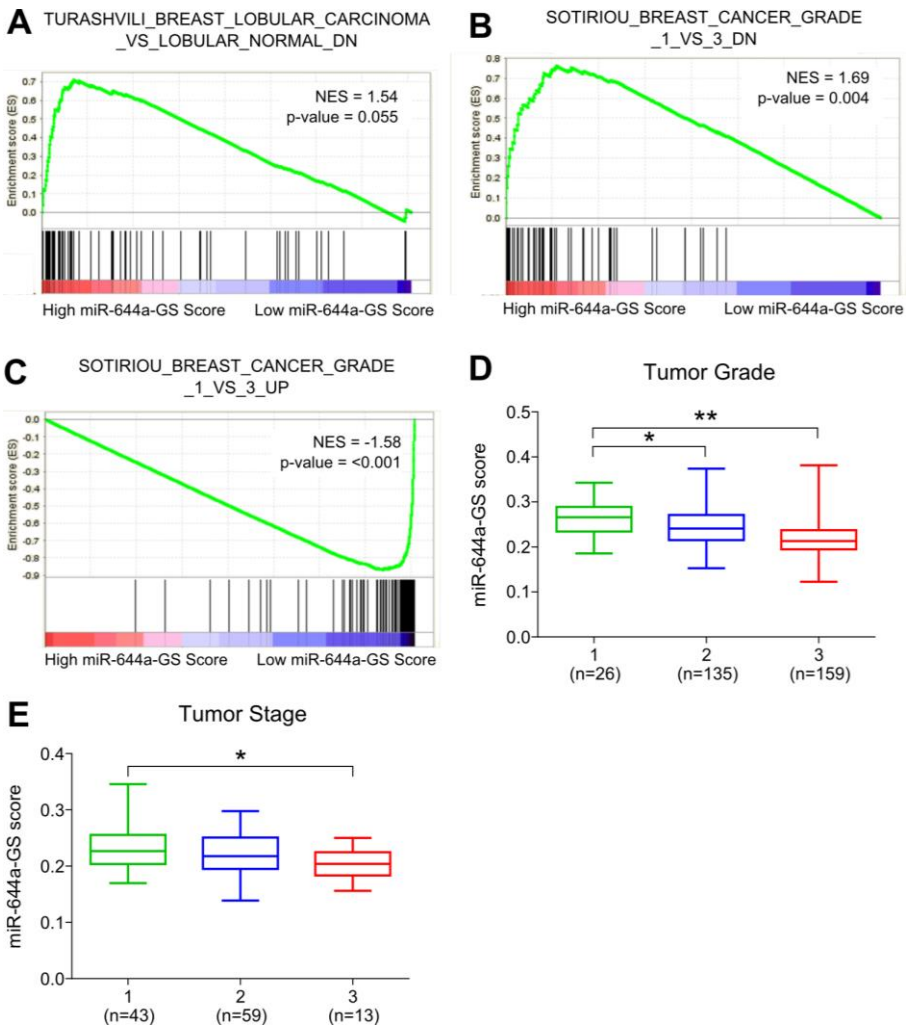

Figure 4.6. Loss of miR-644a correlates with breast cancer progression. (A-C) Enrichment plots of patients from GSE58644 (*n* = 320) with low and high miR-644a-GS scores. Genes downregulated in breast lobular carcinoma as compared to normal lobular breast cells were enriched in patients with high miR-644a-GS scores **(A)**. Genes downregulated as breast tumors progress through histologic grade 3 were enriched in patients with high miR-644a-GS score **(B)**. Genes up-regulated as breast tumors progress through histologic grade 3 were enriched in patients with low miR-644a-GS score **(C)**. **(D and E)** Changes in miR-644a-GS score with tumor grade (D) and stage (E) in patients from GSE58644.

Finally, miR-644a status was correlated with the formation and progression of not only breast cancer, but also of a variety of cancers, including melanoma, liver, lung and ovarian cancers (Table 4.1), all supporting the tumor suppressive roles of miR-644a.

Table 4.1. Enrichment of gene sets related to cancer formation and progression of different cancer types in patients with low and high miR-644a-GS scores.

Name of the gene set	**NES***	**p-value**
Gene Sets associated with low miR-644a-GS score		
LOPEZ_MESOTELIOMA_SURVIVAL_TIME_UP	-1.499	0.008
WEST_ADRENOCORTICAL_CARCINOMA_VS_ADENOMA_UP	-1.704	0.008
POMEROY_MEDULLOBLASTOMA_PROGNOSIS_DN	-1.714	0.012
MONTERO_THYROID_CANCER_POOR_SURVIVAL_UP	-1.420	0.012
SHEDDEN_LUNG_CANCER_POOR_SURVIVAL_A6	-1.633	0.021
KAUFFMANN_MELANOMA_RELAPSE_UP	-1.543	0.035
MEINHOLD_OVARIAN_CANCER_LOW_GRADE_DN	-1.538	0.037
Gene Sets associated with high miR-644a-GS score		
WAMUNYOKOLI_OVARIAN_CANCER_GRADES_1_2_DN	1.683	0.003
WOO_LIVER_CANCER_RECURRENCE_UP	1.480	0.050
LANDIS_BREAST_CANCER_PROGRESSION_DN	1.664	0.013

*NES: Normalized Enrichment Score

4.1.2. miR-644a inhibits metastasis and correlates with metastasis-free survival in patients

Since we observed that the genes associated with developing distant metastasis in breast cancer are enriched in patients with low miR-644a-GS scores, and the genes downregulated in metastatic tumors are enriched in patients with high miR-644a-GS scores (Table 4.2), we examined the effects of miR-644a mimic on the metastatic potential of breast tumors. Transient miR-644a overexpression significantly inhibited migration of MDA-MB-231 cells as assessed by wound healing assay (Figure 4.7A). We also observed similar results in RTCA migration assay where migration was significantly inhibited in miR-644a mimic transfected MDA-MB-231 and MDA-MB-436 cells as compared to their control counterparts (Figure 4.7B and C). In addition, miR-644a overexpression *via* transient transfection suppressed invasion in highly invasive MDA-MB-231 cells as determined by trans-well matrigel invasion assay (Figure 4.7D). Anchorage-independent growth is another imprtant parameter in metastatic cascade as metastasizing cells need to remain viable in circulation system while travelling to distant organs. Stable expression of miR-644a mimic significantly reduced anchorage-independent growth in MDA-MB-231 breast cancer cells (Figure 4.7E).

Table 4.2. Enrichment of gene sets related to metastasis in patients with low and high miR-644a-GS scores.

Name of the gene set	NES*	p-value
Gene Set associated with low miR-644a-GS score		
WANG_METASTASIS_OF_BREAST_CANCER_ESR1_UP	-1.57	0.032
Gene Set associated with high miR-644a-GS score		
CHANDRAN_METASTASIS_DN	1.494	0.034

*NES: Normalized Enrichment Score

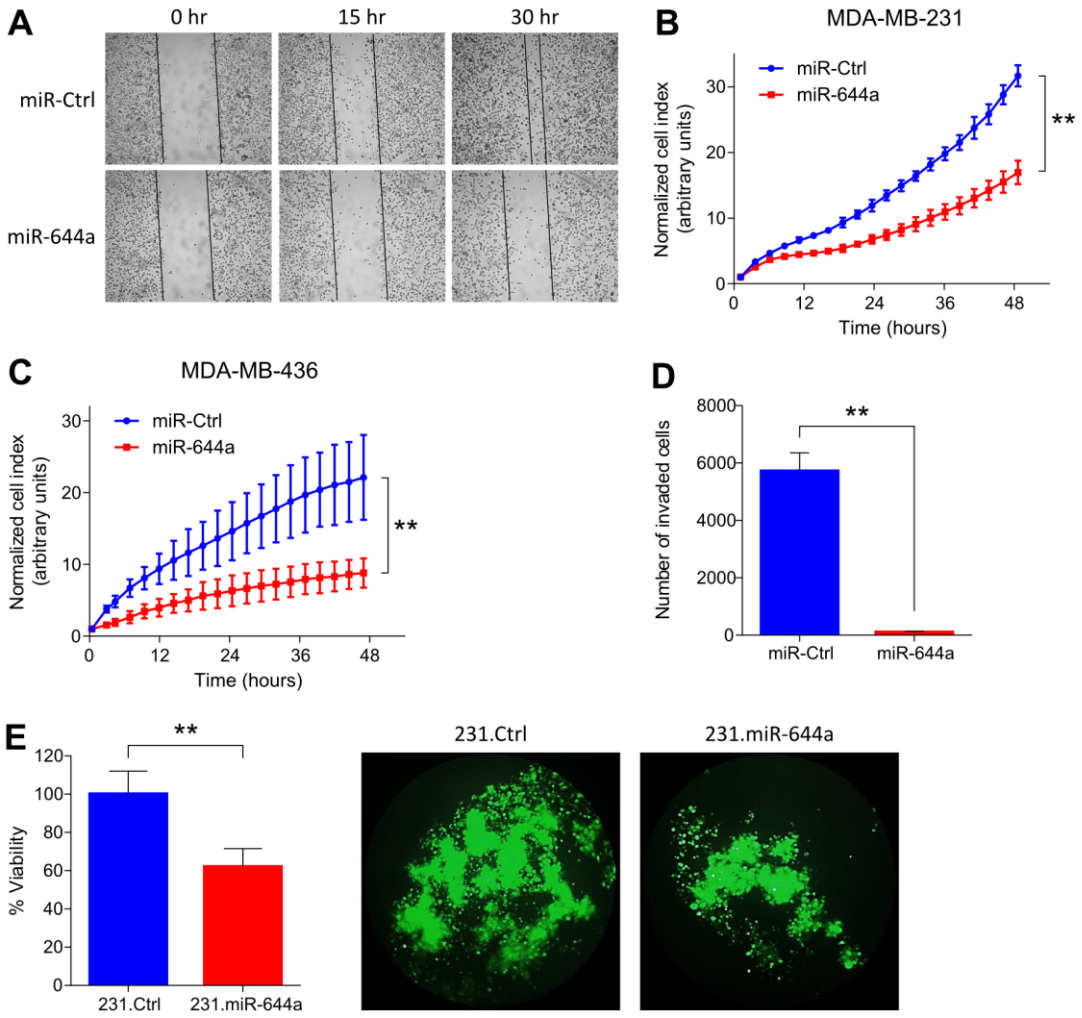

Figure 4.7. miR-644a inhibits migration, invasion and anchorage independent growth *in vitro*. (A) Wound healing assay of MDA-MB-231 cells transfected with miR-Ctrl or miR-644a mimic. Cells were scratched after 48 hours of transfection, and images were taken with 4X Magnification at 0, 15 and 30 hours after making the scratch. **(B and C)** Real-time migration of MDA-MB-231 **(B)** and MDA-MB-436 **(C)** cells transfected with either miR-Ctrl or miR-644a mimic, monitored using an RTCA assay. *n* = 3. **(D)** Number of invaded cells transfected with miR-Ctrl or miR-644a mimic using Matrigel invasion assay. *n* = 3. **(E)** Viability of 231.Ctrl and 231.miR-644a cells grown in anchorage-independent conditions for 7 days, quantified by WST-1 assay (left) together with their fluorescence microscopy images with 10X magnification (right). *n* = 4.

Interestingly, cells showed rearrangements of actin cytoskeletal structures from a mesenchymal to an epithelial-like state upon overexpressing miR-644a (Figure 4.8A)

which is further confirmed by upregulated epithelial markers and downregulated mesenchymal markers both at mRNA and protein level upon miR-644a overexpression (Figure 4.8B-D).

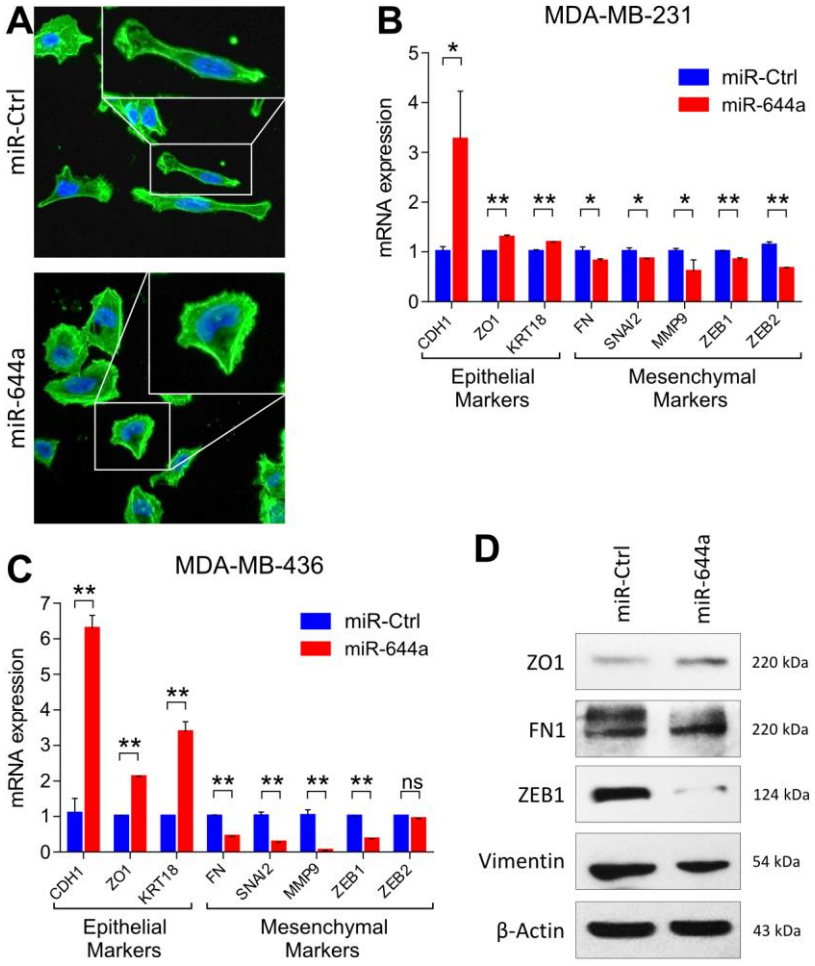

Figure 4.8. miR-644a inhibits EMT *in vitro*. (A) Fluorescence microscopy images of MD-MB-231 cells transfected with miR-Ctrl or miR-644a mimic. Cell nuclei and filamentous actin were stained with DAPI and phalloidin, respectively. Images were taken 72 hours after transfection with 20X magnification. Inset shows cell morphology with higher resolution. **(B and C)** qRT-PCR analysis of epithelial and mesenchymal marker gene expression in MDA-MB-231 **(B)** and MDA-MB-436 **(C)** cells transfected with miR-Ctrl or miR-644a mimic. **(D)** Western Blot analysis of epithelial and mesenchymal markers' expression in MDA-MB-231 cells transfected with miR-Ctrl or miR-644a mimic. Actin was used as a loading control.

Next, we tested the metastatic potential of 231.miR-644a cells in nude mice with tail-vein metastasis assay. Bouin's fixation of lungs and Hematoxylin and Eosin (H&E) staining indicated less colonization of 231.miR-644a cells to lungs as compared to 231.Ctrl cells (Figure 4.9A and B). As these cells are stably labelled with luciferase, we measured luciferase activity of lung lysates, and showed that substantially less metastatic cells reached to the lungs when miR-644a is expressed (Figure 4.9C). These data suggest that miR-644a inhibits lung metastasis *in vivo*.

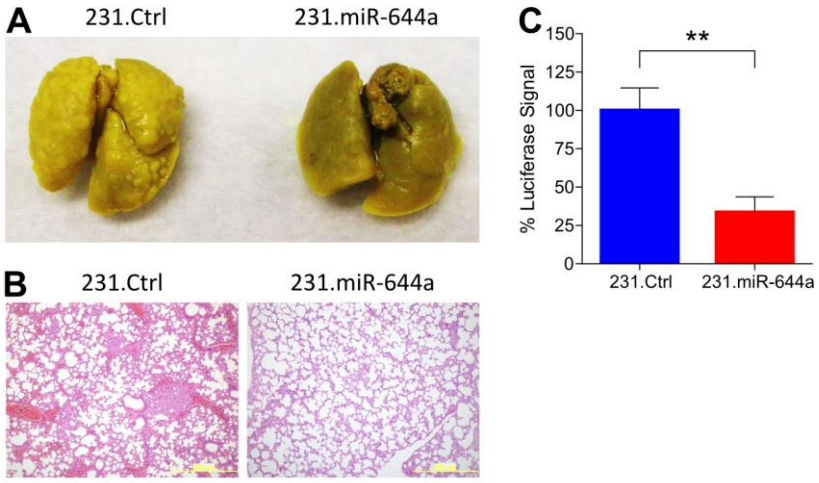

Figure 4.9. miR-644a inhibits metastasis *in vivo*. (A) Representative images of lungs collected from nude mice injected intravenously with 231.Ctrl or 231.miR-644a cells. Mice were sacrificed at week 7 and lungs were fixed in Bouin's Solution. **(B)** Representative Hematoxylin and Eosin staining of metastatic nodules in lungs from **(A)**. **(C)** Luciferase signal coming from metastatic nodules in lungs of **(A)** as quantified by a luciferase assay. $n = 4$.

Next, to validate these *in vitro* and *in vivo* findings in human patient datasets, we first examined GSE38167 dataset, and found that expression of miR-644a is lower in lymph node metastases as compared to primary tumors and normal adjacent tissues (Figure 4.10A). Moreover, miR-644a expression was found to be negatively associated with

metastasis in cancers other than breast as well (Figure 4.10B and C). Finally, we showed an enrichment of genes associated with poor outcome in patients having low miR-644a-GS scores (Figure 4.10D). Consistent with this, breast cancer patients with high miR-644a-GS scores have significantly longer distant metastasis-free survival (DMFS) (Figure 4.10E). Overall, these data suggest that miR-644a is a novel tumor suppressor that is likely to be involved in progression and metastasis of multiple cancer types including breast cancer.

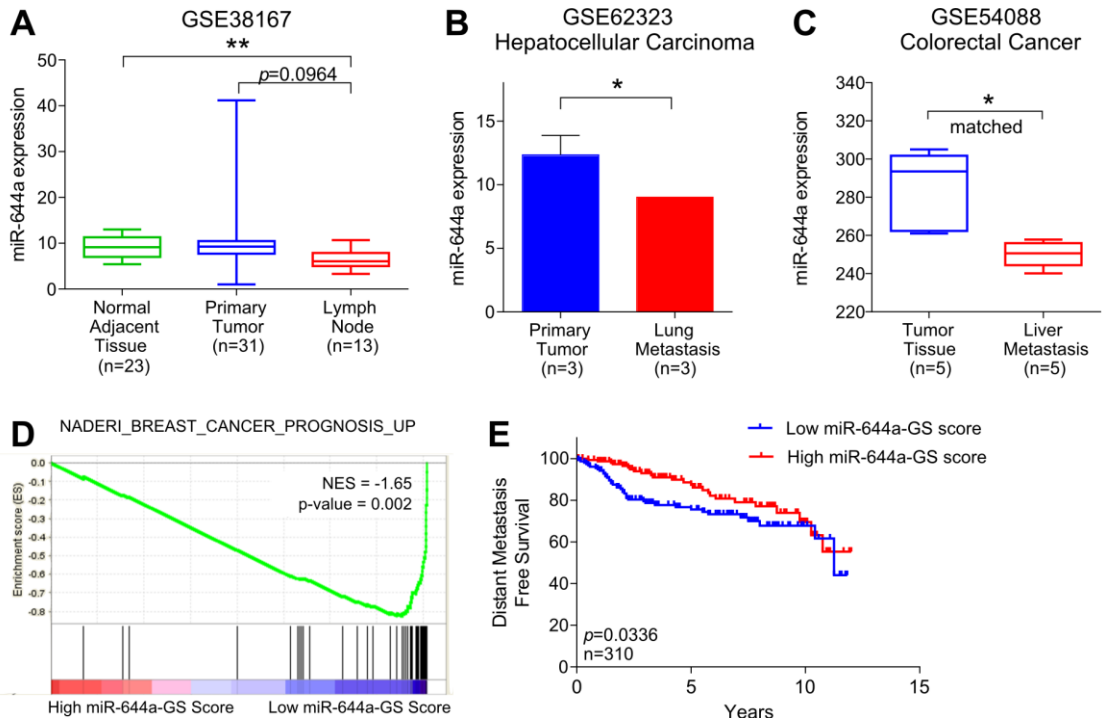

Figure 4.10: miR-644a expression is lower in metastases and correlates with metastasis-free survival. (A) miR-644a expression in 23 normal tissue, 31 primary tumor (IDC) and 13 lymph node metastases in GSE38167 depicted as box-plot. **(B and C)** miR-644a expression in a lung metastases of hepatocellular carcinoma **(B)** and liver metastases of colorectal cancer **(C)** as compared to primary tumors. **(D)** Enrichment plot of patients from GSE58644 (n = 320) with high or low miR-644a-GS score. Genes expressed more in breast cancer patients with poor outcome as compared to those with good outcome were enriched in patients expressing low levels of miR-644a-GS score. **(E)** Kaplan Meier survival curve representing the percentage DMFS in breast cancer patients based on miR-644a-GS score median expression levels in GSE58644 (n = 310).

4.1.3. miR-644a is a pleiotropic therapy sensitizer in breast cancer

Since miR-644a inhibits both breast cancer cell survival and EMT, we hypothesized that it might also work as a therapy sensitizer. To test this hypothesis, we did GSEA with gene sets related to chemotherapy sensitivity and resistance. We observed that genes associated with doxorubicin (topoisomerase II inhibitor) and cisplatin (DNA cross linking agent; promising therapy for BRCA1/2 mutated/deficient tumors) resistance in gastric cancer cell lines and patients, respectively were significantly enriched in patients with low miR-644a-GS scores (Table 4.3) suggesting a close association between miR-644a and chemotherapy resistance. In addition to chemotherapy agents, we found that patients with high miR-644a-GS scores are associated with enhanced sensitivity to tamoxifen (Table 4.3) which is the mainstay targeted therapy for ER+ breast cancer patients for over 40 years [135]. Similarly, we observed that genes downregulated in gefitinib resistant NSCLC cells undergoing prominent growth arrest and apoptosis upon treatment with an irreversible EGFR inhibitor, CL-387,785 [136], were enriched in patients with low miR-644a-GS scores (Table 4.3).

Table 4.3. Enrichment of gene sets related to drug resistance in patients with low and high miR-644a-GS scores.

Name of the gene set	NES*	p-value
Gene Sets associated with low miR-644a-GS score		
KANG_DOXORUBICIN_RESISTANCE_UP	-1.557	0.008
KIM_GASTRIC_CANCER_CHEMOSENSITIVITY	-1.537	0.035
KOBAYASHI_EGFR_SIGNALING_24HR_DN	-1.593	0.017
Gene Set associated with high miR-644a-GS score		
RIGGINS_TAMOXIFEN_RESISTANCE_DN	1.452	0.026

*NES: Normalized Enrichment Score

Indeed, transiently overexpressed miR-644a significantly sensitized p53-*mut* MDA-MB-231 cells to doxorubicin *in vitro* (Figure 4.11A). Similar results were also observed in the case of p53-*wt* MCF-7 cells (Figure 4.11B) Notably, higher miR-644a levels were observed in doxorubicin sensitive tumors developed *in vivo* as compared to resistant ones (Figure 4.11C), further supporting that miR-644a may play a role in chemotherapy resistance also *in vivo*. Furthermore, miR-644a overexpression also sensitized *BRCA1*-mutated MDA-MB-436 breast cancer cells to cisplatin *in vitro* (Figure 4.11D). As we showed that miR-644a-GS score is associated with tamoxifen and gefinitib, we tested if miR-644a overexpression sensitizes breast cancer cells to these targeted therapy agents. We demonstrated that forced miR-644a mimic expression sensitizes cells to tamoxifen in ER+ MCF-7 cells *in vitro* (Figure 4.11E). We then validated this in EGFR overexpressing SK-BR-3 breast cancer cells, where miR-644a overexpression significantly sensitized cells to gefitinib (Figure 4.11F). Overall, multiple lines of evidence support the notion that miR-644a may be a pleiotropic sensitizer for both chemo- and targeted-therapy.

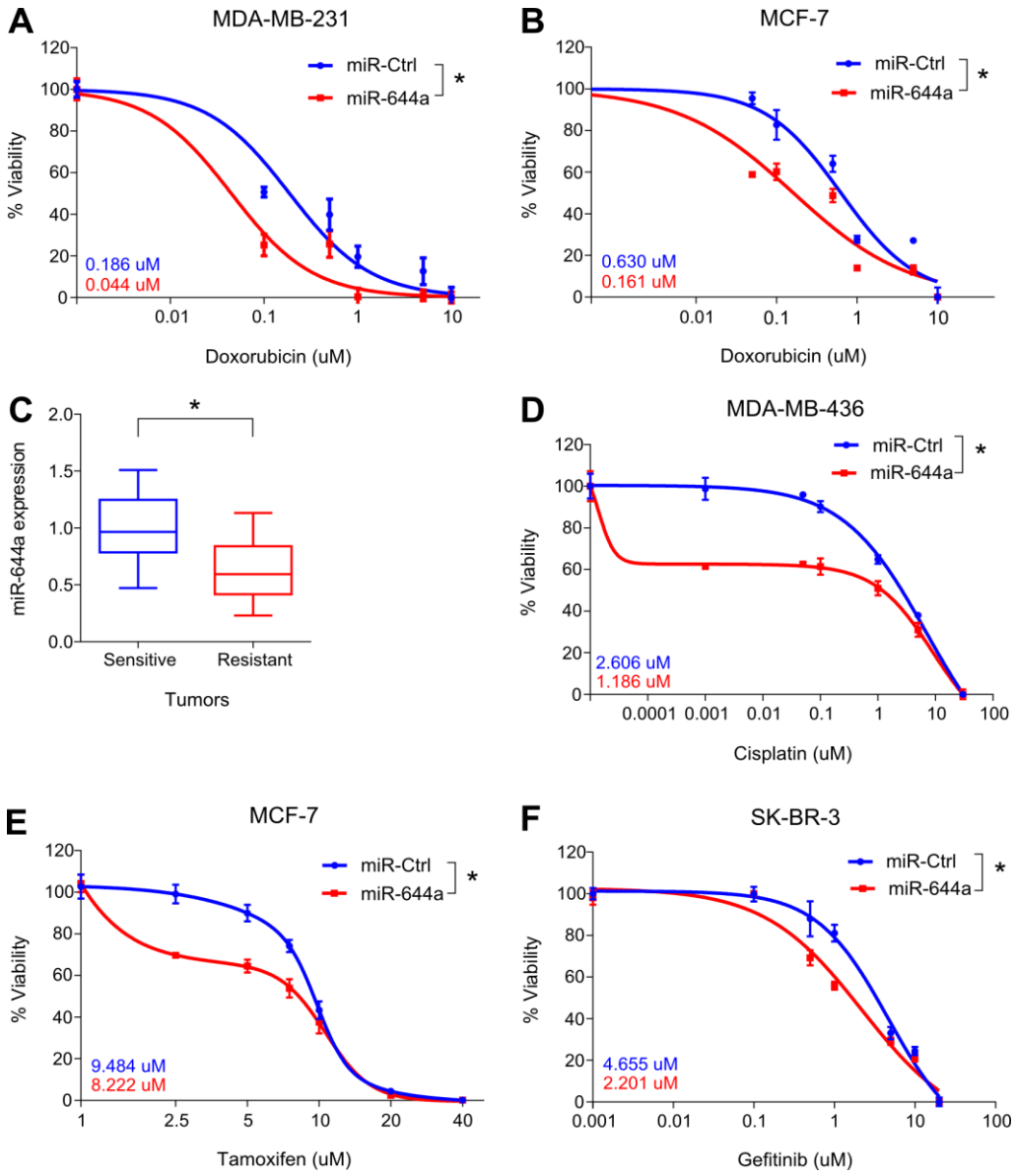

Figure 4.11. miR-644a overexpression acts as a therapy sensitizer in breast cancer cells and its expression correlates with doxorubicin resistance *in vivo*. (A and B) Effect of miR-644a overexpression on the response of MDA-MB-231 **(A)** and MCF-7 **(B)** cells to doxorubicin. *n* = 4. **(C)** qRT-PCR analysis of miR-644a expression in sensitive or resistant xenografts selected based on changes in tumor volumes upon successive doxorubicin treatments. *n* =5. **(D- F)** Effect of miR-644a overexpression on the response of MDA-MB-436 cells to cisplatin **(D)**, MCF-7 cells to tamoxifen **(E)**, and SKBR-3 cells to gefitinib **(F)**. *n* = 4. IC50 values for each condition are given on the left bottom corners of each curve with a color code.

4.1.4. CTBP1 is a direct target of miR-644a

To identify the targets of miR-644a mediating these observed effects related to tumor progression, metastatic spread and therapy resistance, we combined the list of genes downregulated upon miR-644a overexpression in our microarray analysis with targets of miR-644a predicted by three target prediction algorithms. This stringent analysis resulted in 3 common genes: *CHMP7*, *CTBP1* and *NDST1* (Figure 4.12).

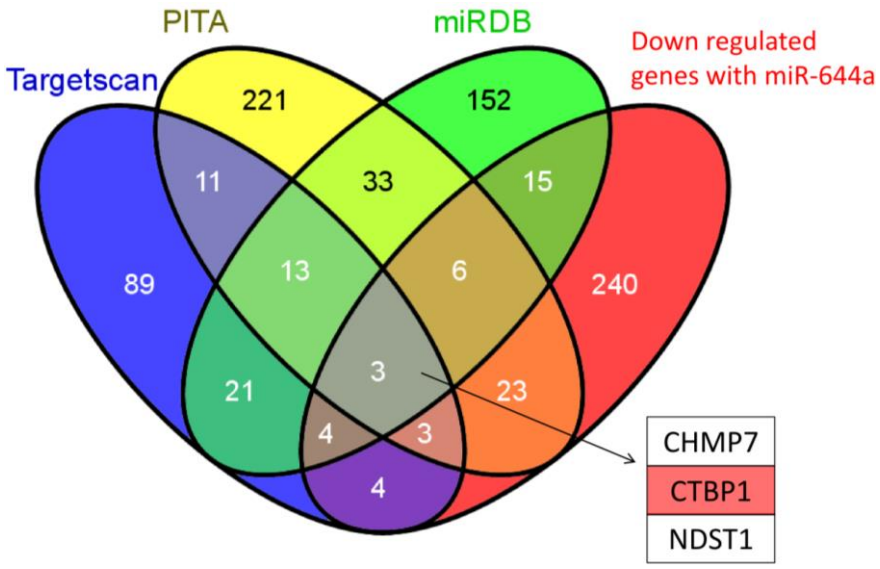

Figure 4.12. Venn diagram for the combinatorial target prediction analysis of miR-644a. List of genes downregulated upon miR-644a mimic transfection in the microarray analysis was combined with genes predicted to be miR-644a targets by three different target prediction algorithms namely TargetScan (blue), PITA (yellow) and miRDB (green). The names of three genes that are common in all four groups are shown, with CTBP1 highlighted in red.

We found CTBP1 (C-Terminal Binding Protein 1) as the most promising candidate since it is an established transcriptional co-repressor which preferentially represses the transcription of tumor suppressor genes and promotes tumor growth *via* playing pivotal roles in tumor pathogenesis [137-139]. Sequence analysis revealed that human *CTBP1*

3’-UTR has one binding site of miR-644a between nucleotides 453-460 conserved among multiple species (Figure 4.13).

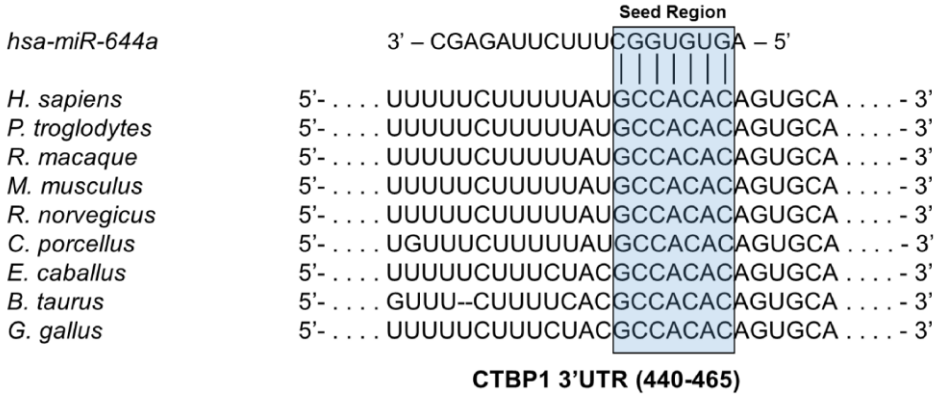

Figure 4.13. Schematic diagram showing miR-644a binding site in *CTBP1* 3’-UTR (453-460) in different species including human.

Transient as well as stable overexpression of miR-644a significantly downregulated CTBP1 mRNA and protein levels in both MDA-MB-231 and MCF-7 cells (Figure 4.14A-D). Inversely, miR-644a inhibition in MDA-MB-231 and MCF-12A cells by using hairpin inhibitors upregulated CTBP1 levels (Figure 4.14E and F).

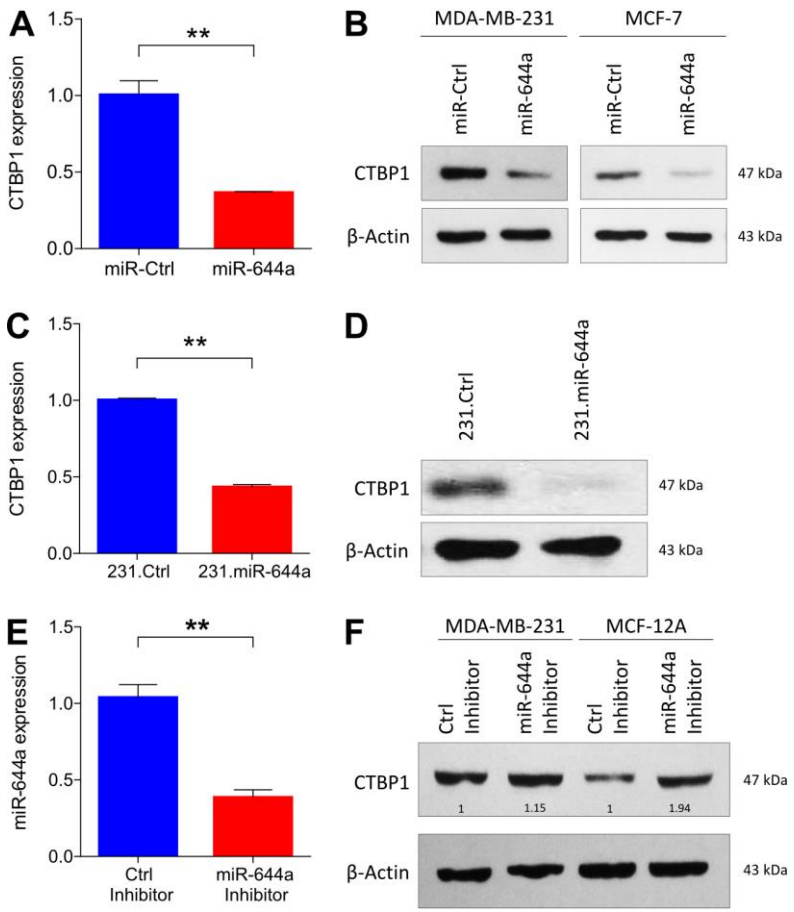

Figure 4.14. Modulating miR-644a expression alters CTBP1 expression inversely *in vitro*. (A and B) Confirmation of CTBP1 downregulation by miR-644a overexpression at transcript and protein levels with qRT-PCR analysis in MDA-MB-231 **(A)** and with Western Blot analysis in MDA-MB-231 (left) and MCF-7 (right) **(B)** cells transfected with either miR-Ctrl or miR-644a mimic. Actin was used as a loading control. **(C and D)** qRT-PCR **(C)** and Western Blot **(D)** analysis of CTBP1 expression in 231.Ctrl and 231.miR-644a cells. Actin was used as a loading control. **(E)** qRT-PCR analysis of miR-644a expression in MDA-MB-231 cells transfected with either a control Inhibitor (Ctrl Inhibitor) or miR-644a Inhibitor. **(F)** Western Blot analysis showing the levels of CTBP1 in MDA-MB-231 and MCF-12A cells transfected with either Ctrl Inhibitor or miR-644a Inhibitor. Actin was used as a loading control.

Next, in order to confirm CTBP1 as a direct target of miR-644a, we measured luciferase expression from *CTBP1* 3'-UTR constructs with or without mutation in the seed-matching of miR-644a in MDA-MB-231 and MCF-7 cells upon miR-644a mimic transfection. In both cell lines, miR-644a overexpression significantly repressed

luciferase expression when co-transfected with vector expressing WT 3'-UTR of CTBP1, but not when co-transfected with vector expressing mutated 3'-UTR of CTBP1 (Figure 4.15A and B). Additionally, through analyzing mRNA and miRNA expression profiles from dataset GSE40059 [115], we observed an inverse correlation between miR-644a and CTBP1 expression in 11 different breast cancer cell lines (Figure 4.15C). Overall, these data confirm that CTBP1 is a direct target of miR-644a.

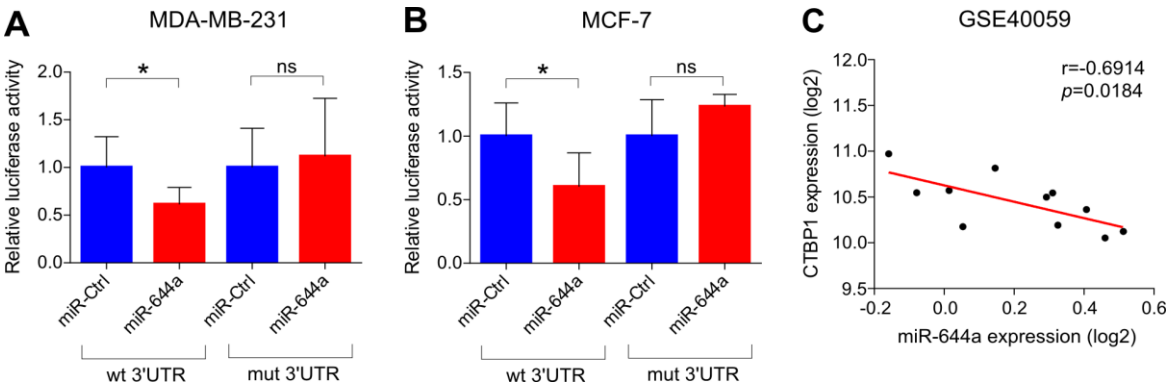

Figure 4.15. miR-644a directly targets CTBP1 and inversely correlates with CTBP1 expression in breast cancer cell lines. (A and B) Luciferase activity of a reporter construct fused with either a *wt* or *mut CTBP1* 3'-UTR co-transfected with miR-Ctrl or miR-644a mimic in MDA-MB-231 **(A)** and MCF-7 **(B)** cells. n = 5. **(C)** Expression of miR-644a negatively correlates with CTBP1 mRNA expression in 9 breast cancer cell lines and 2 normal breast cell line from GSE40059.

4.1.5. Loss of CTBP1 mimics tumor-suppressive roles of miR-644a *in vitro* and *in vivo*

To validate that CTBP1 is a major functional target of miR-644a, we first knocked down CTBP1 with two different siRNA sequences (Figure 4.16A and B), and examined the effects on viability, apoptosis and cell cycle. Similar to miR-644a overexpression, we observed a significant reduction in the viability of all tested cell lines upon CTBP1 knockdown (Figure 4.16C).

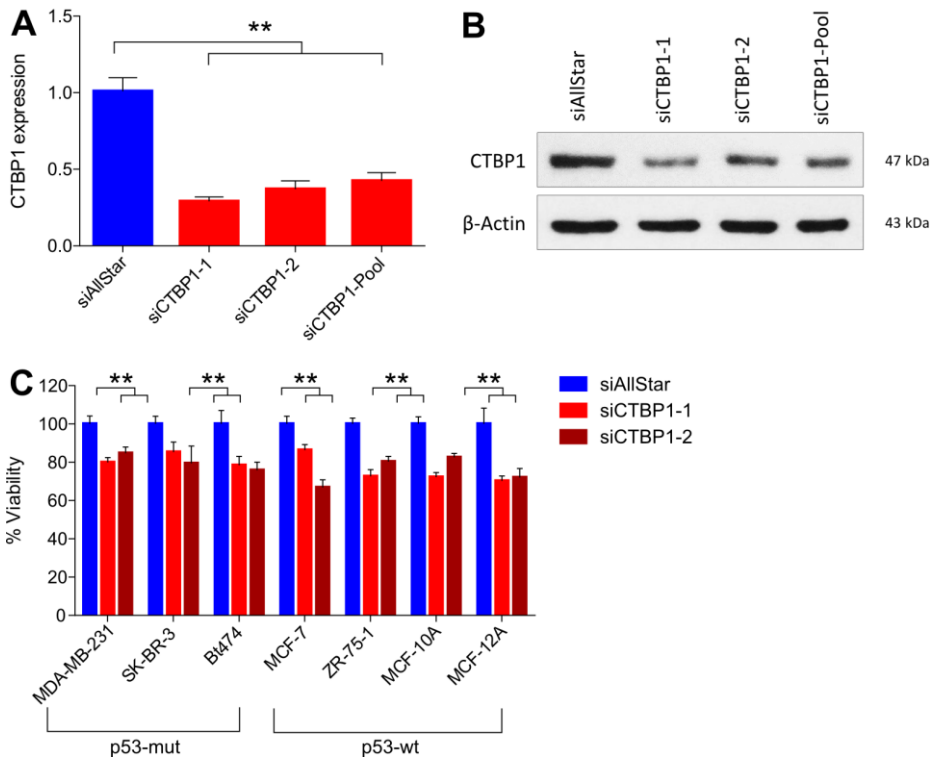

Figure 4.16. CTBP1 knockdown inhibits proliferation of breast cancer cells *in vitro* (A and B) qRT-PCR (**A)** and Western Blot **(B)** analysis of CTBP1 levels in MDA-MB-231 cells transfected with control siRNA (siAllstar) or different CTBP1 targeting siRNAs (siCTBP1-1, siCTBP1-2 and siCTBP1-Pool). Actin was used as a loading control. **(C)** Effect of CTBP1 knockdown on proliferation of cell lines previously used to test the effects of miR-644a overexpression on proliferation as in Figure 4.1C. Cells were transfected with either a non-targeting siRNA control (siAllStar) or different CTBP1 targeting siRNAs (siCTBP1-1, siCTBP1-2) for 48 hours. *n* = 4.

Interestingly, CTBP1 downregulation also mimicked miR-644a overexpression in increasing apoptotic cell death and inducing cleaved caspase-3 exclusively in p53-*mut* breast cancer cell lines, but not in p53-*wt* cell lines (Figure 4.17A and B). Moreover, cell cycle and Western Blot analysis confirmed a G2/M arrest in p53-*mut* MDA-MB-231 cells while a G1 arrest was observed in p53-*wt* MCF-7 cells upon CTBP1 knockdown similar to the effect of miR-644a mimic (Figure 4.17C-E).

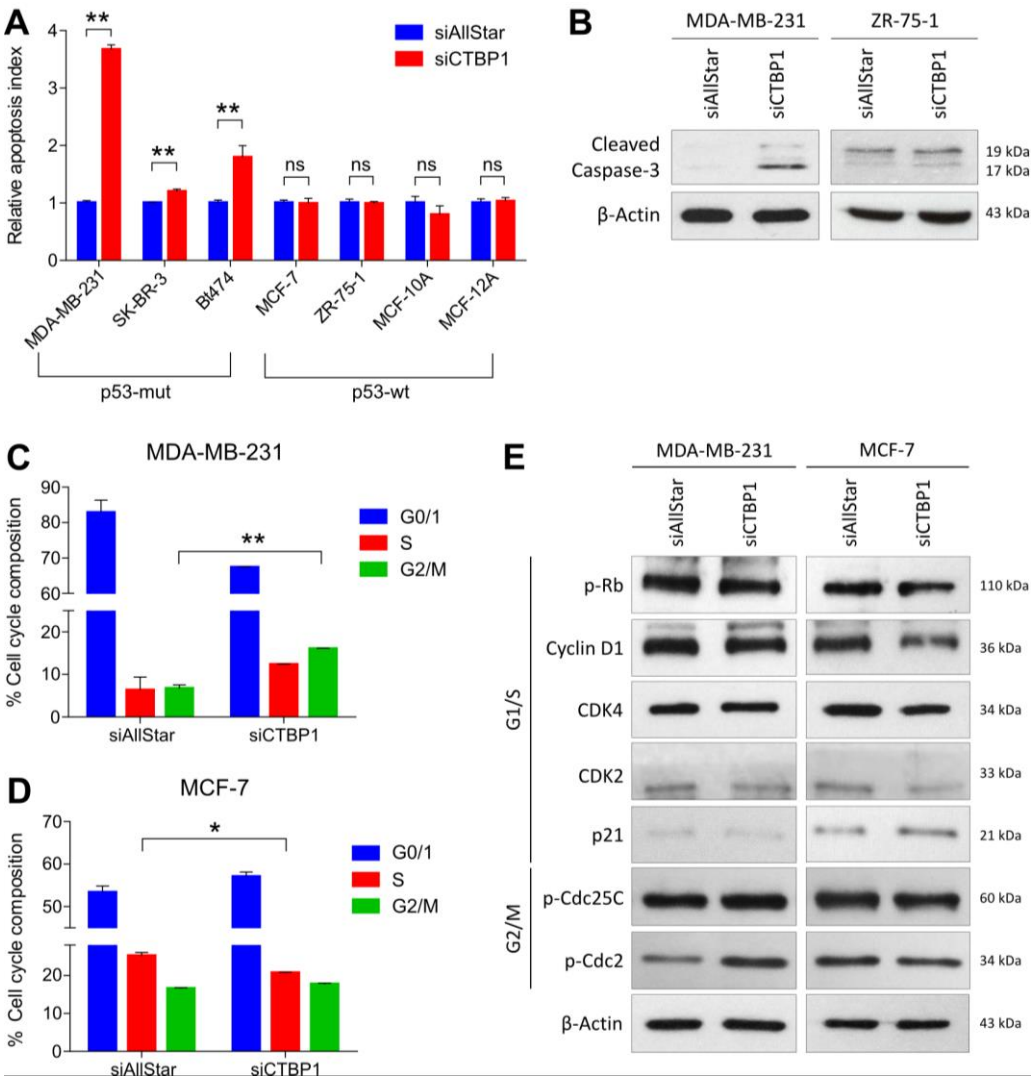

Figure 4.17. CTBP1 knockdown promotes apoptosis in p53-*mut* but G1 cell cycle arrest in p53-*wt* breast cancer cells *in vitro*. (A) Changes in the apoptotic index based on Caspase-3/7 cleavage in 5 breast cancer cell lines and 2 normal breast cell line transfected with siAllStar or siCTBP1-Pool. *n* = 4. **(B)** Western Blot analysis showing the levels of cleaved Caspase-3 in p53-*mut* MDA-MB-231 (left) and p53-*wt* MCF-7 cells (right) 72 hours after transfection with siAllStar or siCTBP1-Pool. Actin was used as a loading control. **(C and D)** Flow cytometric analysis of cell cycle in cells transfected with siAllStar or siCTBP1-Pool showing G2/M arrest in siCTBP1-Pool transfected MDA-MB-231 cells **(C)** and G1 arrest in siCTBP1-Pool transfected MCF-7 cells **(D)**. **(E)** Western Blot analysis showing the levels of cell cycle proteins related to G2/M (p-Cdc25C and p-Cdc2) and G1/S (pRb, Cyclin D1, CDK4, CDK2 and p21) transition in p53-*mut* MDA-MB-231 and p53-*wt* MCF7 cells after 48 hours transfection with siAllStar or siCTBP1-Pool. Actin was used as a loading control.

Next, in order to validate our findings *in vivo* setting, we generated two independent CRISPR-Cas9 mediated CTBP1 knock-outs in MDA-MB-231 cells (referred to herein as 231.sgCTBP1_1 and 231.sgCTBP1_2). Both cell lines showed efficient downregulation of CTBP1 (Figure 4.18A) and exhibited delayed and significantly decreased tumor growth (Figure 4.18B) as compared to 231.sgCtrl cells in nude mice. Correspondingly, tumors developed from these CTBP1 knockout cells were substantially smaller in size and weighed less as well (Figure 4.18C and D). In addition to CTBP1 knock-out cells, we also engineered MDA-MB-231 cell line to express an shRNA targeting CTBP1 (referred to herein as 231.shCTBP1). We observed a significant downregulation in CTBP1 at protein level in these cells (Figure 4.18E). Similar to CTBP1 knock-outs, 231.shCTBP1 cells also exhibited delayed and significantly decreased tumor growth (Figure 4.1F), and collected tumors were substantially smaller in size and weighed less as compared to 231.shCtrl cells (Figure 4.18G and H). These data confirmed that tumor-suppressive effects of miR-644a mainly work *via* targeting CTBP1.

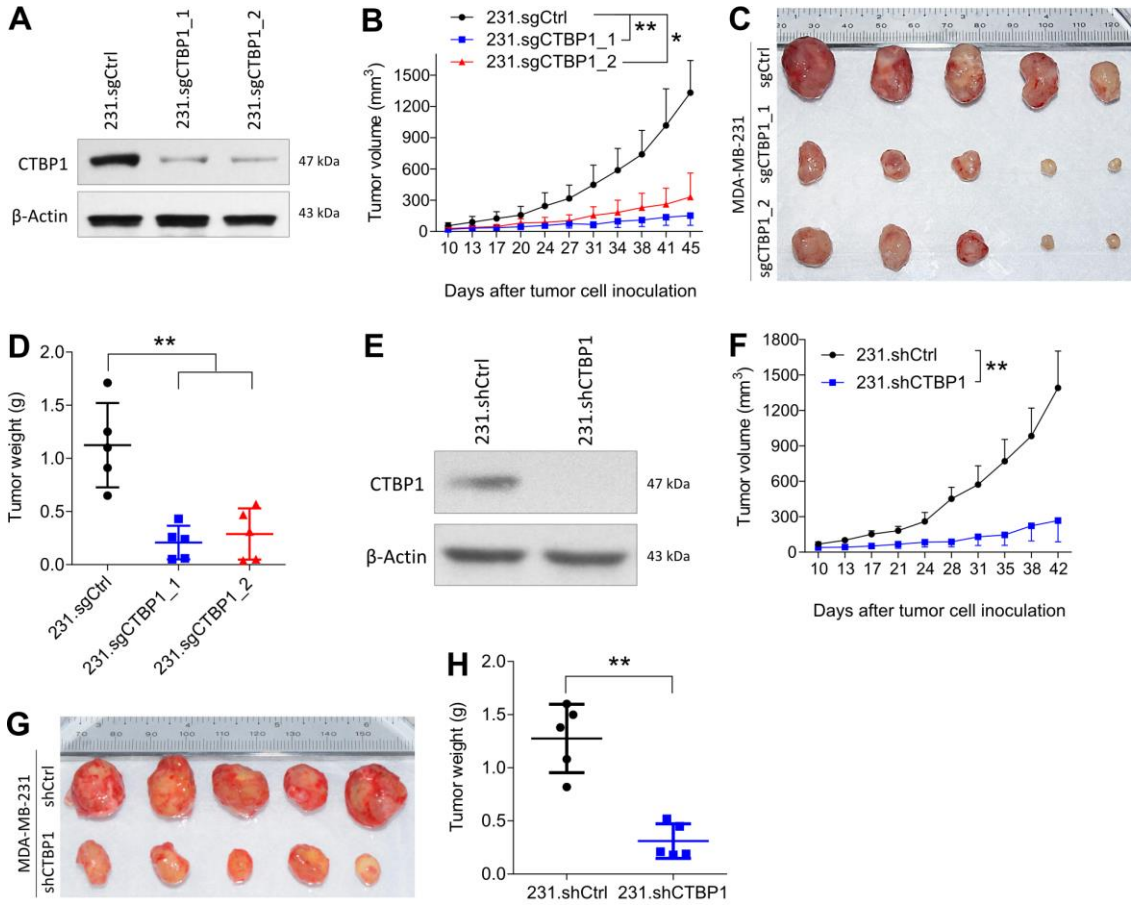

Figure 4.18. Loss of CTBP1 inhibits breast cancer tumor progression *in vivo*. (A) Western Blot analysis of CTBP1 levels in MDA-MB-231.luc cells stably expressing either a non-targeting sgRNA (231.sgCtrl) or different CTBP1 targeting sgRNAs (231.sgCTBP1_1, 231.sgCTBP1_2) confirming stable knock-out of CTBP1. Actin was used as a loading control. **(B)** Tumor progression in xenografts generated with orthotopic subcutaneous injection of 231.sgCtrl, 231.sgCTBP1_1 or 231.sgCTBP1_2. *n* = 5. **(C)** Representative images of tumors collected from xenografts of **(B)** on day 45. **(D)** Tumor weights of tumors from **(C)**. **(E)** Western Blot analysis of CTBP1 levels in MDA-MD-231 cells stably expressing either a non-targeting shRNA (231.shCtrl) or a CTBP1 targeting shRNA (231.shCTBP1) confirming stable knockdown of CTBP1. Actin was used as a loading control. **(F)** Tumor progression in xenografts generated with orthotopic injection of 231.shCtrl or 231.shCTBP1 cells. *n* = 5. **(G)** Representative images of tumors collected from xenografts of **(F)** on day 42. **(H)** Tumor weights of tumors from **(G)** at day 42.

4.1.6. Loss of CTBP1 mimics metastasis-suppressive roles of miR-644a *in vitro* and *in vivo*

Next, we tested if the loss of CTBP1 can mimic the effects of miR-644a on metastasis. CTBP1 knockdown significantly inhibited migration and invasion of both MDA-MB-231 and MDA-MB-436 cells (Figure 4.19A-C), Furthermore, CTBP1 knock-outs by sgRNAs or knockdown by shRNA resulted in a significant reduction in anchorage-independent growth (Figure 4.19 D-G).

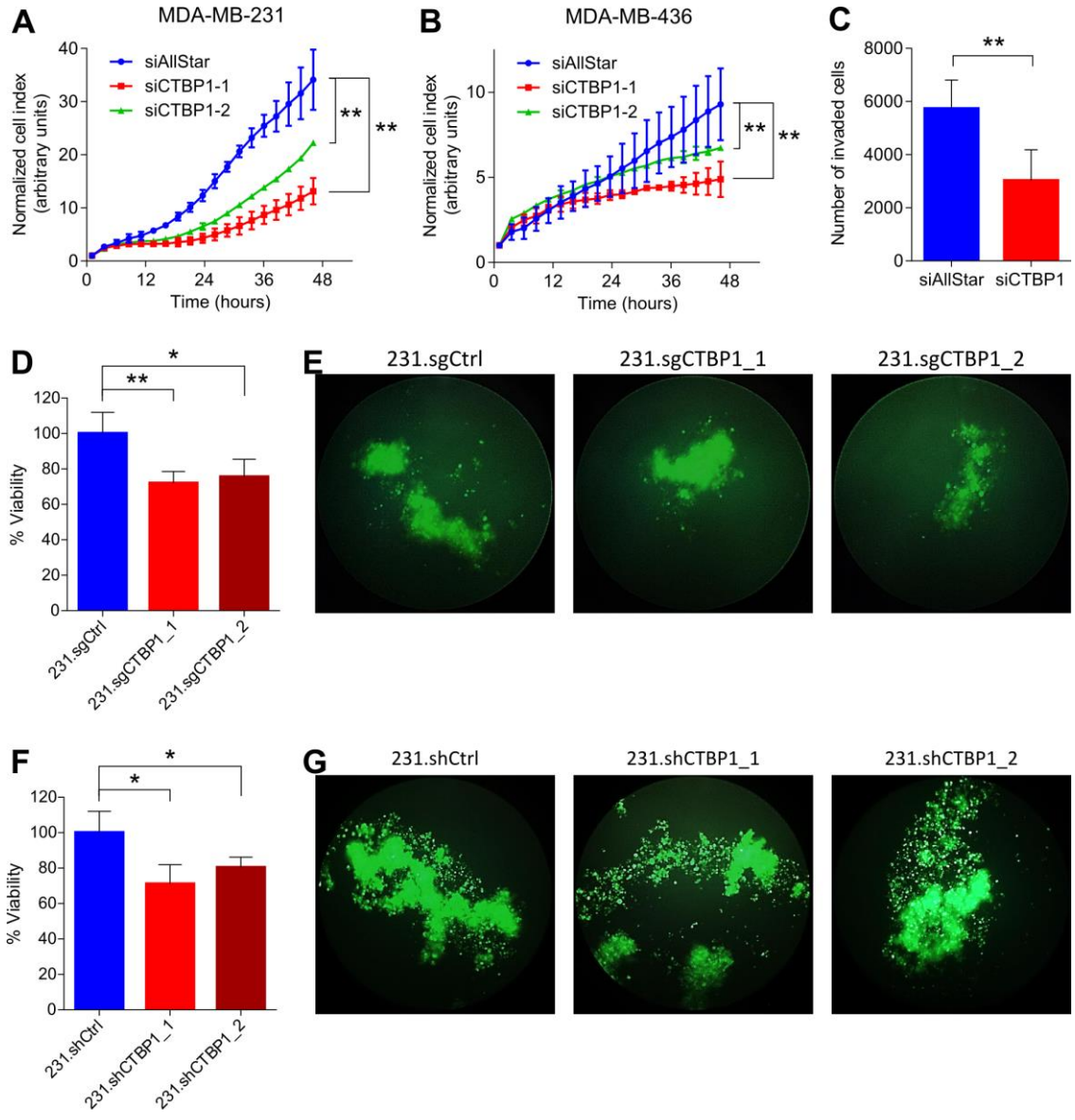

Figure 4.19. Loss of CTBP1 inhibits migration, invasion and anchorage independent growth *in vitro*. (A and B) Real time migration of MDA-MB-231 **(A)** and MDA-MB-436 **(B)**

cells transfected with siAllStar, siCTBP1-1 or siCTBP1-2, monitored using an RTCA assay. *n* = 3. **(C)** Number of invaded cells transfected with siAllStar or siCTBP1-Pool using Matrigel invasion assay. *n* = 3. **(D-G)** Viability of 231.sgCtrl, 231.sgCTBP1_1, 231.sgCTBP1_2 **(D)** 231.shCtrl, 231.shCTBP1_1 and 231.shCTBP1_2 **(F)** cells grown in anchorage-independent conditions for 7 days, together with their fluorescence microscopy images **(E and G)**. *n* = 4.

CTBP1 knockdown also induced an epithelial-like state (Figure 4.20A) as observed by increase in the expression of epithelial markers and downregulation of mesenchymal markers (Figure 4.20B-D) Inversely, CTBP1 overexpression by miR-644a inhibitor transfection promoted mesenchymal-like state (Figure 4.20E).

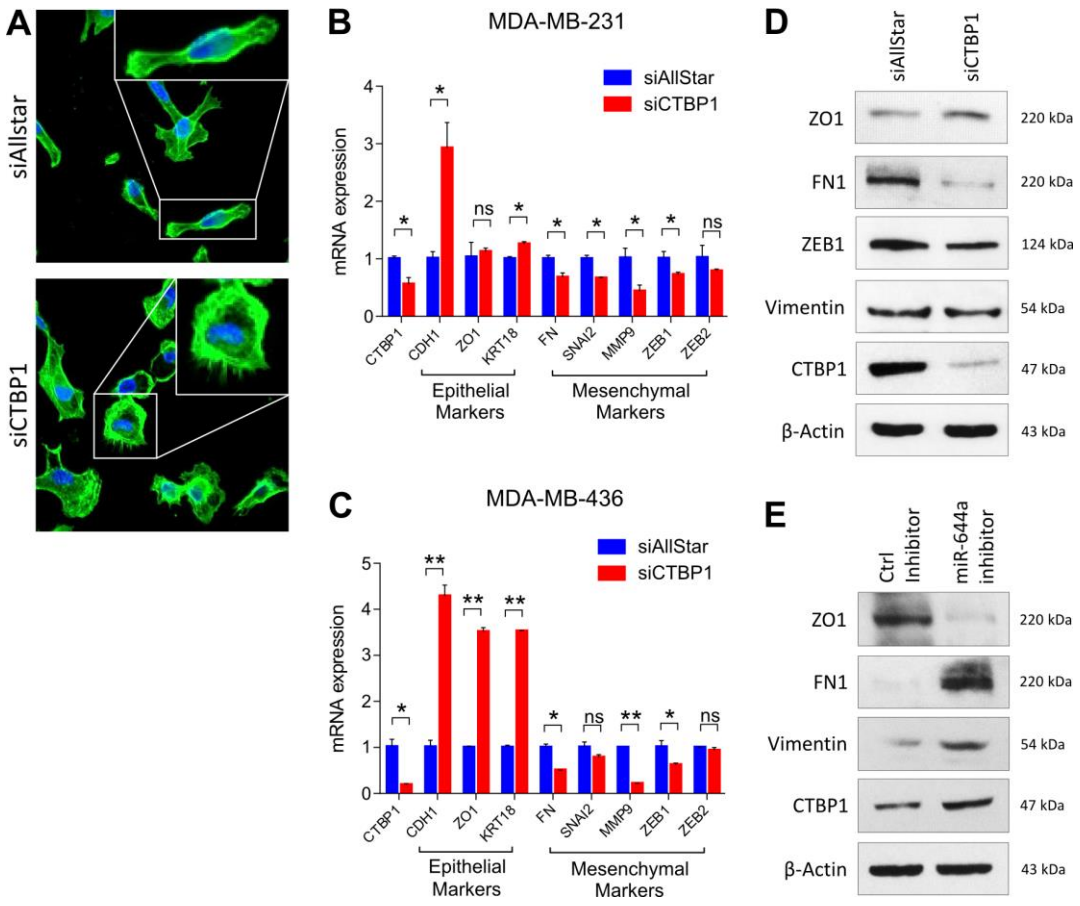

Figure 4.20. Knockdown of CTBP1 inhibits EMT and its upregulation upon miR-644a inhibition promotes EMT *in vitro*. (A) Fluorescence microscopy images of MD-MB-231 cells

transfected with either siAllStar or siCTBP1-Pool. Cell nuclei and filamentous actin were stained with DAPI and Alexa Fluor 488 phalloidin, respectively. Images were taken after 72 hours of transfection with 20X magnification. Insets at the upper right corners of the images show cell morphology with higher resolution. **(B and C)** qRT-PCR analysis of epithelial and mesenchymal marker gene expression in MDA-MB-231 **(B)** and MDA-MB-436 **(C)** cells transfected with either siAllStar or siCTBP1-Pool. **(D and E)** Western Blot analysis of epithelial and mesenchymal marker expression in MDA-MB-231 cells transfected with either siAllStar or siCTBP1-Pool **(D)** and in MCF-12A cells transfected with either Ctrl inhibitor or miR-644a inhibitor **(E)**. Actin was used as a loading control.

We then set to test the effect of CTBP1 in lung metastasis, and observed markedly less colonization of 231.sgCTBP1_1 and 231.sgCTBP1_2 cells to lungs compared to 231.sgCtrl cells (Figure 4.21A-C) suggesting that CTBP1 inhibition mimics miR-644a overexpression in inhibition of breast tumor metastasis.

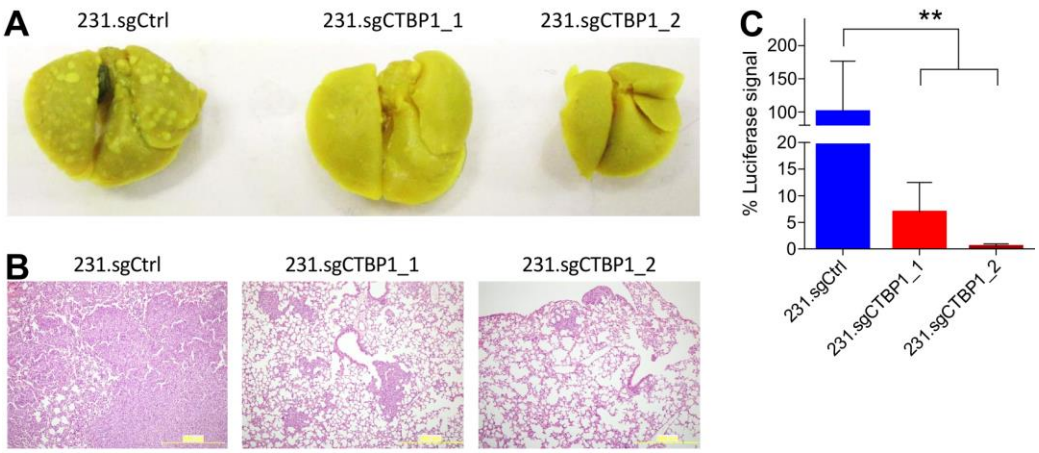

Figure 4.21. Loss of CTBP1 inhibits metastasis *in vivo.* (A) Representative images of lungs collected from nude mice injected intravenously with 231.sgCtrl, 231.sgCTBP1_1 or 231.sgCTBP1_2. Mice were sacrificed at week 7 and lungs were fixed in Bouin's Solution. **(B)** Hematoxylin and eosin (H&E) stainings of metastatic nodules in lungs from **(A)**. **(C)** Luciferase signal coming from metastatic nodules in lungs of **(A)** as quantified by a luciferase assay.

4.1.7. CTBP1 expression correlates with tumor progression and metastatic spread *in silico*

To elucidate the role of CTBP1 in tumor progression and metastasis in breast cancer patients, we analyzed several patient datasets. In GSE4922 and GSE58644 datasets, CTBP1 levels were found to be correlated with higher tumor size and incidence of developing distant metastases (Figure 4.22A and B). In METABRIC data, we observed a significant increase in CTBP1 levels in Stage 4 tumors, characterized by the presence of metastases to organs other than breast (Figure 4.22C). In addition, patients with 20 or more positive lymph nodes had higher CTBP1 in their primary tumors ((Figure 4.22D) suggesting a role of CTBP1 in promoting metastatic spread.

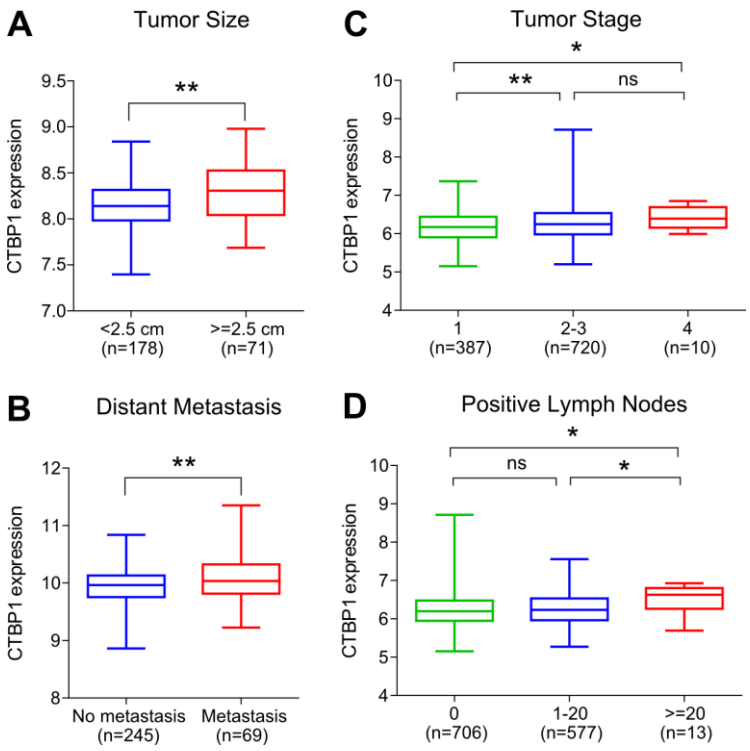

Figure 4.22. CTBP1 expression correlates with tumor progression and metastatic spread *in silico*. (A and B) Changes in CTBP1 expression in breast tumors with tumor size from GSE4922 **(A)** and with presence of distant metastasis **(B)** from GSE58644. **(C and D)** Changes in the CTBP1 expression in breast tumors with tumor stage **(C)** and number of positive lymph nodes **(D)** from METABRIC data.

4.1.8. CTBP1 is a major functional target of miR-644a mediating drug resistance and EMT

We tested if CTBP1 mediates the effect of miR-644a on drug resistance. *In silico* analysis of GSE16446 dataset showed significantly lower levels of CTBP1 in patients with pathological complete response (pCR) compared to patients without complete response against anthracycline treatment (Figure 4.23A). In the same dataset, low CTBP1 level was associated with better DMFS (Figure 4.23B). In GSE58644, among patients treated with chemotherapy, distant metastasis incidence rate was significantly higher in patients with high CTBP1 (Figure 4.23C). All these suggest an important role of CTBP1 in tumor recurrence in chemotherapy-treated patients.

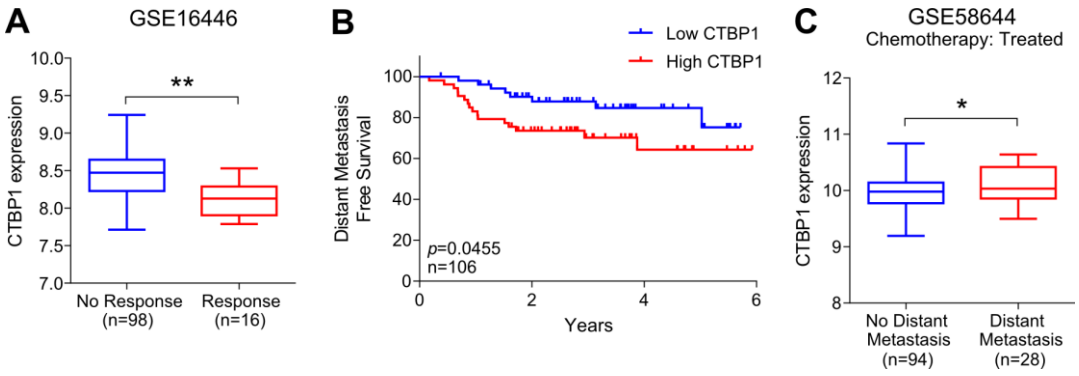

Figure 4.23. CTBP1 expression is associated with poor survival in chemotherapy treated breast cancer patients. (A) CTBP1 expression in anthracycline-treated breast cancer patients from GSE16446 with no response to treatment (n = 98) or pCR (n = 16). **(B)** Kaplan Meier survival curve representing the percentage DMFS in breast cancer patients treated with anthracyclines based on CTBP1 median expression levels in GSE16446 dataset (n = 106). **(C)** CTBP1 expression in patients with no distant metastasis (n = 94) or with distant metastasis (n = 28) among breast cancer patients treated with chemotherapy from GSE58644.

We then tested if we can mimic the effect of miR-644a overexpression on chemotherapy response by knocking down CTBP1. We observed that knockdown of CTBP1 sensitized MDA-MB-231 cells to doxorubicin (Figure 4.24).

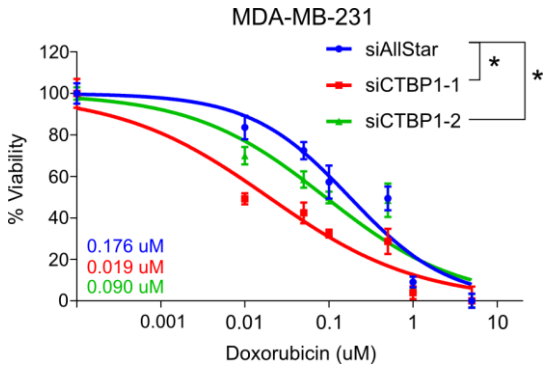

Figure 4.24. CTBP1 knockdown sensitizes MDA-MB-231 cells to doxorubicin. Cells were transfected with siAllStar, siCTBP1-1 or siCTBP1-2 and treated with increasing concentrations of doxorubicin. *n* = 4. Then, cell viability assay was performed.

Rescuing CTBP1 levels along with miR-644a overexpression (Figure 4.25A) not only increased the viability of MDA-MB-231 cells (Figure 4.25B), but also rendered these cells less sensitive to doxorubicin treatment (Figure 4.25C). Furthermore, we observed a significantly lower levels of CTBP1 in doxorubicin sensitive xenografts compared to resistant ones (Figure 4.25D) which is exactly the opposite of miR-644a levels in these tumors (Figure 4.11C).

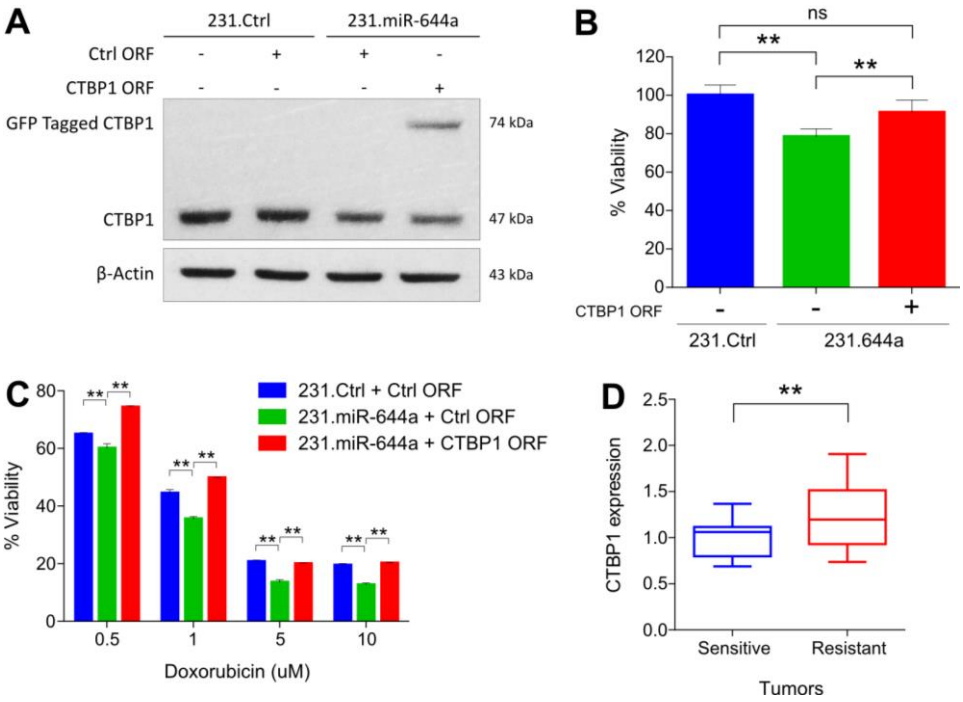

Figure 4.25. CTBP1 rescue overcomes miR-644a associated chemosensitive phenotype. (A and B) 231.Ctrl or 231.miR-644a cells were transfected with Ctrl open reading frame (ORF) or CTBP1 ORF in mentioned combination to rescue the CTBP1 expression. Western Blot analysis showing rescue of CTBP1 expression in MDA-MB-231 **(A)**. Actin was used as a loading control. Effect of CTBP1 rescue on viability of MDA-MB-231 cells **(B)**. **(C)** The effect of CTBP1 rescue as shown in **(C)** on the response of MDA-MB-231 to 4 different doses of doxorubicin. $n = 4$. **(D)** qRT-PCR analysis of CTBP1 expression in xenografts sensitive or resistant to doxorubicin that were previously used to test the changes in miR-644a levels upon drug resistance (Figure 4.11C). $n = 3$.

Finally, we tested if CTBP1 is the functional target of miR-644a regulating EMT. To this point, we rescued CTBP1 *via* miR-644a inhibitor transfection and observed mesenchymal-like state assessed by increase in expression of mesenchymal markers and decrease in expression of epithelial markers; and this phenotype was reversed upon CTBP1 knockdown (Figure 4.26). Overall, all these data confirm that CTBP1 is a major functional target of miR-644a mediating drug resistance and EMT in breast cancer.

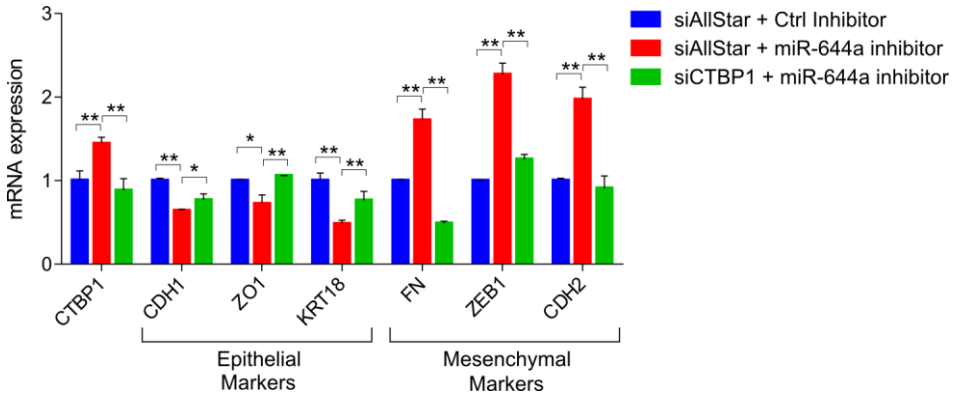

Figure 4.26. Loss of CTBP1 reverses miR-644a inhibition associated mesenchymal phenotype to epithelial like state. qRT-PCR analysis of epithelial and mesenchymal marker gene expression in MCF-12A cells upon CTBP1 rescue by miR-644a inhibitor and further knockdown by siCTBP1.

4.1.9. miR-644a/CTBP1-mediated wild type or mutant p53 upregulation acts as a switch deciding on G1 arrest or apoptosis

The *in vitro* findings that overexpression of miR-644a or loss of its target CTBP1 induces apoptosis in p53-*mut*, but not in p53-*wt* cells triggered us to investigate the relationship between miR-644a, CTBP1, and p53 mutation status. From GSE22220 dataset, we separated the patients having higher levels of miR-644a as p53-*wt* and p53-*mut* according to their expression levels of a gene signature associated with p53 status [128] (for details, see Methods section). We observed that apoptosis-related genes were significantly enriched in p53-*mut* patients compared to p53-*wt* patients (Figure 4.27A and B).

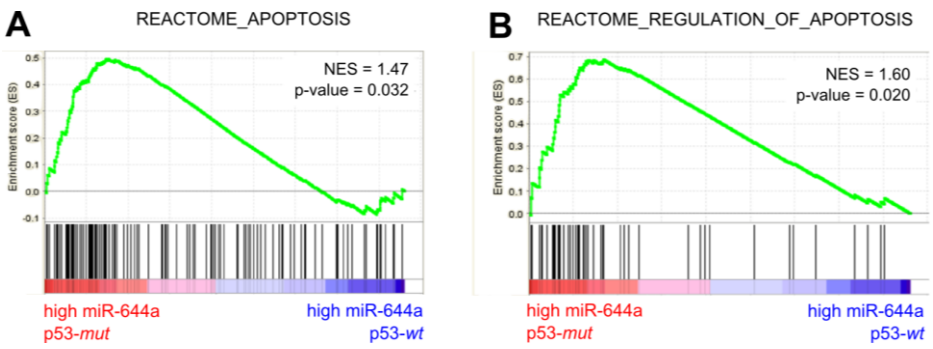

Figure 4.27. Apoptosis associated genes are enriched in p53-*mut* tumors as compared to p53-*wt* ones. (A and B) Enrichment plots of patients from GSE22220 having high miR-644a levels (n = 105). Genes annotated to Apoptosis **(A)** and Regulation of Apoptosis **(B)** pathways in Reactome were significantly enriched in p53-*mut* group as compared to p53-*wt* group.

While investigating the underlying mechanisms, we found that miR-644a overexpression or CTBP1 knockdown increased the expression of p53 level in both p53-*mut* MDA-MB-231 and p53-*wt* MCF-7 cells (Figure 4.28A and B). Furthermore, in 231.miR-644a cells, p53 level was reduced upon CTBP1 ORF expression, which shows miR-644a mediated upregulation of p53 is *via* CTBP1 downregulation (Figure 4.28C). Notably,

overexpression of miR-644a or knockdown of CTBP1 in MCF-7 cells did not change p53 mRNA levels (Figure 4.28D and E), which indicates a possible post-transcriptional regulation of p53 expression. Overall, these results show that miR-644a mimic induces p53 expression/activity in a p53 status-independent manner.

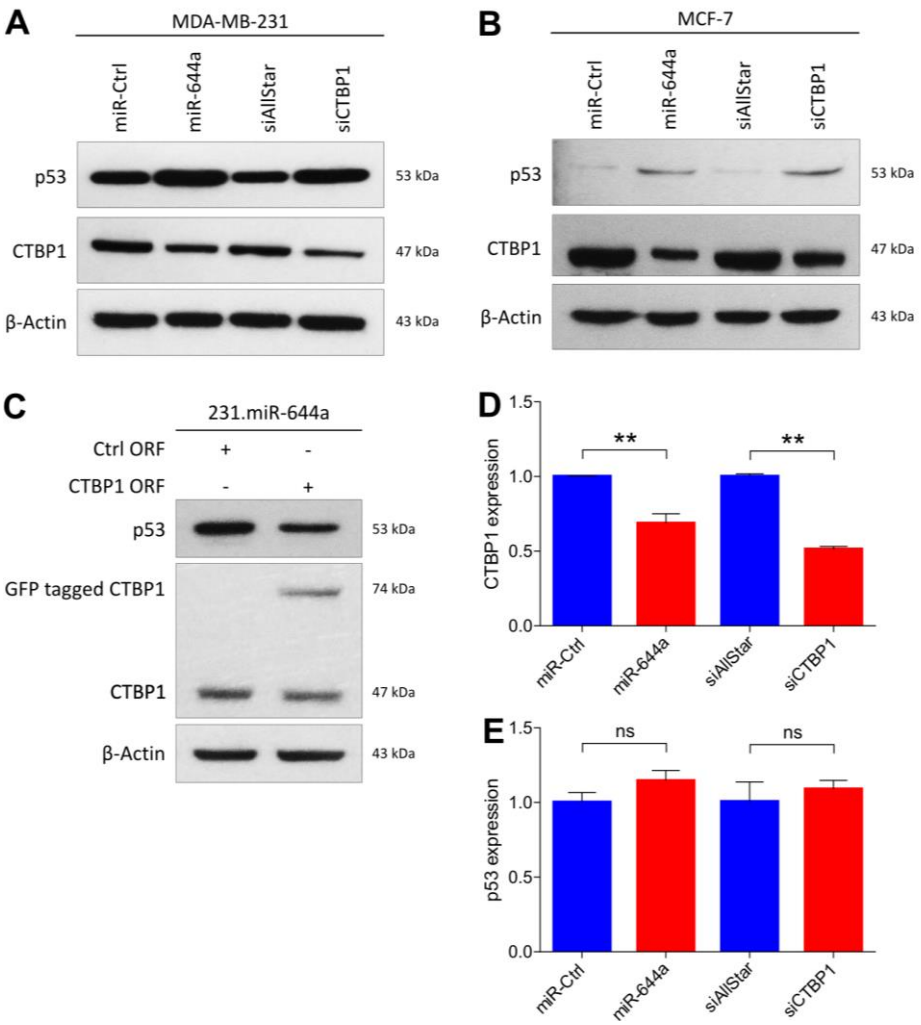

Figure 4.28. miR-644a regulates p53 at post-transcriptional level independent of its mutation status. (A and B) Western Blot analysis showing the regulation of p53 in MDA-MB-231 **(A)** and MCF-7 cells **(B)** upon miR-644a overexpression or CTBP1 knockdown. Actin was used as a loading control. **(C)** Western Blot analysis of p53 and CTBP1 levels in 231.miR-644a cells transfected with either Ctrl ORF or CTBP1 ORF showing downregulation of p53 with rescue of CTBP1 expression. Actin was used as a loading control. **(D and E)** qRT-PCR analysis of CTBP1 **(D)** and p53 **(E)** expression in MCF-7 cells upon miR-644a overexpression or CTBP1 knockdown with siCTBP1-Pool.

Stabilized p53 has been shown to activate several genes that induce cell cycle arrest (e.g. p21) and apoptosis (e.g. Noxa, Bax and Puma) [140]. Furthermore, CTBP1 knock-out cells were shown to express high levels of pro-apoptotic genes Noxa and Bax [141]. Therefore, we examined the expression of these genes upon miR-644a overexpression. While the expression of p21 was only upregulated in p53-*wt* MCF-7 cells, Noxa (neither Bax nor Puma) was significantly upregulated in p53-*mut* MDA-MB-231 cells upon miR-644a mimic transfection (Figure 4.29A-F). Analysis of commonly upregulated genes by *wt*-p53 in breast cancer patients from Troester *et al* [128] and by loss of CTBP1 in MCF-7 cells from Di et *al* [142] also identified only p21 and BTG2 which further supported that miR-644a mimic mediated upregulation of *wt*-p53 and p21 is *via* CTBP1 downregulation.

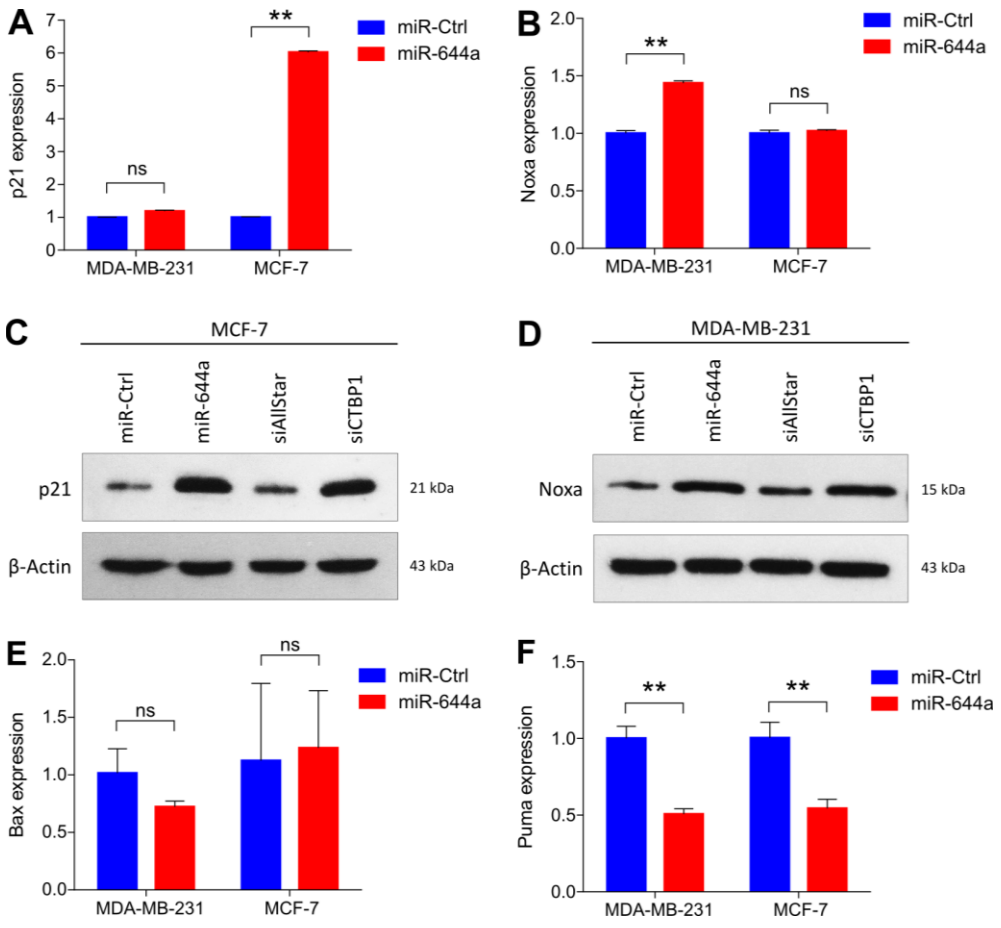

Figure 4.29. miR-644a/CTBP1 mediated wild type or mutant p53 regulates p21 or Noxa, respectively at downstream. (A-D) qRT-PCR **(A and B)** and Western Blot **(C and D)** analysis of p21 and Noxa gene expression in MDA-MB-231 and MCF-7 cells upon miR-644a overexpression or CTBP1 knockdown. Actin was used as a loading control. **(E and F)** qRT-PCR analysis of Bax **(E)** and Puma **(F)** expression in MDA-MB-231 and MCF-7 cells transfected with miR-Ctrl or miR-644a mimic.

We then asked whether we can induce apoptosis upon miR-644a mimic expression or CTBP1 knockdown in p53-*wt* MCF-7 cells if *mut*-p53 was co-expressed. After confirming successful overexpression of *mut*-p53 with western blot (Figure 4.30A and D), we performed an apoptosis assay followed by qRT-PCR of Noxa. Overexpression of *mut*-p53 alone in p53-*wt* MCF-7 cells induced a certain level of apoptosis and Noxa expression, which is further enhanced either by overexpression of miR-644a or by knockdown of CTBP1 (Figure 4.30B, C, E and F). This confirms that miR-644a mediates apoptosis in the presence of *mut*-p53 mainly by the pro-apoptotic gene Noxa.

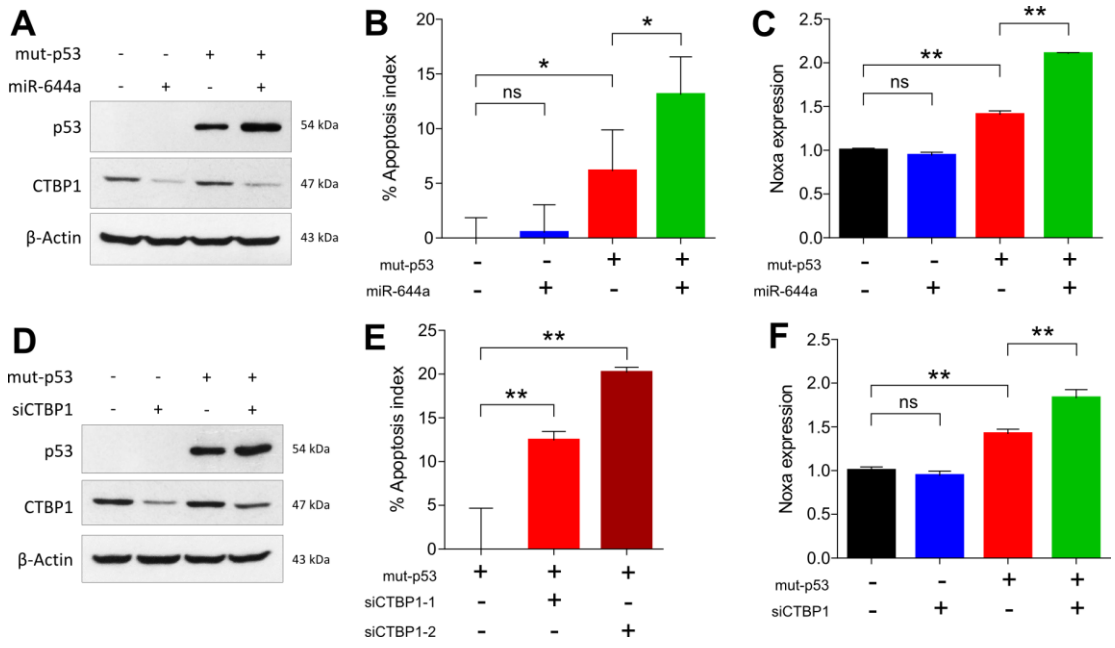

Figure 4.30. miR-644a overexpression or CTBP1 knockdown promotes apoptosis in p53-*wt* cells in the presence of mutant p53. **(A-F)** Changes in the apoptotic index based on Caspase-3/7 cleavage in p53-*wt* MCF-7 cells transfected with miR-644a mimic **(B)** or siCTBP1-1, siCTBP1-2 **(E)** together with *mut*-p53 ORF. Regulation of Noxa expression upon miR-644a overexpression **(C)** or CTBP1 knockdown **(F)** in the presence of *mut*-p53 was shown with qRT-PCR analysis. Overexpression of *mut*-p53 in p53-*wt* MCF-7 cells was confirmed with Western Blot analysis **(A and D).** Actin was used as a loading control. $n = 4$ for **(B)** and **(E)**.

Furthermore, presence of *mut*-p53 did not affect downregulation of CTBP1 (Figure 4.30A and D and Figure 4.31A and C) suggesting that there is no feedback regulation of CTBP1 by p53 in the miR-644a/CTBP1/p53 axis.

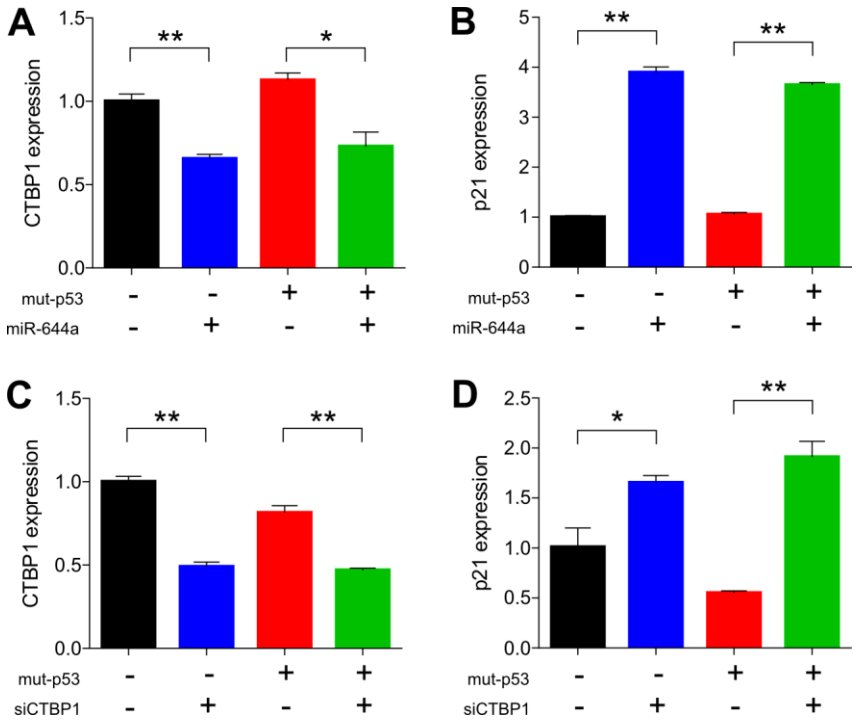

Figure 4.31. Ectopic p53 expression does not affect CTBP1. (A-D) qRT-PCR analysis of CTBP1 **(A and C)** and p21 **(B and D)** expression in p53-*wt* MCF-7 cells either upon miR-644a overexpression or after knockdown of CTBP1 in the absence or presence of *mut*-p53.

Lastly, to validate that p53 serves as a switch in miR-644a/CTBP1/p53 axis in breast cancer, we checked the downstream effects of miR-644a in 6 different breast cancer cell lines (three p53-*wt* and three p53-*mut*) after forced miR-644a expression using mimics. We demonstrated that depending on the p53 status, miR-644a/CTBP1/p53 axis leads to either p21 upregulation (in case of p53-*wt* cells) or Noxa upregulation (in case of p53-*mut* cells) explaining the observed G1 arrest or apoptosis induction, respectively (Figure 4.32).

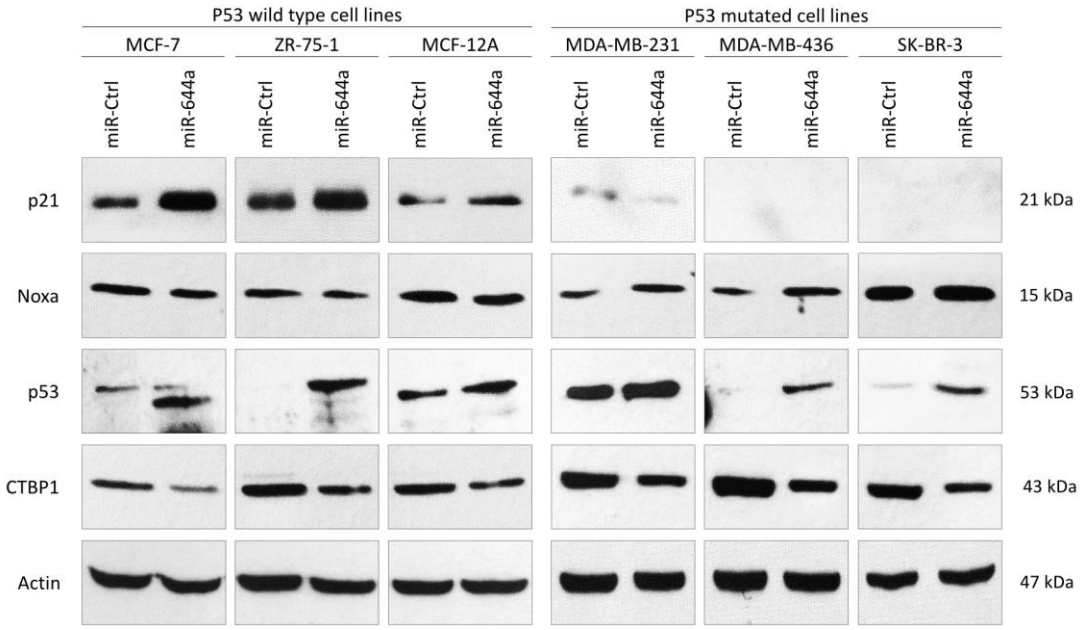

Figure 4.32. Modulation of miR-644a/CTBP1/p53 axis upon miR-644a overexpression in different breast cancer cell lines. Western Blot analysis showing CTBP1, p53, Noxa and p21 expression upon miR-644a mimic transfection in 6 different breast cancer cell lines. Actin was used as a loading control.

4.1.10. p53 mutant patients with high CTBP1 level are predicted to have a worse survival

It has been known that p53-*wt* patients have better survival as compared to p53-*mut* ones [117, 143, 144]. We confirmed this by analyzing published patient data and showed that

p53-*mut* patients survive less than p53-*wt* patients (Figure 4.33). Unlike the prognostic relevance of miR-644a-GS, no correlation of CTBP1 mRNA levels with the survival of breast cancer patients from GSE58644 and GSE19536 datasets was found (Figure 4.34).

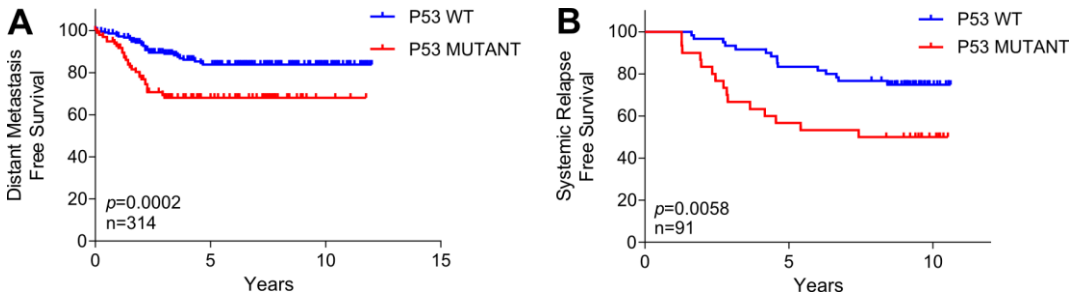

Figure 4.33. Mutant p53 is associated with poor survival in breast cancer patients as compared to wt p53. (A and B) Kaplan Meier survival curves of breast cancer patients based on p53 status in datasets GSE58644 representing percentage DMFS **(A)** and in GSE19536 representing percentage systemic relapse-free survival (RFS) **(B)**.

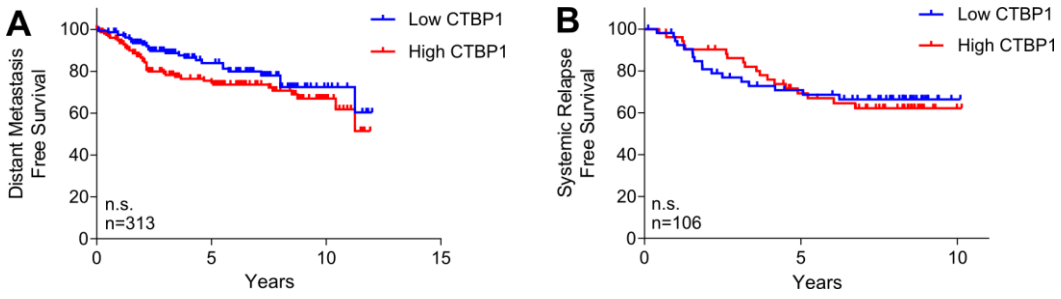

Figure 4.34. CTBP1 expression is not associated survival in breast cancer patients. (A and B) Kaplan Meier survival curves of breast cancer patients based on CTBP1 status in datasets GSE58644 representing percentage DMFS **(A)** and in GSE19536 representing percentage systemic RFS **(B)**.

Therefore, we asked if the expression level of CTBP1 can be associated with the survival of p53-*mut* patients in these datasets. This was indeed the case for both datasets as well as an online survival analysis tool, Kaplan-Meier (KM) Plotter [145] (Figure 4.35A-C).

However, in p53-*wt* patients CTBP1 expression level did not have any significant effect on survival of the patients (Figure 4.35D-F).

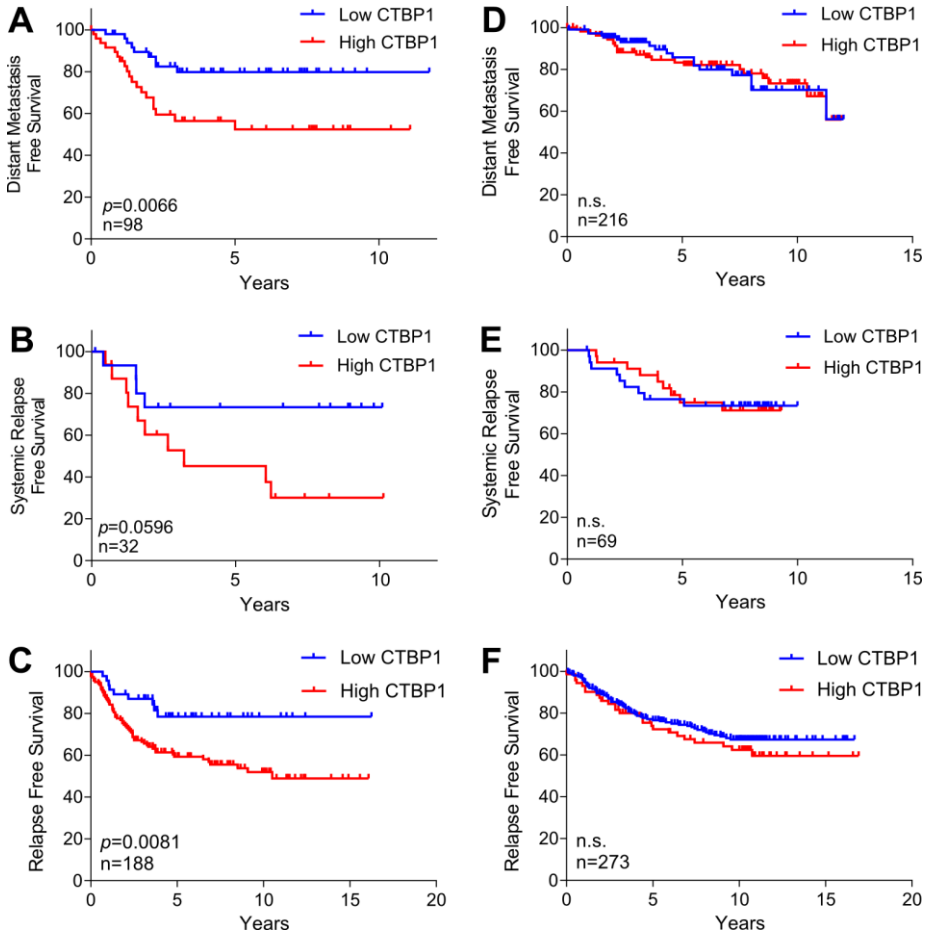

Figure 4.35. CTBP1 expression is associated with poor survival in p53-*mut* but not in p53-*wt* breast cancer patients. (A and B) Kaplan Meier survival curves of breast cancer patients with p53 mutation based on CTBP1 median expression levels in datasets GSE58644 (n = 98) representing percentage DMFS **(A)** and in GSE19536 (n = 32) representing percentage systemic RFS **(B). (C)** Kaplan Meier survival curve of breast cancer patients with p53 mutation based on 'best cut-off' for CTBP1 expression levels in KM Plotter (n = 188) representing percentage RFS. **(D and E)** Kaplan Meier survival curves of p53-*wt* breast cancer patients based on CTBP1 median expression from datasets in GSE58644 **(D)** and in GSE19536 **(E)**. **(F)** Kaplan Meier survival curve of p53-*wt* breast cancer patients based on best cut-off for CTBP1 expression levels in KM Plotter (n = 273) representing percentage RFS.

We observed a similar pattern in ovarian cancer as well, where p53-*mut* patients with high CTBP1 levels are less likely to survive compared to patients with low CTBP1 (Figure 4.36). Overall, these data suggest that CTBP1 expression may be associated with survival of p53-*mut* breast and ovarian cancer patients.

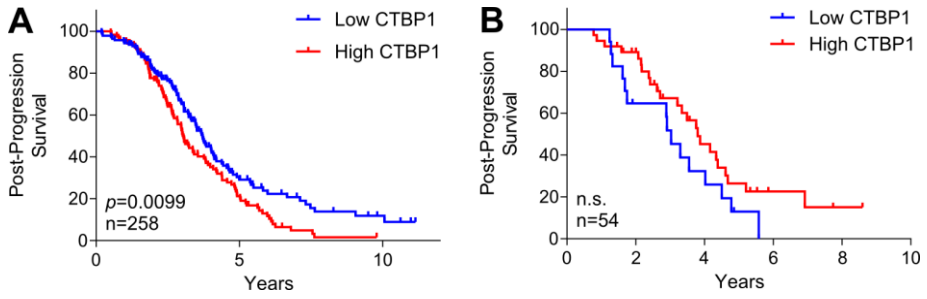

Figure 4.36. CTBP1 expression is associated with poor post-progression survival in p53-*mut* but not in p53-*wt* ovarian cancer patients. (A) Kaplan Meier survival curve of ovarian cancer patients with p53 mutation based on 'best cut-off' for CTBP1 expression levels in KM Plotter (*n* = 258) representing percentage post-progression survival. **(B)** Kaplan Meier survival curve of p53-*wt* ovarian cancer patients based on best cut-off for CTBP1 expression levels in KM Plotter (*n* = 54) representing percentage post-progression survival.

PART II.

Targeting hypoxia-induced lysyl oxidase overcomes chemotherapy resistance in triple negative breast cancer

4.2.1. Whole transcriptome sequencing combined with pathway analyses identifies integrin signaling as a key mediator of chemoresistance in TNBCs

To elucidate the underlying mechanisms of chemotherapy resistance in TNBCs and to identify novel drug targets overcoming resistance, we developed doxorubicin resistant TNBC tumors in nude mice using MDA-MB-231 TNBC cell line. We treated tumor-bearing mice with doxorubicin over a period of 3-4 months. Initially, tumors showed sensitivity to the treatment and gradually decreased in size. Some of these tumors were collected as "doxorubicin sensitive" samples. Over time, tumors started resisting doxorubicin in some mice and showed increase in size; these tumors were collected as "doxorubicin resistant" samples. We performed RNA sequencing to obtain the differentially expressed transcripts between doxorubicin sensitive and resistant tumors (Figure 4.37; for details, see Methods section). Ingenuity Pathway Analysis (IPA) of differentially expressed mRNAs showed integrin-linked kinase (ILK) signaling as the top deregulated pathway (Figure 4.38).

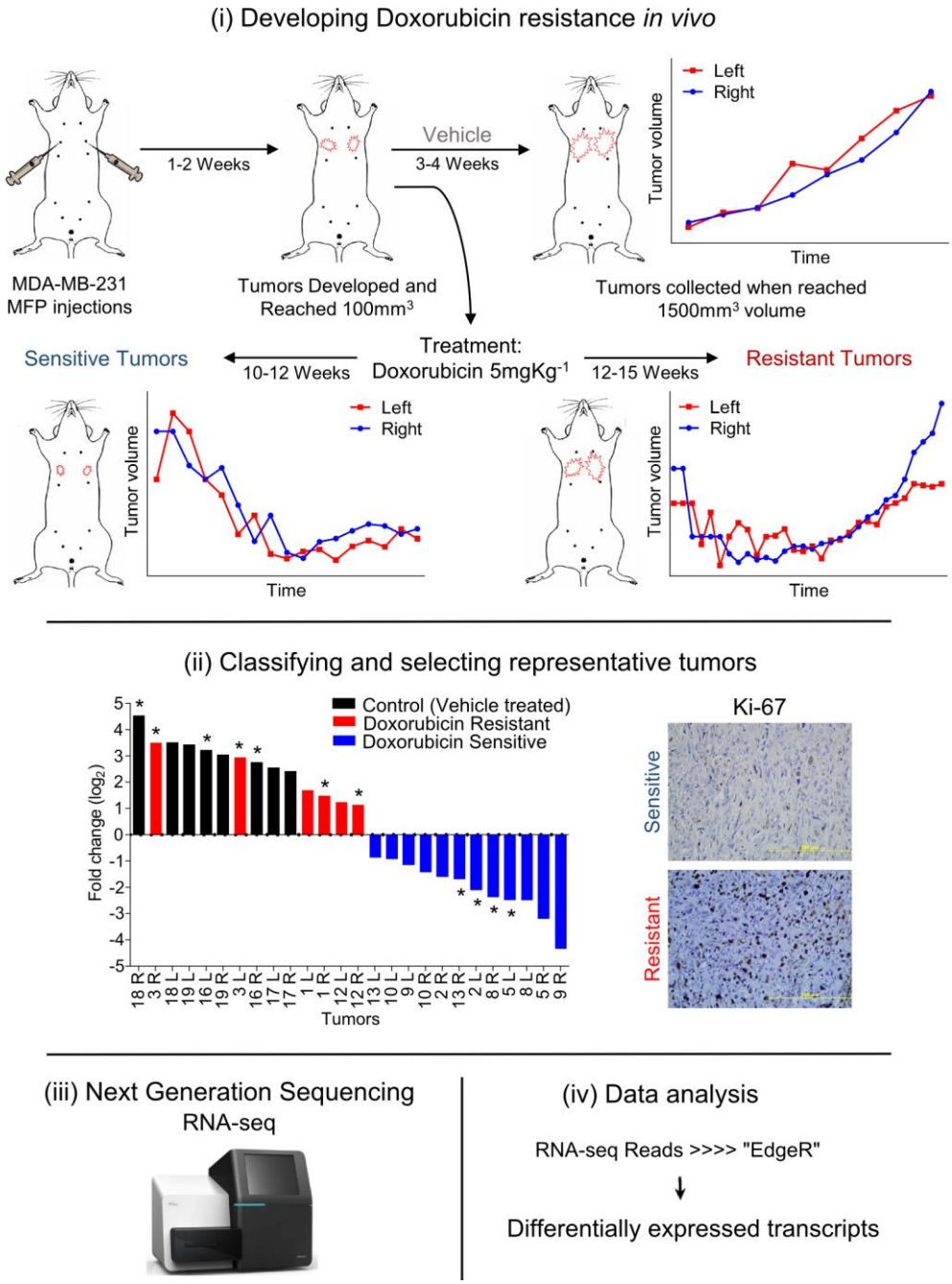

Figure 4.37. Schematic representation of developing doxorubicin resistance in mice using MDA-MB-231 TNBC cells. (i), classification of tumors (ii), RNA sequencing of selected tumors (iii), and data analysis platforms to identify differentially expressed genes between tumor groups (iv). Waterfall plot in (ii) shows Log2 fold change in tumor volume of control and doxorubicin-treated mice. Latter was divided into doxorubicin sensitive and resistant groups depending on the net change in tumor volume over the course of treatment. * indicates the tumors profiled by RNA sequencing. Ki-67 staining shows the difference in proliferative potential between doxorubicin sensitive and resistant tumors.

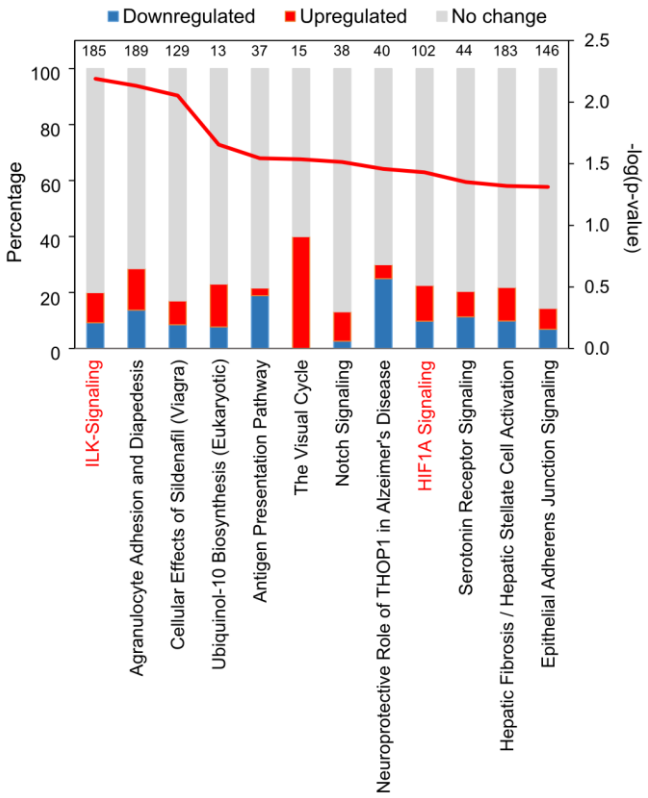

Figure 4.38. Summary of IPA-based mRNA core analysis showing top deregulated pathways in doxorubicin resistance. Numbers at the top are the number of genes associated with each pathway at IPA platform.

Next, we derived a DoxoR-GS comprising of top 441 differentially expressed mRNAs (-0.80>Log2FC>0.80 and p-value of <0.05) between sensitive and resistant xenografts and analyzed GEO patient datasets after calculating DoxoR-GS scores (for details, see Methods section). Using GSEA, we found that genes associated with integrin signaling and focal adhesion were significantly enriched in chemotherapy-treated TNBCs that have high DoxoR-GS scores (Figure 4.39A). The patients with high DoxoR-GS scores showed poor overall survival (OS) and metastasis-free survival (MFS) as compared to their counterparts having low DoxoR-GS score (Figure 4.39B and C) validating our *in vivo* chemoresistant TNBC model. Furthermore, we observed an enrichment of focal adhesion-associated gene signature in TNBC patients after chemotherapy treatment

(Figure 4.39D) supporting the involvement of integrin signaling in chemotherapy response in TNBC.

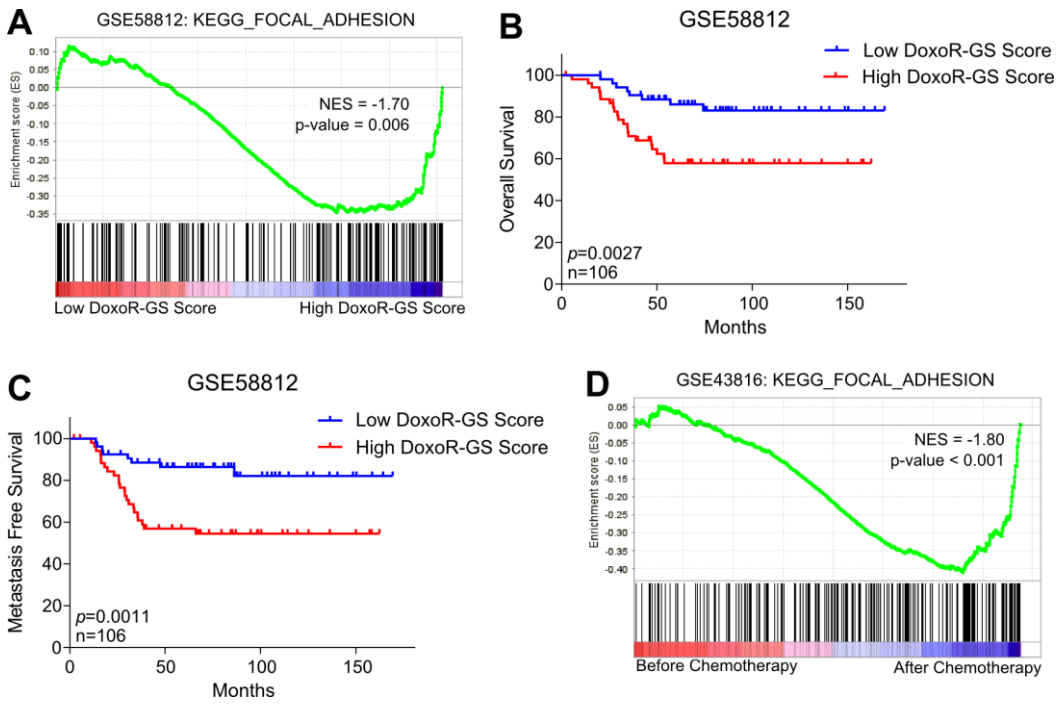

Figure 4.39. DoxoR-GS having enriched integrin/focal adhesion signaling predicts worst survival in chemotherapy-treated TNBC. (A) Enrichment plot of chemotherapy-treated TNBC tumors from GSE58812 (*n* = 106) with low or high DoxoR-GS scores. Genes associated with focal adhesion signaling are enriched in tumors with high DoxoR-GS scores. **(B and C)** Kaplan-Meier survival curve representing the percentage OS **(B)** and MFS **(C)** in chemotherapy-treated TNBC patients from GSE58812 (*n* = 106) based on low vs high DoxoR-GS scores. **(D)** Enrichment plot of TNBC patients from GSE43816 showing that genes associated with focal adhesion signaling get enriched after chemotherapy treatment.

Human genome has 24 different integrins (18 alpha and 8 beta subunits), which heterodimerize to produce cell surface receptors, involved in cellular adhesion to ECM, cell-cell communication, and signal transduction [146]. We examined the mRNA expression of all these integrins in doxorubicin sensitive and resistant tumors, and we

found that three integrins namely ITGA5, ITGA10 and ITGB5 were significantly (cut-off: log2FC=±0.59, p-value<0.05) upregulated in Doxorubicin resistant tumors (Figure 4.40A and Figure 4.41A and B). Next, we asked whether changes in the expression of these integrins have any effects on the outcomes of chemotherapy treatment in TNBC patients, and observed that higher expression of ITGA5, but not that of ITGA10 or ITGB5, is associated with poor RFS only in chemotherapy-treated basal subtype breast cancer patients, but neither in untreated basal subtype nor in other subtypes of breast cancer (Figure 4.40B-D and Figure 4.41C and D).

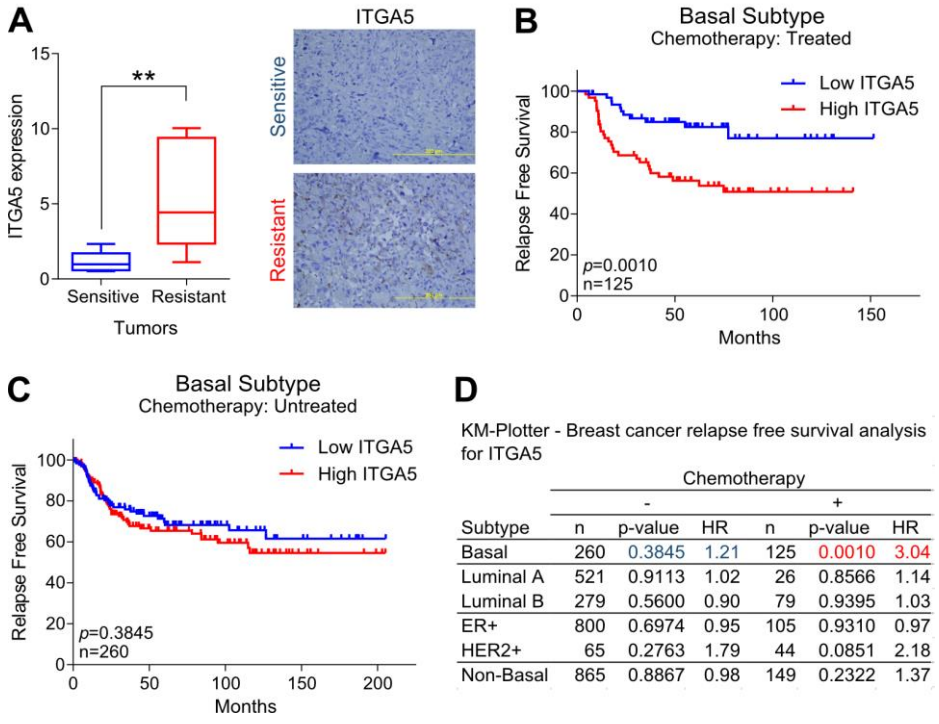

	Chemotherapy					
	-			+		
Subtype	n	p-value	HR	n	p-value	HR
Basal	260	0.3845	1.21	125	0.0010	3.04
Luminal A	521	0.9113	1.02	26	0.8566	1.14
Luminal B	279	0.5600	0.90	79	0.9395	1.03
ER+	800	0.6974	0.95	105	0.9310	0.97
HER2+	65	0.2763	1.79	44	0.0851	2.18
Non-Basal	865	0.8867	0.98	149	0.2322	1.37

Figure 4.40. ITGA5 is upregulated in doxorubicin resistant tumors and is associated with worst RFS specifically in chemotherapy-treated TNBCs. (A) Expression of ITGA5 in doxorubicin sensitive and resistant tumors at mRNA (left), and protein levels (right). *n* = 4. **(B and C)** Kaplan-Meier survival curves representing the percentage RFS in chemotherapy-treated basal patients (n = 125) **(B)** and untreated basal patients (n = 260) **(C)** based on low vs high ITGA5 expression. **(D)** Table summarizing ITGA5 expression-based Kaplan-Meier RFS analysis of patients representing different breast cancer subtypes either treated or not treated with chemotherapy.

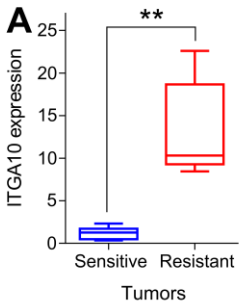

C

KM-Plotter - Breast cancer relapse free survival analysis for ITGA10

	Chemotherapy					
	-			+		
Subtype	n	p-value	HR	n	p-value	HR
Basal	260	0.8333	1.05	125	0.8507	0.94
Luminal A	521	0.3632	0.86	26	0.8210	0.85
Luminal B	279	0.4065	0.86	79	0.0007	0.25
ER+	800	0.2343	0.87	105	0.0055	0.39
HER2+	65	0.6863	1.23	44	0.4144	0.70
Non-Basal	865	0.2756	0.88	149	0.0021	0.44

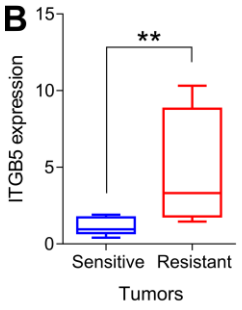

D

KM-Plotter - Breast cancer relapse free survival analysis for ITGB5

	Chemotherapy					
	-			+		
Subtype	n	p-value	HR	n	p-value	HR
Basal	260	0.8009	1.06	125	0.0418	1.86
Luminal A	521	0.1439	1.27	26	0.7803	0.82
Luminal B	279	0.3544	1.19	79	0.0345	2.24
ER+	800	0.0746	1.24	105	0.1232	1.68
HER2+	65	0.2908	1.73	44	0.7235	1.17
Non-Basal	865	0.0354	1.28	149	0.0967	1.56

Figure 4.41. ITGA10 and ITGA5 expression in doxorubicin sensitive and resistant xenografts and association of their expression with survival in different breast cancer subtypes with or without chemotherapy treatment. (A and B) qRT-PCR analysis showing expression of ITGA10 **(A)** and ITGB5 **(B)** in doxorubicin sensitive and resistant tumors. *n* = 4. **(C and D)** Table summarizing ITGA10 **(C)** and ITGB5 **(D)** expression-based Kaplan-Meier R analysis results of patients representing different breast cancer subtypes either treated or not treated with chemotherapy.

As 70% of TNBCs are shown to be basal subtype, and 76% of basal subtype is TNBCs [147], we repeated the survival analysis by classifying the patients as TNBCs based on the expression of ERα, PR and HER2, and observed a stronger RFS separation between high and low ITGA5 expressing, chemotherapy-treated TNBC patients (Figure 4.42A and B). Furthermore, high ITGA5 expression was also associated with poor OS (Figure 4.42C) and MFS (Figure 4.42D) in another independent, chemotherapy-treated TNBC patient dataset. Overall, our data suggest an important role for ITGA5 in modulating chemotherapy response in TNBC patients.

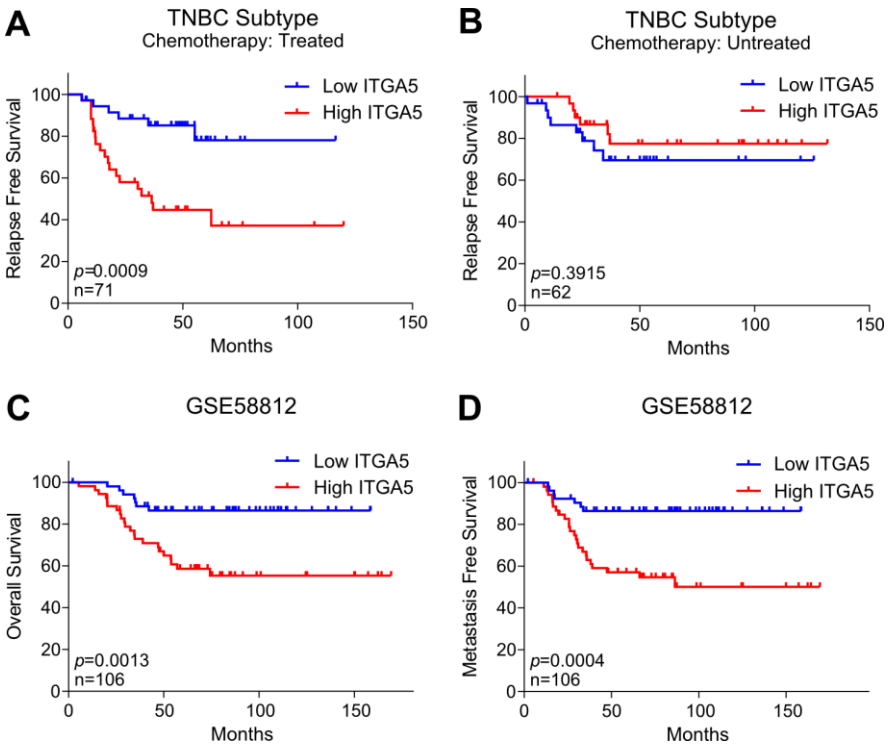

Figure 4.42. ITGA5 expression is associated with worst survival in chemotherapy-treated TNBC patients. (A and B) Kaplan-Meier survival curve representing the percentage RFS in chemotherapy-treated TNBC patients (*n* = 71) **(A)** and untreated TNBC patients (*n* = 62) **(B)** based on low vs. high ITGA5 expression. Data was retrieved from KM-plotter online survival analysis tool. **(C and D)** Kaplan-Meier survival curve representing the percentage OS **(C)** and MFS **(D)** in chemotherapy-treated TNBC patients from GSE58812 (*n* = 106) based on low vs. high ITGA5 expression.

4.2.2. Hypoxia-induced LOX regulates ITGA5 and is associated with poor RFS in chemotherapy-treated TNBC patients

As solid tumors grow in size, inner core often gets deprived of oxygen leading towards hypoxic microenvironment. Tumor cells usually counteract this by adapting to hypoxia *via* upregulating HIFs [148]. Importantly, we observed that HIF1A signaling was among the top deregulated pathways between doxorubicin resistant and sensitive tumors (Figure 4.38). Furthermore, genes upregulated in hypoxic conditions were significantly enriched in chemotherapy-treated TNBC tumors that displayed a high DoxoR-GS scores as

compared to those with low DoxoR-GS scores (Figure 4.43A). The same set of genes was also enriched in TNBC tumors after chemotherapy treatment further supporting the involvement of hypoxia signaling in chemotherapy response of patients (Figure 4.43B). IPA-based "Upstream Regulator" analysis predicted that HIF1A is activated in resistant tumors, with 28 of 39 HIF1A target genes showing an expression direction consistent with the activation of HIF1A (Figure 4.43C and Table 4.4).

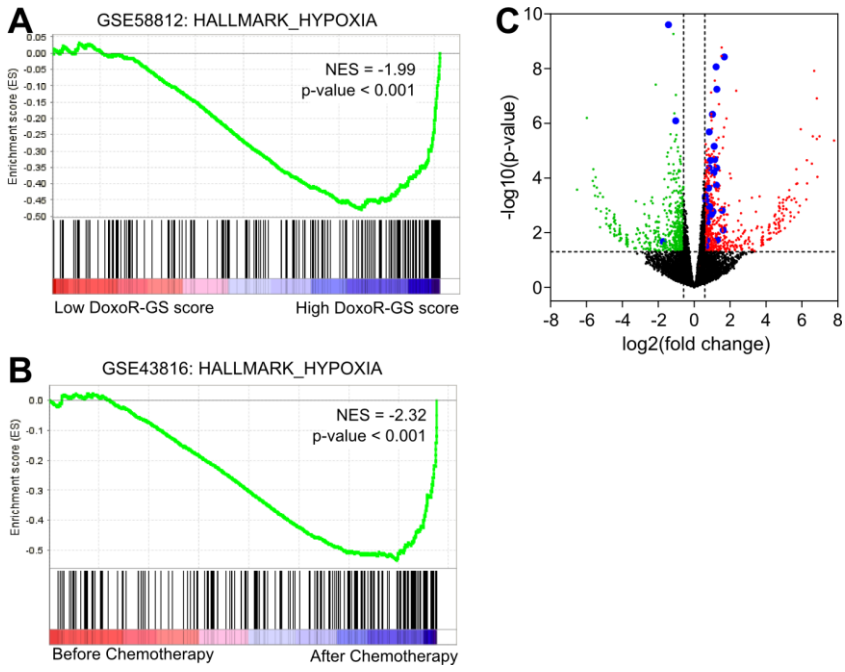

Figure 4.43. Hypoxia signaling is associated with chemotherapy resistance and HIF1A signaling is predicted to be activated in doxorubicin resistant xenografts. (A) Enrichment plot of chemotherapy-treated TNBC patients from GSE58812 (n = 106) with low or high DoxoR-GS scores. Genes upregulated upon low levels of oxygen are enriched in patients with high DoxoR-GS score. **(B)** Enrichment plot of TNBC patients from GSE43816 showing that genes upregulated upon low levels of oxygen get enriched after chemotherapy treatment. **(C)** Volcano plot showing significantly downregulated genes (green), upregulated genes (red) and the genes in IPA-based HIF1A gene signature (blue) in doxorubicin resistant versus sensitive tumors.

Table 4.4. IPA-based Upstream Regulator Analysis using RNA-Seq data of chemoresistant TNBC xenografts. mRNA core analysis was performed at IPA platform using top differentially

expressed mRNA data (-0.59>Log2FC>0.59 and p-value of 0.05) from doxorubicin sensitive and resistant xenografts. Genes and their expression values are shown, based on which, IPA predicted that HIF1A signaling is upregulated in doxorubicin resistant tumors.

Gene ID	Log2 FC	Prediction (based on expression direction)	Literature findings
ADM	1.684	Activated	HIF1A upregulates
ANGPTL4	1.220	Activated	HIF1A upregulates
BHLHE40	0.735	Activated	HIF1A upregulates
BNIP3	0.729	Activated	HIF1A upregulates
BNIP3L	1.117	Activated	HIF1A upregulates
C9orf9	1.285	Activated	HIF1A upregulates
CXorf40B	1.021	Activated	HIF1A upregulates
EGLN3	1.615	Activated	HIF1A upregulates
EREG	1.046	Activated	HIF1A upregulates
ERO1L	0.626	Activated	HIF1A upregulates
FN1	1.091	Activated	HIF1A upregulates
HILPDA	0.966	Activated	HIF1A upregulates
HK2	0.862	Activated	HIF1A upregulates
ITGA5	0.838	Activated	HIF1A upregulates
L1CAM	0.703	Activated	HIF1A upregulates
LOX	0.800	Activated	HIF1A upregulates
MMP1	0.876	Activated	HIF1A upregulates
NDRG1	1.228	Activated	HIF1A upregulates
NEK8	0.707	Activated	HIF1A upregulates
PFKFB3	1.264	Activated	HIF1A upregulates
PFKFB4	0.795	Activated	HIF1A upregulates
PTGS2	1.567	Activated	HIF1A upregulates
SLC2A1	0.905	Activated	HIF1A upregulates
SLC2A3	1.256	Activated	HIF1A upregulates
AKAP12	1.146	Affected	HIF1A regulates
ANKRD37	0.741	Affected	HIF1A regulates
ANKZF1	0.625	Affected	HIF1A regulates
BRCA1	-1.434	Affected	HIF1A regulates
CITED2	0.858	Affected	HIF1A regulates
DNASE1	-1.025	Affected	HIF1A regulates
FAM13A	0.783	Affected	HIF1A regulates
IL17RA	0.646	Affected	HIF1A regulates
MMP9	-1.726	Affected	HIF1A regulates
TAF9B	0.622	Affected	HIF1A regulates
SSBP1	0.660	Inhibited	HIF1A downregulates

Among these genes was LOX, which is transcriptionally regulated by HIF1A, and has been previously shown to regulate integrin signaling whereby promoting metastatic spread of cancer by modulating ECM [149]. After confirming the upregulation of LOX in doxorubicin resistant xenografts both at mRNA and protein levels (Figure 4.44A), we performed GSEA with respect to LOX expression levels (low vs. high) using the expression profiles of chemotherapy-treated TNBCs (from GSE58812). We showed that the genes upregulated upon low levels of oxygen were significantly enriched in patients having high LOX expression (Figure 4.44B and Table 4.5) suggesting a potential key role for LOX in hypoxia in the chemotherapy-treated TNBC patients.

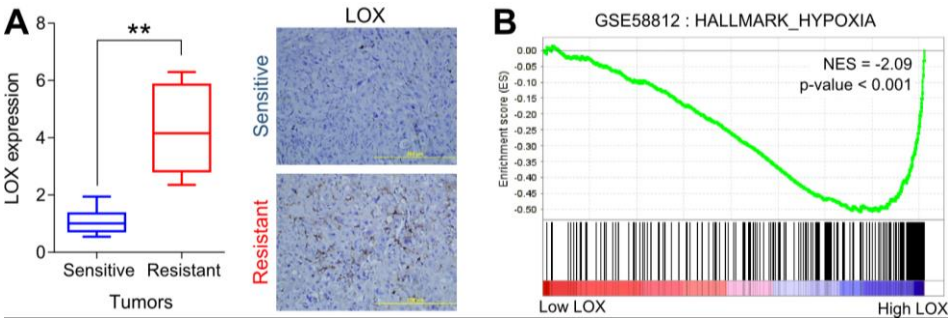

Figure 4.44. LOX, a key regulator in hypoxia, is upregulated in doxorubicin resistant xenografts. (A) Expression of LOX in doxorubicin sensitive and resistant tumors at mRNA (left) and protein levels (right). *n* = 4. **(B)** Enrichment plots of chemotherapy-treated TNBC patients from GSE58812 (n = 106) with low or high LOX expression. Genes upregulated upon low levels of oxygen are enriched in patients with high LOX expression.

Table 4.5. GSEA of GEO datasets having chemotherapy-treated TNBC patients. In GSE43816, expression data was available for before and after chemotherapy treatment. Analysis was done as "Before_Chemotherapy" vs "After_Chemotherapy". Patients in GSE58812 were separated either on the basis of DoxoR-GS score or LOX expression. Analysis was done as "Low_DoxoR-GS_Score" vs. "High_DoxoR-GS_Score" and "Low_LOX" vs. "High_LOX", respectively. A positive NES value shows enrichment of geneset in former group whereas a negative NES value shows enrichment in latter group.

Name of the gene set	GSE43816 Before vs After chemotherapy		GSE58812 Low vs High DoxoR-GS Score		GSE58812 Low vs High LOX expression	
	NES	p-value	NES	p-value	NES	p-value
HARRIS_HYPOXIA	-2.37	< 0.001	-2.06	< 0.001	-2.26	< 0.001
MANALO_HYPOXIA_UP	-2.14	< 0.001	-1.94	< 0.001	-2.27	< 0.001
PID_HIF1_TFPATHWAY	-2.57	< 0.001	-1.74	0.005	-2.04	< 0.001
WINTER_HYPOXIA_METAGENE	-2.47	< 0.001	-2.02	< 0.001	-2.08	< 0.001

*NES: Normalized Enrichment Score

Interestingly, genes associated with integrin signaling/focal adhesions were also enriched in patient tumors expressing high LOX levels (Figure 4.45), indicating a close association between LOX and integrin signaling in chemotherapy-treated TNBC patients.

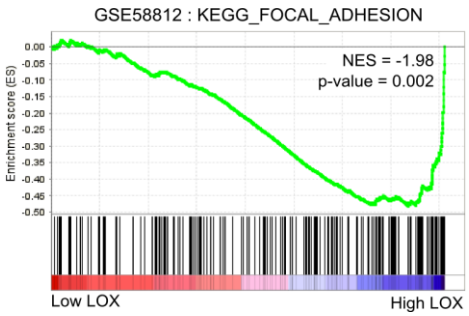

Figure 4.45. LOX is associated with integrin signaling in chemotherapy treated TNBC tumors. Enrichment plot of chemotherapy-treated TNBC patients from GSE58812 (n = 106) with low or high LOX expression**.** Genes associated with focal adhesion signaling are enriched in patients with high LOX expression.

Importantly, mRNA expression correlation analysis from 10 different breast cancer patient datasets also confirmed high correlation of HIF1A with LOX and ITGA5, but not with other integrins (ITGB5 and ITGA10) upregulated in doxorubicin resistant tumors. Strikingly, we observed the highest expression correlation between LOX and ITGA5 (Figure 4.46A). In order to examine possible regulatory relationship between LOX and ITGA5, we knocked down LOX in MDA-MB-231.Luc.GFP (referred to herein as 231.shLOX) at different levels and measured the ITGA5 expression levels in xenografts generated from these cells. We observed a strong positive correlation between LOX and ITGA5 mRNA expression *in vivo* (Figure 4.46B) suggesting a regulatory role for LOX on ITGA5 expression.

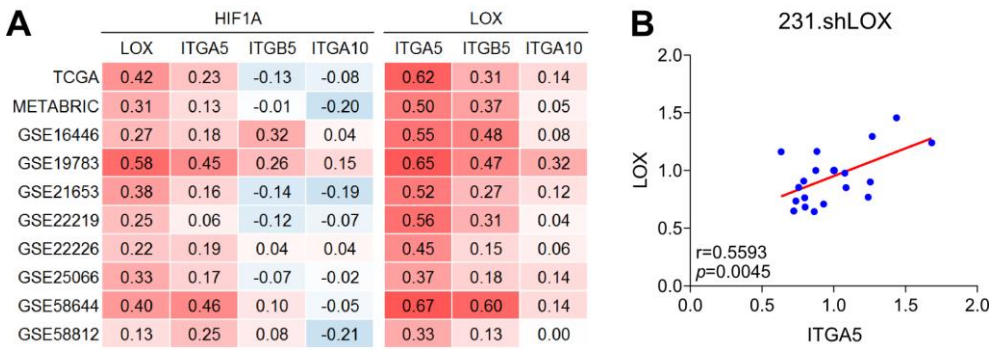

Figure 4.46. HIF1A expression correlates with LOX and ITGA5 expression *in silico* whereas LOX expression is highly correlated with ITGA5 both *in silico* and *in vivo*. (A) Heatmap summarizing the Pearson's correlation coefficient between HIF1A and LOX, between HIF1A and integrins and between LOX and Integrins from different breast cancer patient datasets. **(B)** Dot-plot showing the correlation between LOX and ITGA5 mRNA expression in xenografts developed using 231.Luc.GFP cells engineered to express inducible shLOX.

Notably, similar to ITGA5, higher LOX expression was also associated with poor RFS only in chemotherapy-treated basal breast cancer patients, but not in other subtypes or

untreated cases (Figure 4.47A-C). Altogether, these data demonstrate that hypoxia-induced LOX regulates ITGA5 expression, and that LOX expression associates with the survival of chemotherapy-treated patients.

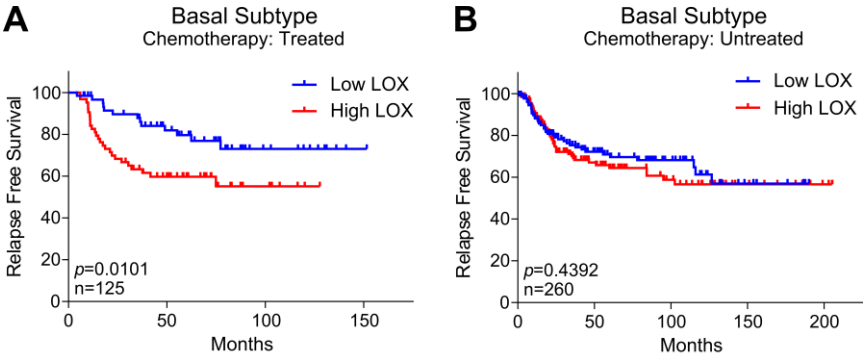

C

KM-Plotter - Breast cancer relapse free survival analysis for LOX

	Chemotherapy					
	-			+		
Subtype	n	p-value	HR	n	p-value	HR
Basal	260	0.4392	1.18	125	0.0101	2.33
Luminal A	521	0.6971	0.94	26	0.7897	0.83
Luminal B	279	0.1737	1.28	79	0.3565	1.41
ER+	800	0.6040	1.07	105	0.3811	1.34
HER2+	65	0.4217	0.66	44	0.7989	1.12
Non-Basal	865	0.6681	1.05	149	0.5149	1.19

Figure 4.47. LOX is associated with poor RFS in chemotherapy-treated TNBC patients. (A and B) Kaplan-Meier survival curve representing the percentage RFS in chemotherapy-treated (*n* = 125) **(A)** and untreated basal patients (*n* = 260) **(B)** based on LOX expression. **(C)** Table summarizing LOX expression based Kaplan-Meier RFS analysis results of patients representing different breast cancer subtypes either treated or not treated with chemotherapy.

4.2.3. LOX hyperactivates ITGA5/FAK/Src axis to confer doxorubicin resistance which is overcome by suppressing LOX

In order to test the functional role of LOX in doxorubicin resistance and to elucidate how LOX-mediated ITGA5 regulation may lead to resistance, we first induced hypoxia by culturing 231.Luc.GFP cells under low oxygen environment in hypoxia chambers for different time points. We observed an increase in HIF1A expression at protein level,

which was concomitant with the upregulation of LOX and ITGA5 at mRNA and protein levels (Figure 4.48A and B). This hypoxia-driven increase in ITGA5 levels under hypoxia was reflected to the elevated integrin signaling as shown by an increase in p-FAK (Y397) and p-Src (Y416) (Figure 4.48C). Moreover, we observed an increase in the LOX enzymatic activity under hypoxia as compared to normoxia (Figure 4.48D), showing that the increased expression of LOX is reflected to its activity.

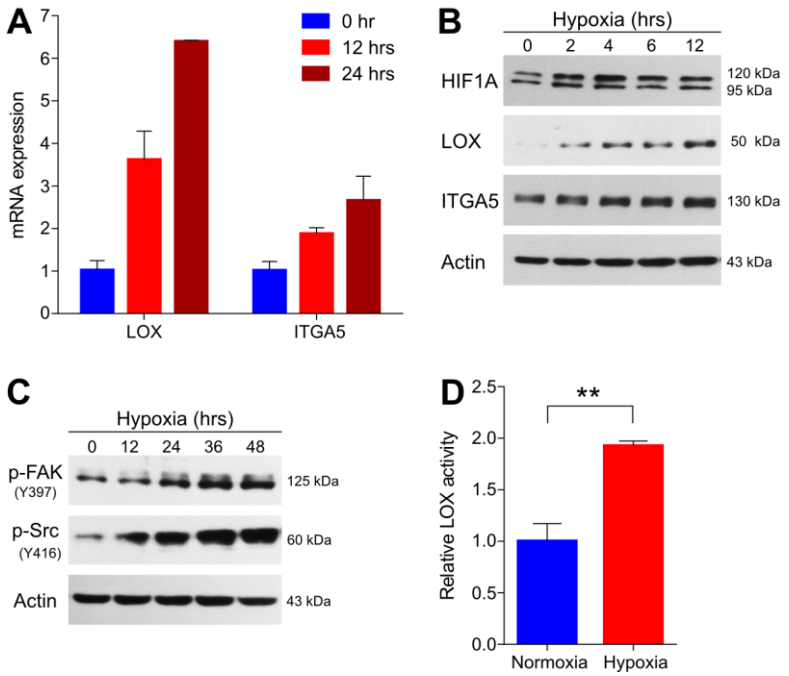

Figure 4.48. Hypoxia-induced LOX and ITGA5 hyperactivate integrin signaling. (A) qRT-PCR analysis showing changes in the mRNA expression levels of LOX and ITGA5 after induction of hypoxia for different time points using hypoxia chambers. **(B)** Western Blot analysis showing changes in expression of HIF1A, LOX and ITGA5 after induction of hypoxia. Actin was used as a loading control. **(C)** Western Blot analysis showing changes in p-FAK (Y397) and p-Src (Y416) after induction of hypoxia. Actin was used as a loading control. **(D)** Bar graph showing the relative LOX activity after hypoxia induction for 24 hours.

In addition, inhibiting LOX using two different siRNAs (with different knockdown levels) downregulated ITGA5 both at mRNA (Figure 4.49A) and protein levels (Figure 4.49 B) and inhibited the downstream signaling as shown by a decrease in p-FAK (Y397) and p-Src (Y416) in a dose-dependent manner (Figure 4.49A and B). These data further confirmed that hypoxia-mediated hyperactivation of integrin signaling mainly works *via* LOX-mediated upregulation of ITGA5.

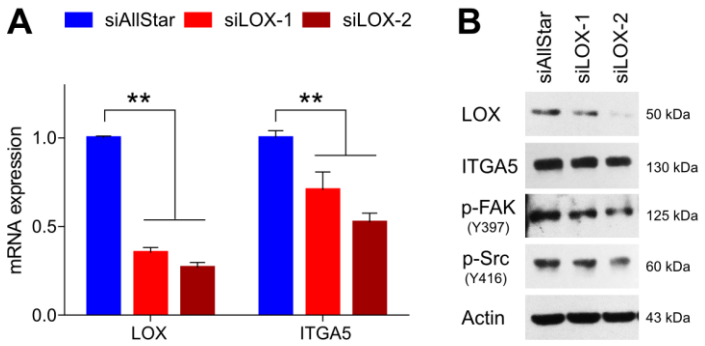

Figure 4.49. LOX hyperactivates integrin signaling by regulating ITGA5. (A) qRT-PCR analysis showing changes in the mRNA expression of LOX and ITGA5 48 hours after transfection with siAllStar or siLOX. **(B)** Western Blot analysis showing changes in LOX, ITGA5, p-FAK (Y397) and p-Src (Y416) 48 hours after transfection with siAllStar or siLOX. Actin was used as a loading control.

Considering the key role of tumor microenvironment in conferring therapy resistance and LOX being an enzyme modulating ECM, we performed doxorubicin sensitization assay in 3D culture settings. It is important to note that uneven distribution of O_2 in 3D culture mimics the natural hypoxic tumor environment [150]. We observed that LOX activity inhibitor, BAPN, (Figure 4.50A) clearly sensitized two different TNBC cell lines to doxorubicin treatment (Figure 4.50B-E). Altogether, our *in vitro* experiments demonstrate that inhibition of LOX overcomes chemotherapy resistance in hypoxic environments by inhibiting ITGA5/FAK/Src axis in TNBC.

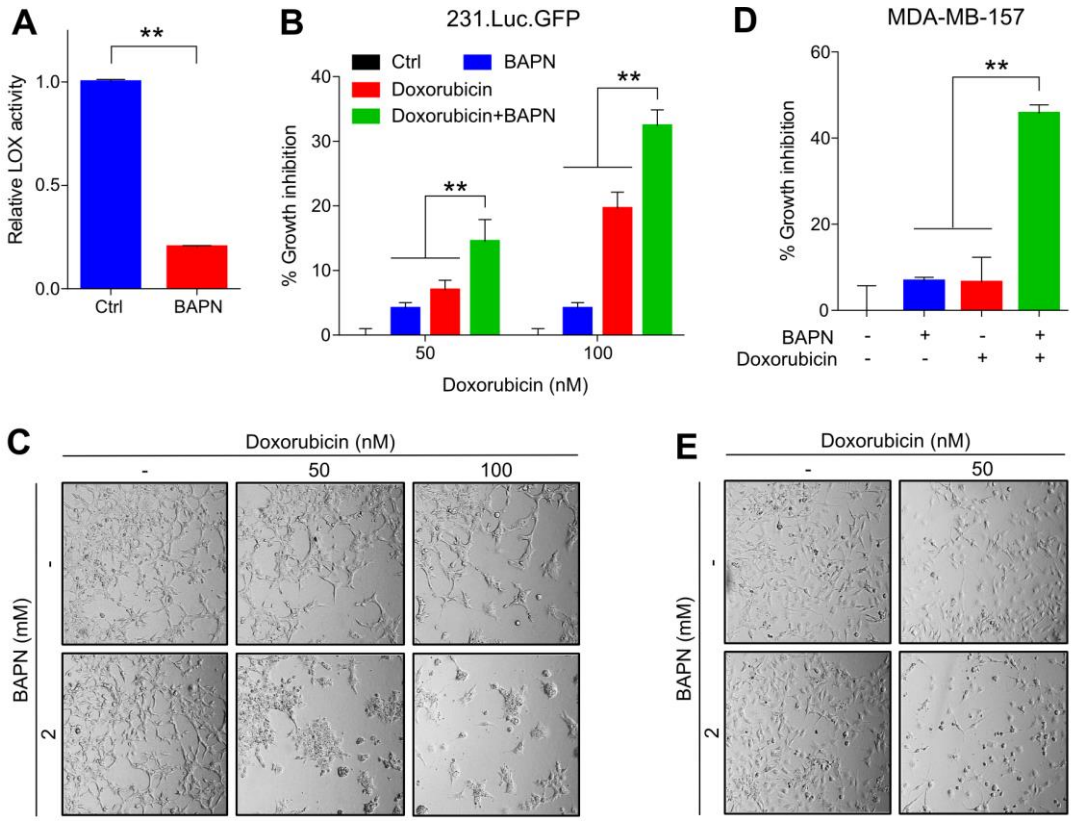

Figure 4.50. Inhibiting LOX activity sensitizes cells to doxorubicin treatment in 3D. (A) Bar graph showing relative LOX activity after treatment with LOX inhibitor, BAPN (1mM) for 24 hours. **(B)** Bar graph showing percent growth inhibition in 231.Luc.GFP cells grown in 3D matrigel after treatment with BAPN and doxorubicin alone and in combination. *n* = 3. **(C)** Representative microscopy images from **(B)**. **(D)** Bar graph showing percent growth inhibition in MDA-MB-157 cells grown in 3D matrigel after treatment with BAPN and doxorubicin alone and in combination. *n* = 3. **(E)** Representative microscopy images from **(D)**.

4.2.4. Targeting LOX overcomes doxorubicin resistance in TNBCs *in vivo*

In order to validate our findings *in vivo*, we engineered 231.Luc.GFP cells to inducibly express an shRNA targeting LOX mRNA (referred to herein as 231.shLOX) under the control of doxycycline (Figure 4.51A and B).

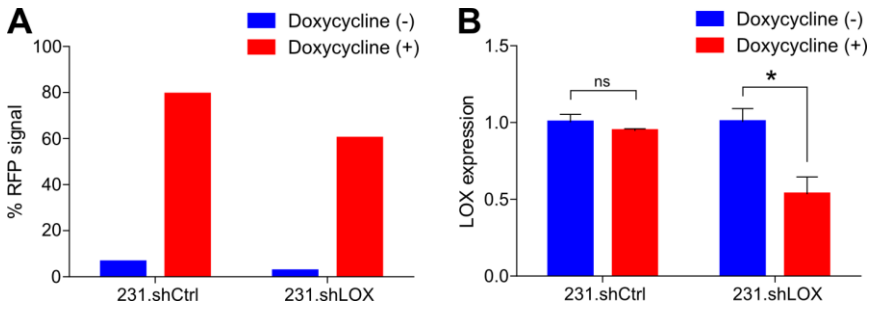

Figure 4.51. Validation of LOX downregulation upon induction of shLOX using doxycycline. (**A)** Changes in shRNA induction-associated red fluorescent protein (RFP) upon doxycycline treatment. Cells were treated with 2ug/ml doxycycline for 48 hours. **(B)** Bar graphs showing changes in LOX mRNA expression after induction of shRNA upon doxycycline treatment. 231.Luc.GFP cells were treated with 2ug/ml doxycycline for 48 hours.

Later, we developed primary tumor xenografts using abovementioned cell line in nude mice. Once tumors became palpable (around 100 mm^3), we started drug treatment along with the inhibition of LOX by inducing shRNA using doxycycline (for details, see Methods Section). We showed that combination of LOX inhibition and doxorubicin treatment resulted in a stronger growth-inhibitory effect on tumors than individual treatments in 231.Luc.GFP xenografts (Figure 4.52A-C). In addition, tumors in combined LOX inhibition and doxorubicin treatment group were smaller in size and weighed less as compared to individual treatments in these xenografts (Figure 4.52D and E).

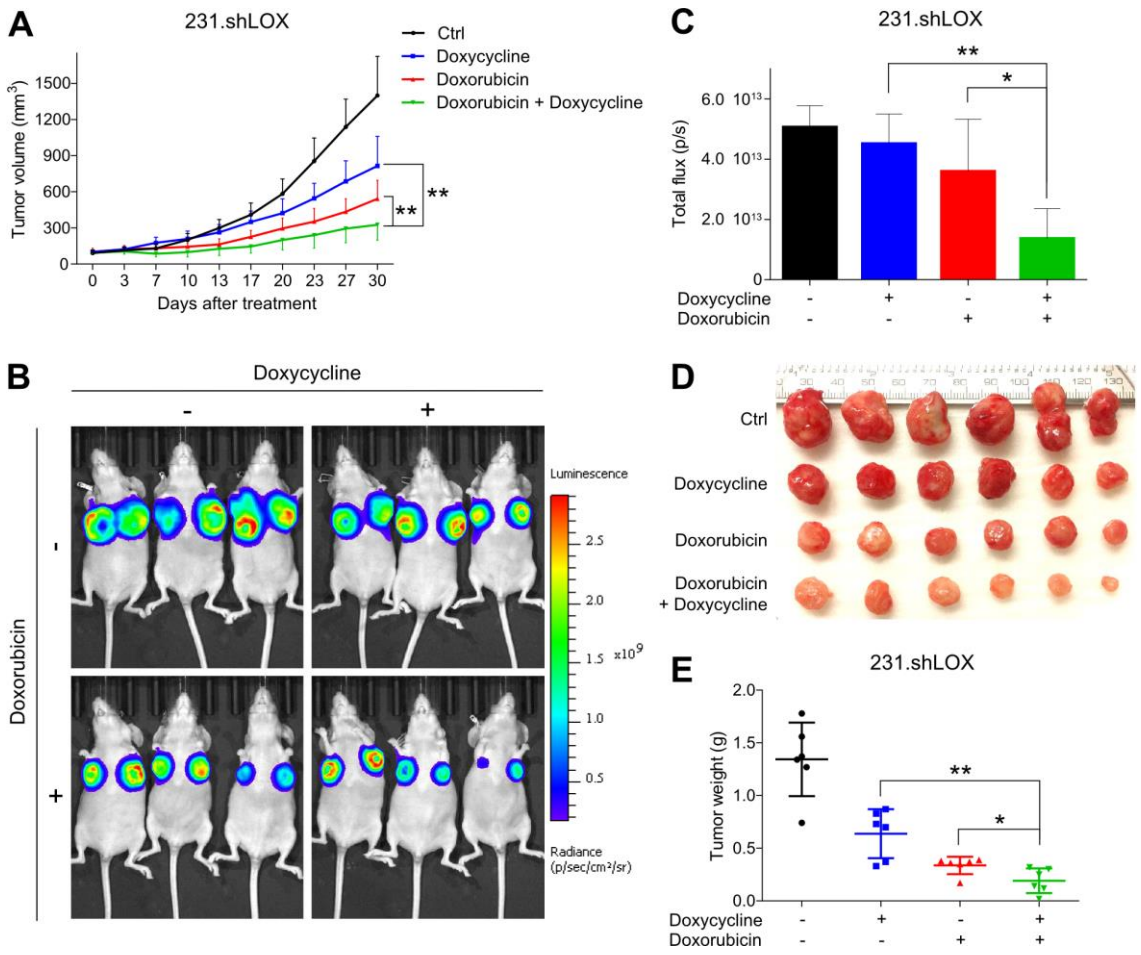

Figure 4.52. Knocking down LOX increases tumor suppressive effects of doxorubicin in TNBCs *in vivo*. A) Tumor volume changes upon shLOX induction and doxorubicin treatment alone or in combination as compared to control in nude mice (n = 6). **B)** IVIS images of mice from **(A)**. **C)** Bar graph showing changes in luciferase intensity from tumors in **(B)**. **D)** Images showing isolated tumors from **(B)**. **E)** Dot plot showing changes in tumor weights from **(D)**.

We observed a reduction in proliferation marker Ki-67 (Figure 4.53A) while an increase in the expression of cleaved Caspase-3 (Figure 4.53B) was observed in combination groups as compared to LOX inhibition or doxorubicin treatment alone confirming attenuated cell proliferation and activated apoptosis in this group. Notably, we observed a decreased expression of ITGA5 and phosphorylation of Src (p-Y416) at the downstream of LOX (Figure 4.53C and D) validating our *in vitro* findings.

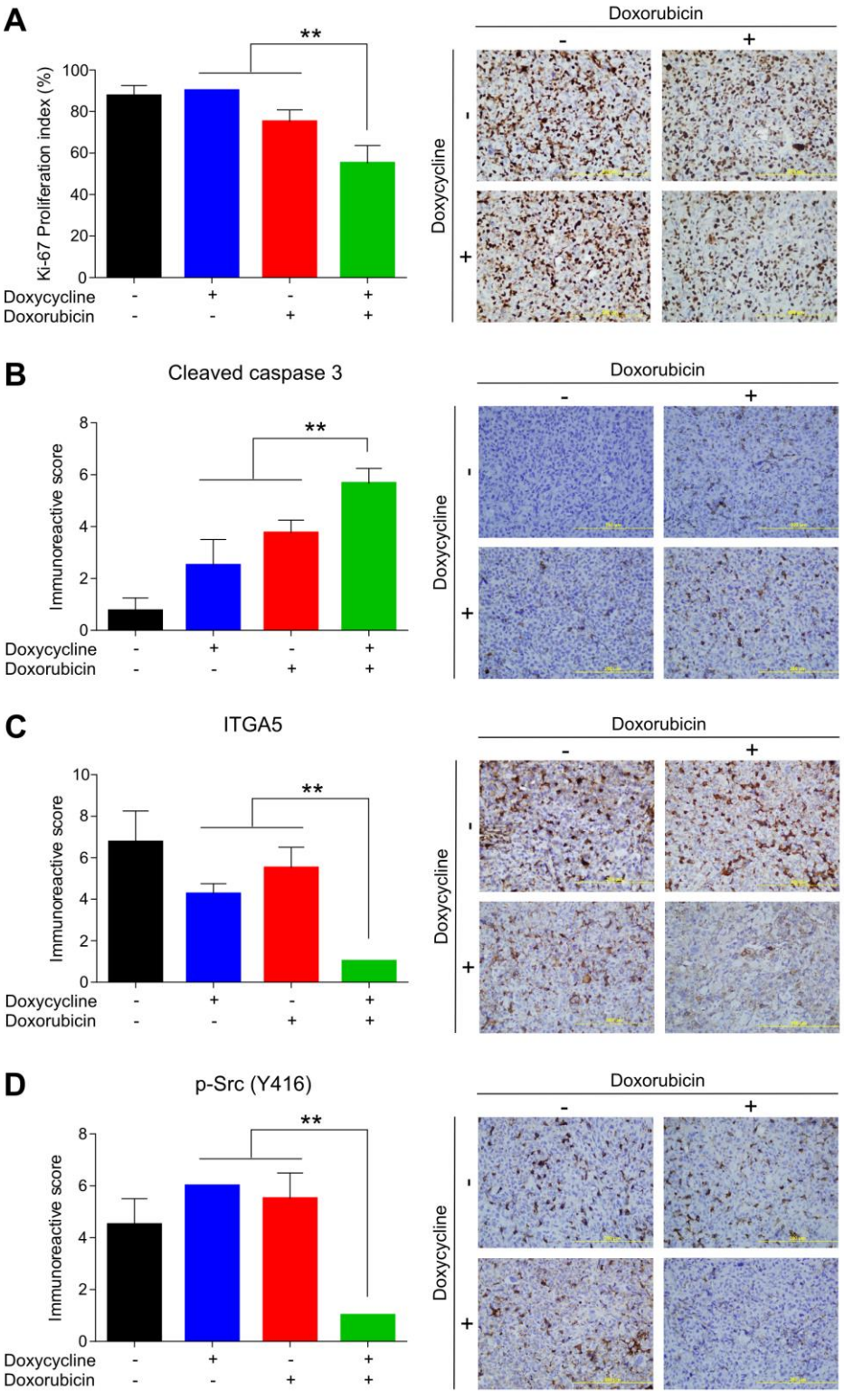

Figure 4.53. Combinatorial treatment of xenografts with shLOX and doxorubicin resulted in least proliferation, higher apoptosis and less active integrin signaling. (A) Ki-67 proliferation index for tumors shown in Figure 4.52 (left) and representative IHC images (right). **(B-D)** Immunoreactive scores of cleaved caspase-3 **(B)**, ITGA5 **(C)** and p-Src (Y416) **(D)** expression in tumors shown in Figure 4.52 (left) and representative IHC images (right). (n = 4).

Next, we aimed to validate our *in vivo* xenograft results in an immunocompetent setting where we employed a syngeneic model by producing TNBC tumors using 4T1 mouse mammary tumor cell line in Balb/c mice. Once tumors became palpable, we started doxorubicin treatment along with the inhibition of LOX using LOX activity inhibitor, BAPN, which we used previously for doxorubicin sensitization in 3D culture (Figure 4.50). Importantly, we observed a stronger effect of combined LOX activity inhibition and doxorubicin treatment compared to individual treatments in terms of tumor growth inhibition in immunocompetent tumor microenvironment (Figure 4.54A). In addition, tumors in combination group were smaller in size and weighed less as compared to individual treatments (Figure 4.54B and C). LOX activity assay confirmed that LOX activity was significantly suppressed in all BAPN treated tumors (Figure 4.54D). Altogether, these data demonstrate that inhibition of LOX increases the efficacy of chemotherapy in TNBC tumors *in vivo*.

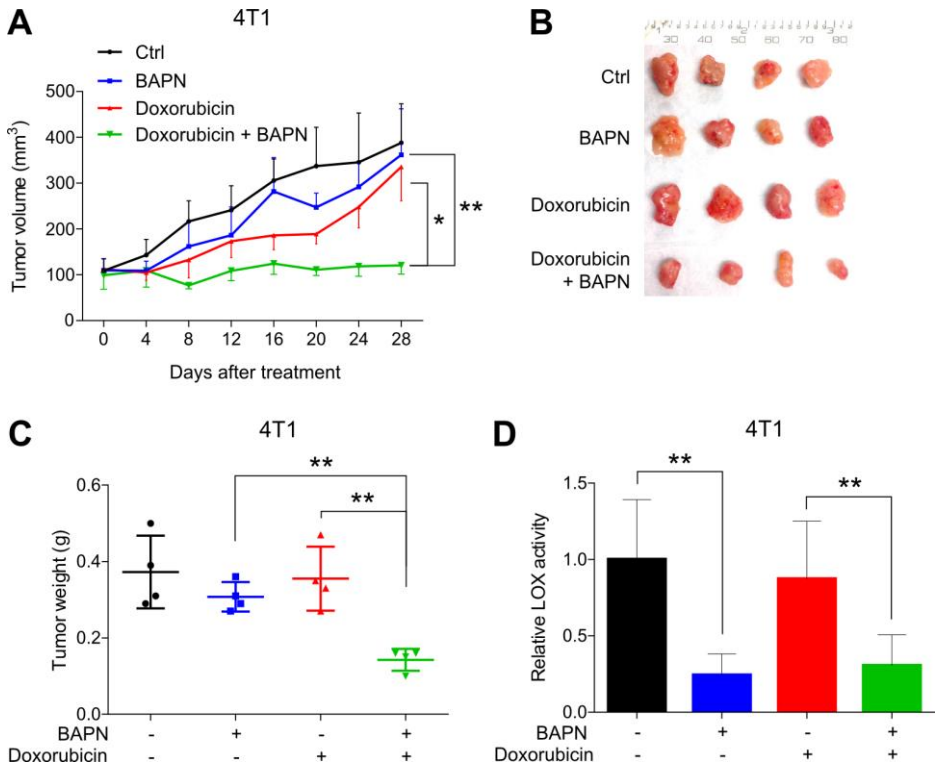

Figure 4.54. Inhibiting LOX activity increases the efficacy of doxorubicin in syngeneic tumor model of TNBCs. (A) Tumor volume changes upon treatment with BAPN and doxorubicin alone or in combination as compared to control in TNBC tumors developed from 4T1 cell line in Balb/c mice (n = 4). **(B)** Images showing isolated tumors from **(A)**. **(C)** Changes in weights of tumors from **(B)**. **(D)** Changes in LOX activity in tumors from **(B).**

4.2.5. Hypoxia-mediated downregulation of miR-142-3p is a master regulator of HIF1A/LOX/ITGA5 axis sensitizing TNBCs to doxorubicin, and is associated with worse survival only in chemotherapy-treated TNBC patients

As we are interested in the possible effects of miRNAs in chemoresistance, and miRNAs have shown tendency to work in pathway-centric manner targeting multiple genes [151, 152], we searched for miRNA modulators of HIF1A/LOX/ITGA5-mediated chemotherapy resistance. To this end, we first examined all conserved miRNAs targeting HIF1A, LOX and ITGA5 and found 8 common miRNAs having binding sites in the 3'-UTRs of all these three genes (Figure 4.55).

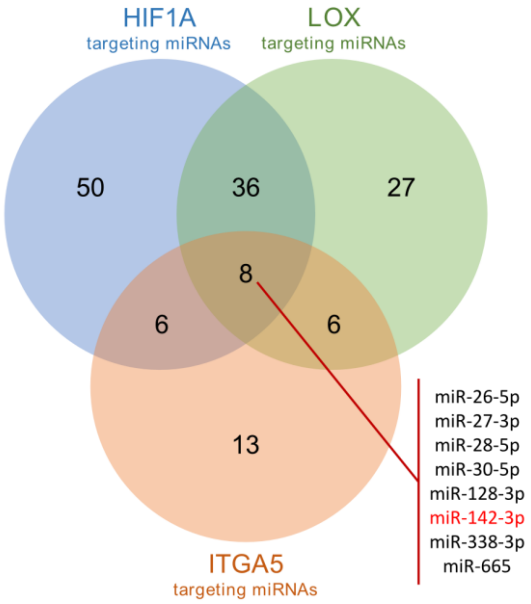

Figure 4.55. miRNAs predicted to target HIF1A, LOX and ITGA5. Venn diagram for the combinatorial target prediction analysis. Number of miRNAs targeting HIF1A (blue), LOX

(green) and ITGA5 (orange) is shown. Names of eight miRNAs predicted to target all three genes are shown. Data was retrieved from online target prediction tool, TargetScan release 7.2.

Out of these 8 miRNAs, only two miRNAs, miR-142-3p and miR-128-3p, showed high inverse correlation with HIF1A gene signature, LOX and ITGA5 expression (Figure 4.56A and Figure 4.57A-G) in basal subtype breast cancer. One of these two miRNAs, miR-142-3p, showed a strong positive correlation with OS specifically in chemotherapy-treated TNBC patients (Figure 4.56B-D and Figure 4.58A-G).

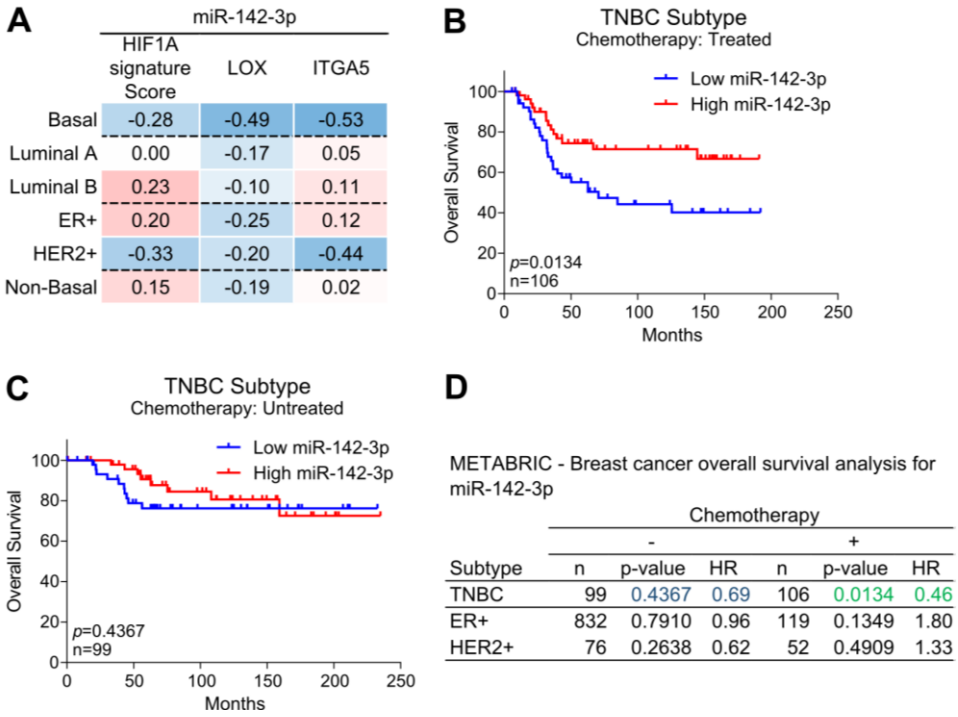

	Chemotherapy					
	-			+		
Subtype	n	p-value	HR	n	p-value	HR
TNBC	99	0.4367	0.69	106	0.0134	0.46
ER+	832	0.7910	0.96	119	0.1349	1.80
HER2+	76	0.2638	0.62	52	0.4909	1.33

Figure 4.56. miR-142-3p expression is inversely correlated with HIF1A, LOX and ITGA5 and is associated with better OS in chemotherapy-treated TNBC patients. (A) Heatmap showing Pearson's correlation coefficient between miR-142-3p and HIF1A gene signature score, LOX and ITGA5 mRNA expression in patients from GSE19783. **(B and C)** Kaplan-Meier survival curve representing the percentage OS in chemotherapy-treated (n = 106) **(B)** and untreated (n = 99) **(C)** TNBC patients based on low vs high miR-142-3p expression. **(D)** Table summarizing LOX expression-based Kaplan-Meier OS analysis results of patients representing different breast cancer subtypes either treated or not treated with chemotherapy.

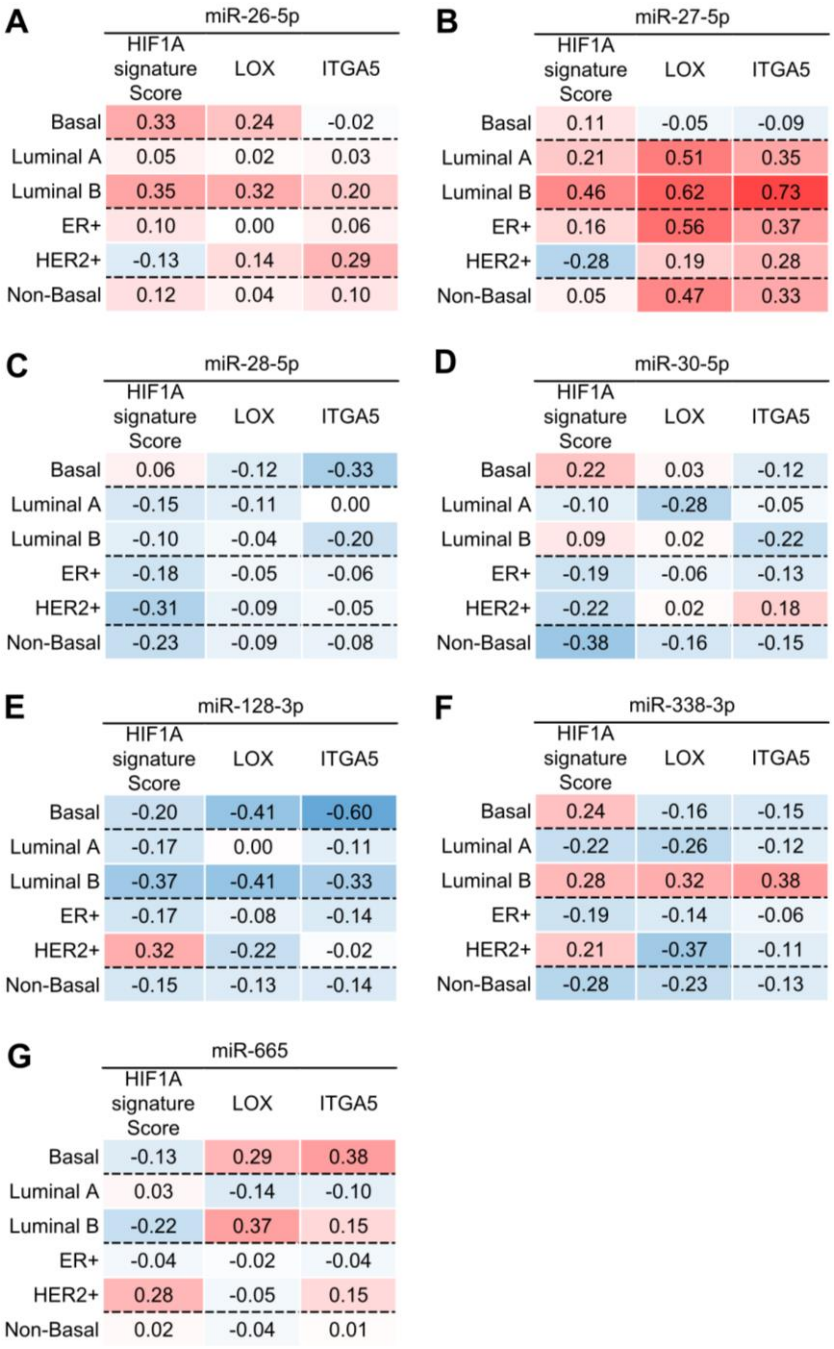

Figure 4.57. Correlation analysis of miRNAs (other than miR-142-3p) predicted to target HIF1A, LOX and ITGA5. (A-G) Heatmaps summarizing Pearson's correlation coefficients for HIF1A gene signature score, LOX or ITGA5 mRNA expression and miR-26-5p **(A)** miR-27-5p **(B)** miR-28-5p **(C)** miR-30-5p **(D)** miR-128-3p **(E)** miR-338-3p **(F)** and miR-665 **(G)** in patients from GSE19783.

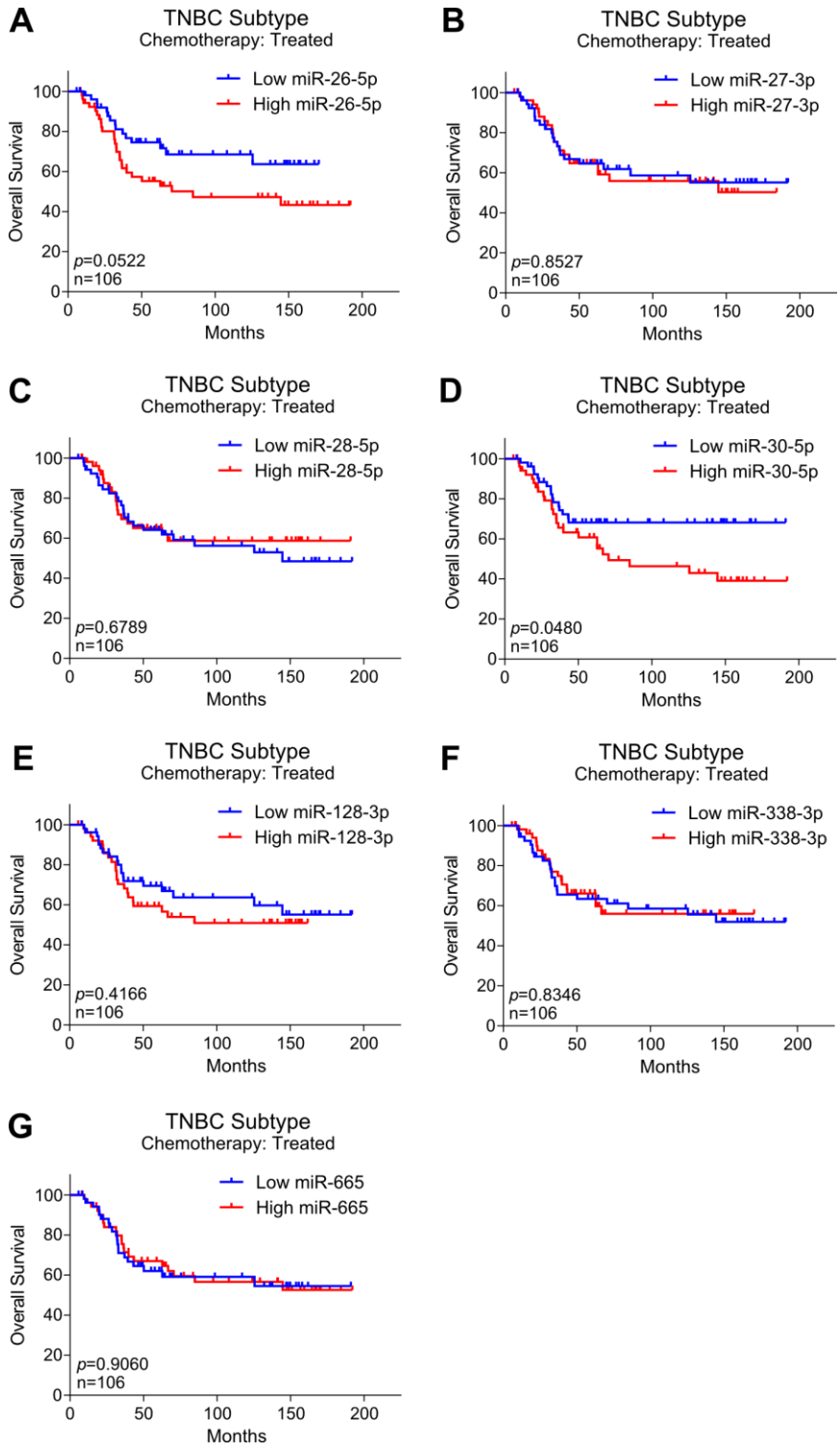

Figure 4.58. Survival analysis of miRNAs (other than miR-142-3p) predicted to target HIF1A, LOX and ITGA5. (A-G) Kaplan-Meier survival curve representing the percentage OS in chemotherapy-treated basal patients (n = 106) (right) based on low vs. high miR-26-5p **(A)** miR-27-5p **(B)** miR-28-5p **(C)** miR-30-5p **(D)** miR-128-3p **(E)** miR-338-3p **(F)** and miR-665 **(G)** expression. Data was retrieved from METABRIC project.

Furthermore, miR-142-3p was significantly downregulated in doxorubicin resistant tumors developed *in vivo* as compared to sensitive ones (Figure 4.59A). Importantly, induction of hypoxia inhibited the expression of miR-142-3p (Figure 4.59B) further suggesting the potential role of this miRNA in hypoxia-induced doxorubicin resistance.

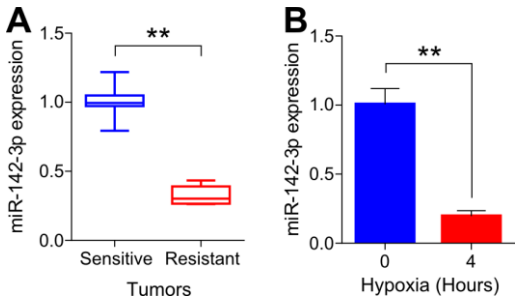

Figure 4.59. miR-142-3p is downregulated in doxorubicin resistant xenografts *in vivo* and upon hypoxia *in vitro*. (A) qRT-PCR analysis showing the expression of miR-142-3p in doxorubicin sensitive and resistant tumors. *n* = 4. **(B)** qRT-PCR analysis showing the expression of miR-142-3p in 231.Luc.GFP cells under hypoxia for 4 hours.

We observed a significant downregulation in HIF1A, LOX and ITGA5 both at mRNA and protein levels upon overexpression of miR-142-3p (Figure 4.60A and B).

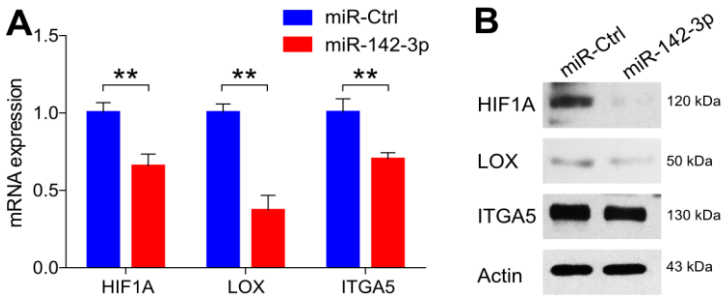

Figure 4.60: HIF1A, LOX and ITGA5 are downregulated upon miR-142-3p ectopic expression. (A) qRT-PCR showing changes at the mRNA levels of HIF1A, LOX and ITGA5 upon miR-142-3p transfection in 231.Luc.GFP cells for 48 hours. **(B)** Western Blot analysis

showing changes in protein level of HIF1A, LOX and ITGA5 upon miR-142-3p transfection in 231.Luc.GFP cells for 48 hours. Actin was used as a loading control.

Next, we confirmed HIF1A, LOX and ITGA5 as direct targets of miR-142-3p by measuring the luciferase expression from reporter constructs containing 3′-UTRs of their mRNAs in 231.Luc.GFP cells upon miR-142-3p transfection (Figure 4.61A and B).

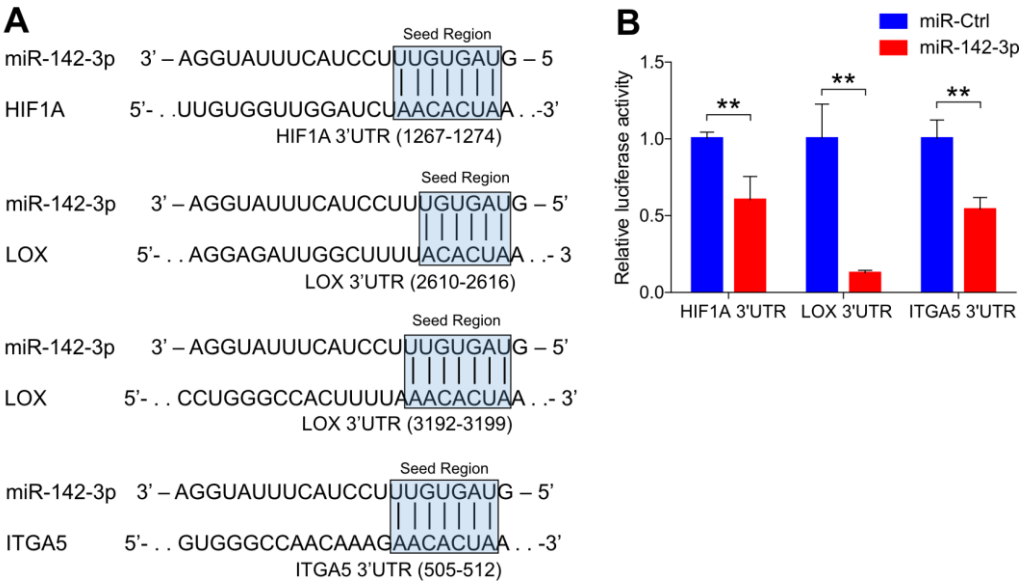

Figure 4.61. miR-142-3p directly targets HIF1A, LOX and ITGA5. (A) Graphical representation of miR-142-3p binding sites within the 3'-UTRs of HIF1A, LOX and ITGA5. **(B)** Luciferase activity of a reporter construct fused with 3′-UTRs of HIF1A, LOX or ITGA5 in 231.Luc.GFP cells transfected with miR-Ctrl or miR-142-3p.

Lastly, under 3D culture hypoxic conditions, ectopic expression of miR-142-3p clearly sensitized cells to doxorubicin treatment (Figure 4.62A and B). Overall, we showed that miR-142-3p sensitizes cells to doxorubicin by regulating the HIF1A/LOX/ITGA5 axis, and is associated with the chemotherapy response in TNBC patients.

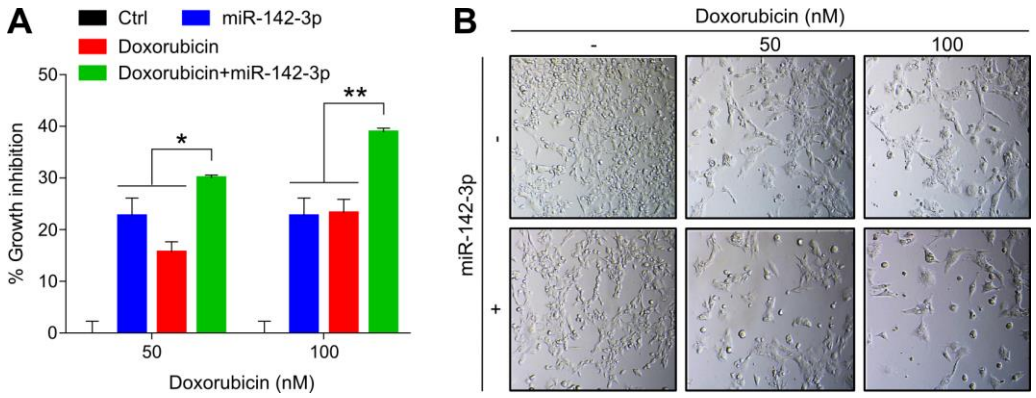

Figure 4.62. miR-142-3p sensitizes TNBC cells to doxorubicin treatment in 3D. (A) Bar graph showing percent growth inhibition in 231.Luc.GFP cells grown in 3D matrigel after transfection with miR-142-3p and/or treatment with doxorubicin. *n* = 3. **(B)** Microscopy images from A.

Chapter 5

Discussion

This dissertation has identified two different miRNAs, namely miR-644a and miR-142-3p, former suppressing therapy resistance and EMT in breast cancer, in general, whereas latter inhibiting chemotherapy resistance particularly in TNBCs. In the first part of the dissertation, I have identified the multifactorial role of miR-644a in regulating tumor growth, metastatic potential and therapy resistance in breast cancer. In the second part, developing chemotherapy resistant model *in vivo* and using next generation sequencing technology, I have unraveled the underlying molecular changes of doxorubicin resistance in TNBC and have shown a novel mechanism of hypoxia-induced LOX, a pro-metastatic enzyme, to regulate chemotherapy resistance in TNBCs. Furthermore, I identified miR-142-3p as an important chemo-sensitizer by targeting LOX, HIF1A and ITGA5 simultaneously.

PART I.

The miR-644a/CTBP1/p53 axis suppresses drug resistance by simultaneous inhibition of cell survival and epithelial-mesenchymal transition in breast cancer

In this part of the dissertation, I demonstrated that miR-644a acts as a tumor suppressor in breast cancer by regulating tumor progression, metastasis, and drug resistance affecting the patient survival. Mechanistically, miR-644a targets transcriptional co-repressor CTBP1 whose loss on one hand leads to increased E-Cadherin to inhibit EMT and metastasis, on the other hand leads to increased p53 expression. Apoptosis induced by miR-644a/CTBP1 is dependent on p53 mutation. Increased expression of wild-type p53

induces p21 expression, which leads to G1 arrest; while increased expression of mutant p53 induces pro-apoptotic Noxa expression, which leads to apoptosis in breast cancer cells. Collectively, our results establish the miR-644a/CTBP1/p53 axis as a key modulator of cell survival, EMT, and drug resistance in breast cancer (Figure 5.1).

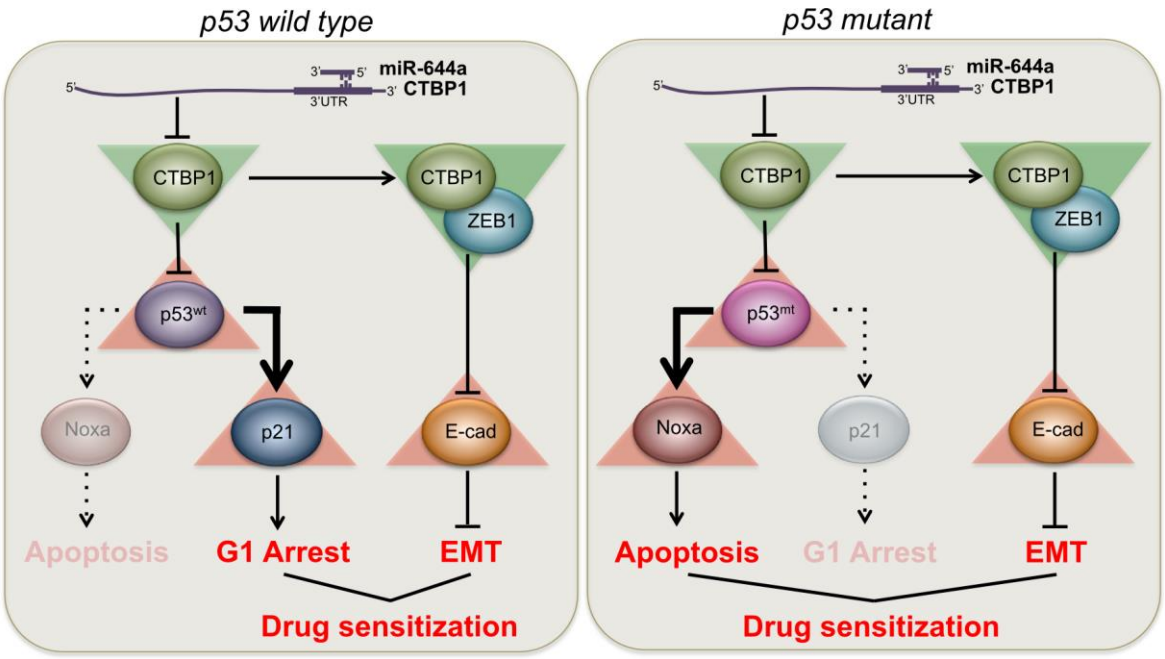

Figure 5.1. Schematic representation of miR-644a/CTBP1/p53 axis-mediated drug resistance by simultaneous modulation of cell survival and EMT in p53-*wt* (left) and p53-*mut* (right) cells. Downregulation of CTBP1 by miR-644a targets results in p53 upregulation irrespective of its mutation status. WT p53 then transcriptionally activates p21 leading towards G1 cell cycle arrest whereas mutant p53 activates pro-apoptotic Noxa. On the other hand, downregulation of CTBP1 by miR-644a inhibits EMT by promoting epithelial-like state. This inhibition of EMT combined with cell cycle arrest (in p53-wt cells) or apoptotic cell death (in p53-mut cells) sensitizes cells to therapy treatment. Active interactions are shown with bold and solid whereas inactive interactions with dotted lines.

5.1.1. miR-644a and cancer

Little is known about the deregulation of miR-644a in cancer. It has been shown that high expression of miR-644a (previously known as miR-644 according to miRBase release 21 [153]) is correlated with shorter OS in Acute myeloid leukemia (AML) [154], and miR-644a is found to be upregulated in bladder cancer [155]. On the contrary, miR-644a overexpression was shown to downregulate an isoform of the androgen receptor, and decrease viability in prostate cancer cell lines [156]. However, there was no functional study on miR-644a, and its deregulation in breast cancer had not been reported (prior to our publication [104]). For the first time, we showed that miR-644a acts as a tumor suppressor in breast cancer by regulating tumor progression, metastasis, and drug resistance. In addition, we corroborated our findings with online available clinical patient data, where we demonstrated that miR-644a expression is reduced in breast tumors compared to matching normal tissues, and its expression is significantly reduced with increased tumor size, grade and stage in breast cancer. We also observed a trend for the reduced expression of miR-644a in lymph nodes compared to primary tumors. Notably, patients with low miR-644a-GS scores experience worse DMFS. All these data suggest that in contrast to AML and bladder cancer, miR-644a likely acts as a tumor suppressor in breast cancer similar to the case of prostate cancer. This highlights the tissue-specific roles of miRNAs, in general, and of miR-644a, in particular.

Following our study, miR-644a has been shown to inhibit aggressiveness and stem-like traits in esophageal squamous cell carcinoma and its lower expression was associated with tumor recurrence and/or metastasis [157]. More importantly, CTBP1 has been again demonstrated as major functional target of miR-644a and its inhibition by miR-644a was shown to suppress cell proliferation and invasion in gastric cancer cells [158] further supporting our findings.

5.1.2. CTBP1 and cancer

We identified the transcriptional co-repressor CTBP1 as a major functional target of miR-644a phenocopying all its effects on cell proliferation, apoptosis, EMT and drug resistance. In addition to the loss-of-function experiments, rescue experiments showed the key role of CTBP1 in phenocopying the effects of miR-644a. CTBPs were first identified as oncogenic proteins interacting with the C-terminus of the E1A protein from adenoviruses [159]. In vertebrates, there are two loci, CTBP1 and CTBP2, and they share 78% amino acid homology; however, they may have differential roles in development and breast tumorigenesis [138]. This effect could, in part, be explained by the poor homology between the 3'-UTR regions of the CTBP1 and CTBP2 genes. In our case, we did not find any binding site for miR-644a in the 3'-UTR of CTBP2 in contrast to that of CTBP1. The oncogenic role of CTBP1 has been shown in several tumors including prostate [160], breast [137], melanoma [161] and hepatocellular carcinoma [162]. However, little is known on its miRNA regulation. Deng *et al* reported that miR-137 targets CTBP1 and inhibits EMT by increasing the expression of E-Cadherin in melanoma cell lines [163], which is in line with our findings in breast cancer.

5.1.3. p53 mutation status: "gain of pathway" paradigm

It has been known that activated p53 can either lead to apoptosis or cell cycle arrest in a highly context dependent manner. As reviewed by Haupt *et al* [164] and Fridman *et al* [165], cell type, strength and nature of the stimulus as well as the presence of collateral signals can determine cell fate in the presence of a stress stimulus. Importance of the latter has been shown in case of DNA damage during which Myc shifts the balance of cell fate from cell cycle arrest to apoptosis by blocking p21 induction *via* recruiting Miz-1 to p21 promoter site, and thereby preventing p53-mediated transcription [166, 167].

Therefore, we also checked changes in Myc expression with miR-644a overexpression, but did not observe an induction in Myc levels (data not shown), which might be due to the presence of a stimulus other than DNA damage in our system. Here, we propose that the mutation status of p53 is yet another factor that is important for the decision of undergoing either to cell cycle arrest or to apoptosis. Our results demonstrated that increase in p53 levels upon miR-644a overexpression or CTBP1 knockdown increases p21 which protects cells from p53-dependent apoptosis [17], and causes cell cycle arrest in p53-wt cells whereas it induces apoptosis *via* increasing the expression of pro-apoptotic gene Noxa in p53-*mut* cells. We showed that overexpression of *mut*-p53 in p53-*wt* MCF-7 cells was enough to shift the balance between cell cycle arrest and apoptosis in favor of apoptosis through upregulation of an established pro-apoptotic BH3-only protein, Noxa, even though p21 was still induced (Figure 4.31B and D).

p53 is mutated in 30% of breast cancer which causes several defects in p53 functioning like altered DNA binding affinity or loss of transcriptional activity [168, 169]. However, there is substantial evidence showing that mutant p53 is still able to induce apoptosis through different mechanisms. It has been shown that a transcriptionally inactive mutant p53 can still activate the pro-apoptotic gene Bax upon DNA damage [170], and some transcription-defective mutants retain significant apoptotic activity independent of Bax induction [171, 172]. These suggest that in case of p53 mutation, a "gain of pathway" phenomenon occurs which may involve either transcription-dependent or independent activation of a different set of pro-apoptotic genes [173]. Our results support these findings with regard to induction of apoptosis by miR-644a in p53-mutant breast cancer cells by activation of Noxa.

Notably, although we found no correlation of CTBP1 levels with the survival of breast cancer patients (Figure 4.34, Figure 4.35D-F and Figure 4.36B), in all datasets that

we analyzed, we confirm that p53-*mut* patients with breast or ovarian cancer that show high CTBP1 level are associated with a worse survival as compared to the patients with low CTBP1 group (Figure 4.35A-C and Figure 4.36A). This suggests that CTBP1 could be a potential prognostic factor for breast cancer patients with p53 mutations which may be due to the fact that apoptosis induction is more effective on prolonging OS of patients than p53-dependent growth arrest.

5.1.4. miR-644a/CTBP1/p53 axis: Biomarker of drug response in breast cancer

As EMT and cell survival are closely related with drug resistance, we examined the effects of miR-644a and its target CTBP1 in drug sensitization, and observed that overexpression of miR-644a sensitized different breast cancer cells representing different subtypes to both chemotherapy and targeted therapy agents e.g. tamoxifen and gefitinib. In addition, low CTBP1 correlated with better response (Figure 4.23A) and longer DMFS of breast cancer patients treated with chemotherapy (Figure 4.23B). We have previously shown that miR-375 blocks EMT and sensitizes MCF-7 cells to tamoxifen [89]. Similarly, it has been shown that miR-147 blocks EMT and sensitizes colon cancer cells to gefinitib [174]. Although these drugs have different targets and mechanisms of action, we reveal miR-644a as a pleotropic sensitizer, which suggests that the inhibition of EMT might be a common nominator for sensitization to all drugs tested. However, as CTBP1 can increase the expression of MDR1 gene transcriptionally [175], we cannot rule out the alternative of possible downregulation of MDR1 upon miR-644a expression, which leads to inhibition of multi-drug resistance. Nevertheless, our results suggest that miR-644a or its target CTBP1 could be a potential drug candidate which can simultaneously block primary tumor growth, metastasis, and finally sensitize cancer cells to several different drugs.

A recent study reported a small molecule, NSC95397, which inhibits the interaction between CTBP1 and its binding partners and blocks the CTBP1-mediated transcriptional repression [176]. Although using miRNAs as potential drugs could need longer time, small molecules targeting CTBP1 could act as potential drugs for cancer therapy in the near future. In conclusion, the miR-644a/CTBP1/p53 axis acts not only as biomarker of progression and drug response, but also could be targeted for cancer therapy.

PART II.

Targeting hypoxia-induced lysyl oxidase overcomes chemotherapy resistance in triple negative breast cancer

In the second part of the dissertation, I have uncovered a novel molecular mechanism for chemotherapy resistance in TNBCs, which involves over-activation of LOX/ITGA5/FAK/Src axis due to the hypoxia-driven downregulation of miR-142-3p (Figure 5.2A). Mechanistically, in hypoxic chemoresistant tumor microenvironment, HIF1A transcriptionally activates LOX which then hyper-activates integrin signaling indirectly due to reduced matrix crosslinking and *via* regulating ITGA5 expression. Hypoxia also inhibits miR-142-3p, a miRNA able to target all three main players (HIF1A, LOX and ITGA5) of doxorubicin resistance in TNBCs. Therefore, we propose that suppressing LOX by a LOX inhibitor, e.g. BAPN, or activating miR-142-3p can modulate ITGA5/FAK/Src axis and sensitize cells to chemotherapy (Figure 5.2B).

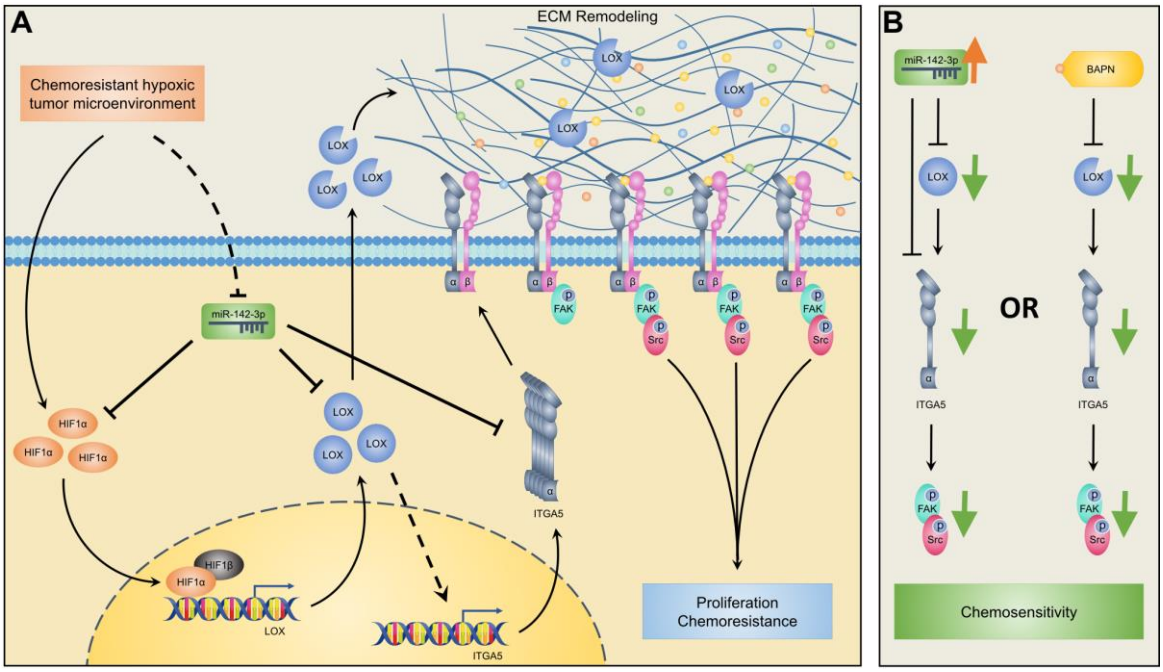

Figure 5.2. Schematic representation of hypoxia-induced LOX/ITGA5/FAK/Src axis mediated therapy resistance in TNBCs and targeting approaches for chemosensitization. **(A)** Hypoxia-induced HIF1A increases the transcription of LOX which then increases the expression of ITGA5. In meantime, hypoxia-mediated downregulation of miR-142-3p, which normally targets HIF1A, LOX and ITGA5, leads to further activation of the HIF1A/LOX/ITGA5 axis. This culminates in the activation of FAK/Src signaling resulting in chemoresistance in TNBCs. Known interactions are shown by thin arrows while new interactions identified in our study are shown by thick arrows. Indirect interactions are shown as dotted while direct interactions are shown as solid lines. **(B)** Upregulating miR-142-3p or treatment with LOX inhibitor, BAPN, sensitizes cells to chemotherapy by blocking LOX/ITGA5/FAK/Src axis.

5.2.1. Tumor microenvironment, hypoxia and therapy resistance in TNBC

Deregulation of different cellular processes like apoptosis [47], NFKB signaling [44] or DNA repair [48], as well as alterations in the levels of drug transporter proteins [49] have been previously associated with chemoresistance in TNBCs. Besides modulation of cell intrinsic processes, other components of tumor microenvironment, like ECM remodeling may also confer resistance to given therapy by providing survival signals to drug treated tumors. However, ECM components and re-modelers have so far been studied primarily

in the context of metastasis [177-179], and little is known about their contribution to drug resistance.

Solid tumors often get deprived of oxygen resulting in hypoxic microenvironment. Tumor cells usually counteract this by adapting to hypoxia *via* upregulating HIFs [148]. The strong enrichment of hypoxia-associated genes in our DoxoR-GS was anticipated as the inner core of tumor mass in treatment-refractory, aggressive tumors are often deprived of oxygen due to inadequate vascularization. Most of the molecular changes induced in hypoxic cells were associated with activation of HIF1A as a way to adapt the altered oxygen demand [180, 181]. In the IPA analysis conducted with the genes differentially expressed in doxorubicin resistant tumors, we identified HIF1A as an important upstream regulator of several genes including LOX and ITGA5 (Table 4.4). This is in line with the literature as increased HIF1A protein stability was shown to regulate diverse intracellular processes as well as the ECM composition by activating several matrix modifying enzymes, including LOX, which is proposed as a highly attractive therapeutic target in metastatic tumors [182, 183]. Previously, HIF1A has also been shown to confer therapy resistance by directly regulating multi drug resistance associated genes, MDR1 and MRP, which increase drug eflux against a broad range of structurally and functionally unrelated chemotherapy agents [184]. Additionally, metabolic reprogramming, decrease in cancer cell proliferation, hypoxia driven selection of p53-mutated tumor cells and inhibition of DNA damage has also been proposed as HIF1A or hypoxia driven chemoresistance mechanism [185].

5.2.2. LOX and therapy resistance

LOX belongs to a heterogeneous family of copper-dependent amine oxidases that catalyzes the crosslinking of collagen fibers and elastins to maintain rigidity in ECM. This family consists of five members, LOX and four LOX-like (LOXL1-4) enzymes, each encoded by a different gene [186]. Aberrant expression of LOX family members in multiple cancer tissues has suggested a dual role for these proteins both as tumor suppressor and metastasis promoter [186-188]. However, it has been well established that enzymatic role of these enzymes in extracellular vicinity promotes tumor cells invasion and metastasis [189]. For instance, high expression of LOX in primary tumors has been shown as driving factor towards bone metastasis in breast cancer where it regulates NFAT driven osteoclastogenesis, thus, forming pre-metastatic lesions *via* distrupting normal bone homeostasis [190]. Additionally, high expression of LOX mRNA and/or protein significantly correlated with tumor progression, has been proposed as poor prognostic factor, and was found associated with high grade tumors, increased recurrence rates, and decreased metastasis-free survival in multiple cancer types including breast, head and neck squamous cell, prostate and clear cell renal cell carcinomas [188]. In this study, we found LOX, but not the others members of LOX family (data not shown), was significantly upregulated in doxorubicin resistance in TNBCs, and its pharmacological inhibition sensitized TNBC cells to therapy treatment by inhibiting integrin/focal adhesion signaling. This is in line with the literature where LOX family has been recently shown to promote chemotherapy resistance by limiting intra-tumoral drug distribution in pancreatic ductal adenocarcinoma [191].

5.2.3. Chemoresistance in the context of crosstalk between hypoxia-induced LOX and integrin signaling

I showed that inhibiting LOX mediates doxorubicin sensitization in 3D cultures of TNBC cell line models (Figure 4.50B-E), as well as in *in vivo* models of aggressive TNBCs (Figure 4.52 and Figure 4.54). The demonstrated effect of LOX on FAK/Src activation and drug resistance *via* regulation of integrin signaling could either be 1.) due indirectly to reduced matrix crosslinking or 2.) due to regulation of ITGA5 levels by LOX through activation of transcription factors. Supporting the latter argument, we observed a decrease in ITGA5 mRNA expression upon LOX inhibition in xenografts of 231.Luc.GFP cells (Figure 4.46B). This suggests that the crosstalk between LOX and integrin signaling may not solely be the result of matrix remodeling, but there might rather be a causal indirect transcriptional link between LOX and ITGA5. Interestingly, ITGA5, which is an alpha chain family member of integrins forming heterodimers mainly with beta 1 subunit, ITGB1, was the only member demonstrating a positive correlation with HIF1A in breast cancer patients (Figure 4.46A; Table 4.4). Furthermore, we showed that expression of these two genes has a strong effect on patient survival in chemotherapy-treated TNBC patients (Figure 4.40B-D, Figure 4.42C and Figure 4.47). At the signaling level, ITGA5 expression was following a very similar pattern with the expression of LOX under hypoxia (Figure 4.48A and B), and the increase in both LOX and ITGA5 expression was followed by a profound increase in FAK/Src signaling (Figure 4.48C). This further supported our hypothesis that ITGA5 could be a major effector downstream of LOX in hypoxic TNBC tumors regulating chemoresistance *via* activation of downstream FAK and Src signaling and leading to enhanced cell proliferation and invasion [192, 193]. All these pre-clinical findings support the potential

clinical benefit that can be achieved upon LOX/ITGA5 inhibition in chemotherapy refractory, aggressive TNBCs.

5.2.4. miR-142-3p and therapy resistance

The strong association we have shown between HIF1A, LOX and ITGA5 indicated that these three proteins work in a cascade and therefore, their expression might simultaneously be fine-tuned. We have previously shown that the proteins functioning in the same molecular processes can be co-regulated by miRNAs [152]; therefore, we searched for miRNAs which can fine-tune the expression of this axis and found miR-142-3p as a novel modulator of proposed axis. Despite very few studies posing miR-142-3p as an oncogenic miRNA in a context-dependent manner [194], miR-142-3p has been mainly associated with tumor inhibitory roles in multiple cancer types including osteosarcoma [195, 196], non-small cell lung carcinoma [197], cervical [198], colon [199] and breast cancer [200, 201]. In addition, miR-142-3p has been found significantly downregulated in AML and NSCLC where its overexpression sensitizes cancer cells to different therapy agents [202, 203]. These studies are in line with our findings that miR-142-3p is downregulated upon doxorubicin treatment in TNBCs and is able to mediate Doxorubicin sensitization *via* robust control of HIF1A/LOX/ITGA5 axis under hypoxia-mediated chemoresistance suggesting miR-142-3p as a potential target and a biomarker of chemotherapy resistance in TNBC patients.

Chapter 6

Conclusions and Future Perspectives

PART I.

The miR-644a/CTBP1/p53 axis suppresses drug resistance by simultaneous inhibition of cell survival and epithelial-mesenchymal transition in breast cancer

In the first part of my dissertation, I have uncovered miR-644a as a novel tumor suppressor miRNA which inhibits tumor progression, metastasis, and drug resistance in breast cancer by targeting transcriptional co-repressor CTBP1. Loss of CTBP1, on one hand, leads to increased E-Cadherin to inhibit EMT and metastasis, on the other hand, upregulates p53 independent of its mutation status. Increased expression of wild-type p53 induces p21 expression, which leads to G1 arrest; while increased expression of mutant p53 induces pro-apoptotic Noxa expression, which leads to apoptosis in breast cancer cells. Collectively, our results establish the miR-644a/CTBP1/p53 axis as a key modulator of cell survival, EMT, and drug resistance in breast cancer.

To date, CTBP1 has been mainly studied in the context of transcriptional corepressor and has been associated with multiple “hallmarks of cancer" through its transcriptional regulation of gene networks regulating malignant behavior. CTBP1 has been shown to promote a vast range of pro-tumorigenic, metastatic and cancer stem cell phenotypes, including increased cell survival, evasion from apoptotic cell death, proliferation, migration and invasion, EMT, and stem cell-like features. Huge amount of literature has suggested that CTBP1 regulates all these phenotypes due its ability to influence tumor evolution and progression through suppressing the expression of multiple epithelial and pro-apoptotic genes at transcriptional level [204]. The findings

presented in this dissertation, propose that CTBP1 inhibits p53 expression at a post transcriptional level; thus, it is of importance to understand the underlying the mechanism by which CTBP1 mediated inhibition of p53 occurs. The consistent upregulation of p53 expression at protein level, but not at mRNA level, upon modulating CTBP1 expression in multiple breast cancer cell lines suggests a potential post-transcriptional gene regulation and may involve a direct physical interaction between CTBP1 and p53 proteins, which can be further elucidated by co-immunoprecipitation experiments.

Identifying efficient therapeutic methods to deliver miRNAs specifically to tumor mass with minimal side effects and their use in clinics as drugs in combination with therapy agents is of great interest in the field of miRNA therapeutics. Over last decade, multiple miRNA delivery systems have been introduced but most of these approaches either fail *in vivo* or at clinics. Recently, two different miRNA-based therapeutics (Miravirsen: a miR-122 antisense locked nucleic acid and MRX34: a liposomal miR-34 mimic) have been approved in clinics [205]. The findings presented in this dissertation that miR-644a simultaneously inhibits tumor progression and metastasis, thereby sensitizes cancer cells to both chemo- and targeted-therapy in breast cancer, propose identifying/designing efficient delivery options for miR-644a in combination with therapy agents in clinics.

Although high CTBP1 expression has been associated with progression of multiple cancer types, its expression is generally low or absent in multiple adult tissues; thus, it is anticipated that inhibition of CTBP1 or its activity may not have any drastic effect in most of the tissues; and therefore inhibitors targeting CTBP1 are expected to be well tolerated [204]. To date, efforts have been made in understanding the roles of CTBP1 in tumorigenesis and to target its transcriptional corepressor activity, but it still

remains just as an appealing candidate to be targeted in clinics. A small molecule enzymatic inhibitor, MTOB, and its derivatives have been shown disrupting CTBP1 recruitment to target promoter, thereby antagonizing CTBP1-mediated transcriptional regulation. In addition, chemical modification of MTOB increased the binding affinity and improved the targeting of CTBP1 by these inhibitors [206]. As CTBP1 heterodimerization with CTBP2 or homodimerization is important for its transcriptional activity, targeting CTBP1 dimerization interface using a cyclic peptide, CP61, has been shown to inhibit CTBP1-associated proliferation in MCF-7 breast cancer cells [207]. However, *in vivo* impact of these small molecule inhibitors on CTBP1-mediated transcriptional repression and tumorigenesis has yet to be determined. In addition, rather than targeting specific functions of CTBP1, there is a dire need of identifying/designing a general and specific inhibitor of CTBP1 which can be implicated in clinics.

p53 is a well-known as master regulator of diverse cellular processes e.g. DNA repair, cell cycle arrest, apoptosis, autophagy, senescence, metabolism and aging. It is mutated in more than 50% of human cancers leading towards inactive or dysfunctional p53 protein in tumors. Lot of efforts have been made to identify or develop drugs which can restore wild-type p53 activity or which can deplete mutant p53 and several compounds have already reached to clinical trials. For instance, PRIMA-1^{MET} has been shown inducing wild-type P53 expression and restoring DNA binding activity of mutant-p53 by inducing a conformational change. On the other hand, Hsp90 inhibitors and HDAC inhibitor have potential to deplete mutant p53 and are in clinical trials for cancer therapy [208]. The results presented in this dissertation, propose that CTBP1 inhibits p53 expression at protein level, and p53-mutant patients with low CTBP1 expression are at survival advantage as compared to their counterparts with high CTBP1 expression. Therefore, there is a need to identify drugs/compounds which can promote mutant-p53

expression or evade mutant p53 from inhibition by CTBP1 in p53 mutant patients with high CTBP1 expression.

PART II.

Targeting hypoxia-induced lysyl oxidase overcomes chemotherapy resistance in triple negative breast cancer

In the second part of the dissertation, I found hypoxic tumor microenvironment mediated hyper-activation of LOX/ITGA5/FAK/Src axis as one of the chemoresistance mechanisms in TNBCs. Mechanistically, hypoxia-induced HIF1A transcriptionally activates LOX which then hyper-activates integrin signaling indirectly due to reduced matrix crosslinking and *via* regulating ITGA5 expression. Hypoxia also inhibits miR-142-3p, a miRNA able to target all three main players (HIF1A, LOX and ITGA5) of doxorubicin resistance in TNBCs. Therefore, we propose that suppressing LOX by a LOX inhibitor, e.g. BAPN, or activating miR-142-3p can modulate ITGA5/FAK/Src axis and sensitize TNBC cells to chemotherapy.

LOX belongs to a heterogeneous family of copper-dependent amine oxidases that catalyzes the crosslinking of collagen fibers and elastins to maintain rigidity in ECM. [186]. It has been well-established that changes in collagen crosslinking and ECM stiffness in extracellular vicinity by LOX and other family members promote tumor cells invasion and metastasis [189]. For example, increased ECM crosslinking due to high expression of LOX in primary tumors has been shown as driving factor towards bone metastasis in breast cancer by forming pre-metastatic lesions [190]. The results presented in this dissertation, shows that LOX is upregulated in chemotherapy resistant tumors, works as a regulator of chemotherapy resistance in TNBC and whose inhibition can

sensitize tumor cells to chemotherapy treatment. It is interesing to test whether increased LOX expression-mediated changes in ECM crosslinking and stiffness play any direct or indirect role in regulating chemotherapy resistance or not.

As LOX expression correlated well with ITGA5 expression both *in vivo* and in multiple online available breast cancer patient datasets, it will be interesting to test whether LOX has a direct regulatory effect on ITGA5 expression. Recently, nuclear localization of LOX has been taken into consideration and LOX has been found regulating SNAI2 gene at transcriptional level; thus, promoting metastatic potential of cancer cells [209]. These findings suggest a role of LOX in regulating transcriptional activity from ITGA5 promoter which can be elucidated by co-immunoprecipitation and luciferase-based repoter assays. Findings presented in this dissertation also propose that LOX regulates chemotherapy resistance in TNBCs by hyperactivating ITGA5/FAK/Src axis, and inhibtion of LOX or its activity sensitize tumor cells to therapy treatment. It is of importance to test whether manipulating ITGA5 levels at the downstream of LOX can mimic the inhibition of LOX in sensitizing TNBC cells to chemotherapy treatment.

In vivo experiments have shown that inhibtion of LOX expression or pharmacological inhibition of LOX activity sensitizes cells to doxorubicin treatment. As these experiments were performed by developing tumors using human TNBC cell lines, they do not represent the actual tumor heterogeneity usually observed in patients. Therefore, performing these experiments using chemoresistant pateint-derived xenograft (PDX) models of TNBCs representing actual disease scnenerio will further confirm the findings. In addition, similar experiments will also help in identifying that LOX inhibtion-mediated chemotherapy sensitization of TNBC cells is only restricted to doxorubicin (anthracycline) or it is a general phenomenon extended to other classes of chemotherapy agents as well.

The results presented in this dissertation propose that inhibition of LOX has potential to synergize with chemotherapy treatment; thus, overcoming therapy resistance in TNBCs. In addition, importance of LOX in driving cell proliferation, invasion, and metastasis as well as in promoting angiogenesis and malignant transformation has suggested it as a potent target in solid tumor setting. However, little progress has been made in the development of suitable small molecule inhibitors targeting LOX. One of the major reasons is the lack of a complete crystal structure of LOX precluding it from classical structure driven fragment-based drug development and screening approaches [187]. BAPN has been widely used as the LOX inhibitor since the early 1970s [210]. Unfortunately, BAPN is a non-specific inhibitor of LOX, showing affinity for multiple LOX family members as well as other amine oxidases. In addition, extremely simple structure of BAPN permits unselective biological interactions which can cause multiple unwanted side effects; thus, preventing its use as therapeutics [211]. Notably, *in vitro* dose of BAPN to inhibit LOX is already so high (in mM range) that its quite unlikely to be used as a therapeutics in human. Therefore, it is important to identify novel inhibitors of LOX which can be used in combination with different chemotherapy agents without any combined therapy-associated side effects and toxicities in clinics. Identifying/designing novel LOX inhibitor will not only assist in treating chemotherapy-resistant solid tumors, but will also be helpful in limiting metastatic spread of advance stage cancer in clinics as LOX has been extensively shown as promising candidate to inhibit metastasis.

Bibliography

1. Breastcancer.org, *U.S. Breast Cancer Statistics*. Retrieved from: http://www.breastcancer.org/symptoms/understand_bc/statistics, 2017.

2. Siegel, R., D. Naishadham, and A. Jemal, *Cancer statistics, 2013.* CA Cancer J Clin, 2013. **63**(1): p. 11-30.

3. Jemal, A., et al., *Cancer statistics, 2010.* CA Cancer J Clin, 2010. **60**(5): p. 277-300.

4. de Ronde, J., L. Wessels, and J. Wesseling, *Molecular subtyping of breast cancer: ready to use?* Lancet Oncol, 2010. **11**(4): p. 306-7.

5. Sorlie, T., et al., *Repeated observation of breast tumor subtypes in independent gene expression data sets.* Proc Natl Acad Sci U S A, 2003. **100**(14): p. 8418-23.

6. Morgan, D.A., N.A. Refalo, and K.L. Cheung, *Strength of ER-positivity in relation to survival in ER-positive breast cancer treated by adjuvant tamoxifen as sole systemic therapy.* Breast, 2011. **20**(3): p. 215-9.

7. Gajria, D. and S. Chandarlapaty, *HER2-amplified breast cancer: mechanisms of trastuzumab resistance and novel targeted therapies.* Expert Rev Anticancer Ther, 2011. **11**(2): p. 263-75.

8. Yarden, Y. and G. Pines, *The ERBB network: at last, cancer therapy meets systems biology.* Nat Rev Cancer, 2012. **12**(8): p. 553-63.

9. Ryan, Q., et al., *FDA drug approval summary: lapatinib in combination with capecitabine for previously treated metastatic breast cancer that overexpresses HER-2.* Oncologist, 2008. **13**(10): p. 1114-9.

10. Sorlie, T., et al., *Gene expression patterns of breast carcinomas distinguish tumor subclasses with clinical implications.* Proc Natl Acad Sci U S A, 2001. **98**(19): p. 10869-74.

11. Mayer, E.L. and H.J. Burstein, *Chemotherapy for Triple-Negative Breast Cancer: Is More Better?* J Clin Oncol, 2016. **34**(28): p. 3369-71.

12. Zahreddine, H. and K.L. Borden, *Mechanisms and insights into drug resistance in cancer.* Front Pharmacol, 2013. **4**: p. 28.

13. Osborne, C.K., et al., *Role of the estrogen receptor coactivator AIB1 (SRC-3) and HER-2/neu in tamoxifen resistance in breast cancer.* J Natl Cancer Inst, 2003. **95**(5): p. 353-61.

14. Smith, C.L., Z. Nawaz, and B.W. O'Malley, *Coactivator and corepressor regulation of the agonist/antagonist activity of the mixed antiestrogen, 4-hydroxytamoxifen.* Mol Endocrinol, 1997. **11**(6): p. 657-66.

15. Shou, J., et al., *Mechanisms of tamoxifen resistance: increased estrogen receptor-HER2/neu cross-talk in ER/HER2-positive breast cancer.* J Natl Cancer Inst, 2004. **96**(12): p. 926-35.

16. Turner, N., et al., *FGFR1 amplification drives endocrine therapy resistance and is a therapeutic target in breast cancer.* Cancer Res, 2010. **70**(5): p. 2085-94.

17. Zhang, Y., et al., *Elevated insulin-like growth factor 1 receptor signaling induces antiestrogen resistance through the MAPK/ERK and PI3K/Akt signaling routes.* Breast Cancer Res, 2011. **13**(3): p. R52.

18. Sharma, D., et al., *Release of methyl CpG binding proteins and histone deacetylase 1 from the Estrogen receptor alpha (ER) promoter upon reactivation in ER-negative human breast cancer cells.* Mol Endocrinol, 2005. **19**(7): p. 1740-51.

19. Goetz, M.P., et al., *Pharmacogenetics of tamoxifen biotransformation is associated with clinical outcomes of efficacy and hot flashes.* J Clin Oncol, 2005. **23**(36): p. 9312-8.

20. Desta, Z., et al., *Comprehensive evaluation of tamoxifen sequential biotransformation by the human cytochrome P450 system in vitro: prominent roles for CYP3A and CYP2D6.* J Pharmacol Exp Ther, 2004. **310**(3): p. 1062-75.

21. Garcia-Becerra, R., et al., *Mechanisms of resistance to endocrine therapy in breast cancer: focus on signaling pathways, miRNAs and genetically based resistance.* Int J Mol Sci, 2012. **14**(1): p. 108-45.

22. Jansen, M.P., et al., *Hallmarks of aromatase inhibitor drug resistance revealed by epigenetic profiling in breast cancer.* Cancer Res, 2013. **73**(22): p. 6632-41.

23. Choi, H.J., et al., *Targeting interferon response genes sensitizes aromatase inhibitor resistant breast cancer cells to estrogen-induced cell death.* Breast Cancer Res, 2015. **17**: p. 6.

24. Thiantanawat, A., B.J. Long, and A.M. Brodie, *Signaling pathways of apoptosis activated by aromatase inhibitors and antiestrogens.* Cancer Res, 2003. **63**(22): p. 8037-50.

25. Lee, J.J., K. Loh, and Y.S. Yap, *PI3K/Akt/mTOR inhibitors in breast cancer.* Cancer Biol Med, 2015. **12**(4): p. 342-54.

26. Xu, H., et al., *Recent advances of highly selective CDK4/6 inhibitors in breast cancer.* J Hematol Oncol, 2017. **10**(1): p. 97.

27. Scott, G.K., et al., *A truncated intracellular HER2/neu receptor produced by alternative RNA processing affects growth of human carcinoma cells.* Mol Cell Biol, 1993. **13**(4): p. 2247-57.

28. Christianson, T.A., et al., *NH2-terminally truncated HER-2/neu protein: relationship with shedding of the extracellular domain and with prognostic factors in breast cancer.* Cancer Res, 1998. **58**(22): p. 5123-9.

29. Scaltriti, M., et al., *Expression of p95HER2, a truncated form of the HER2 receptor, and response to anti-HER2 therapies in breast cancer.* J Natl Cancer Inst, 2007. **99**(8): p. 628-38.

30. Lu, Y., et al., *Insulin-like growth factor-I receptor signaling and resistance to trastuzumab (Herceptin).* J Natl Cancer Inst, 2001. **93**(24): p. 1852-7.

31. Garrett, J.T. and C.L. Arteaga, *Resistance to HER2-directed antibodies and tyrosine kinase inhibitors: mechanisms and clinical implications.* Cancer Biol Ther, 2011. **11**(9): p. 793-800.

32. Bailey, T.A., et al., *Mechanisms of Trastuzumab resistance in ErbB2-driven breast cancer and newer opportunities to overcome therapy resistance.* J Carcinog, 2011. **10**: p. 28.

33. Pohlmann, P.R., I.A. Mayer, and R. Mernaugh, *Resistance to Trastuzumab in Breast Cancer.* Clin Cancer Res, 2009. **15**(24): p. 7479-7491.

34. Valabrega, G., F. Montemurro, and M. Aglietta, *Trastuzumab: mechanism of action, resistance and future perspectives in HER2-overexpressing breast cancer.* Ann Oncol, 2007. **18**(6): p. 977-84.

35. Vu, T. and F.X. Claret, *Trastuzumab: updated mechanisms of action and resistance in breast cancer.* Front Oncol, 2012. **2**: p. 62.

36. Lavaud, P. and F. Andre, *Strategies to overcome trastuzumab resistance in HER2-overexpressing breast cancers: focus on new data from clinical trials.* BMC Med, 2014. **12**: p. 132.

37. Sahin, O., et al., *Biomarker-guided sequential targeted therapies to overcome therapy resistance in rapidly evolving highly aggressive mammary tumors.* Cell Res, 2014. **24**(5): p. 542-59.

38. Hurvitz, S.A., et al., *A phase 2 study of everolimus combined with trastuzumab and paclitaxel in patients with HER2-overexpressing advanced breast cancer that progressed during prior trastuzumab and taxane therapy.* Breast Cancer Res Treat, 2013. **141**(3): p. 437-46.

39. Verma, S., et al., *Trastuzumab emtansine for HER2-positive advanced breast cancer.* N Engl J Med, 2012. **367**(19): p. 1783-91.

40. Cortazar, P., et al., *Pathological complete response and long-term clinical benefit in breast cancer: the CTNeoBC pooled analysis.* Lancet, 2014. **384**(9938): p. 164-72.

41. Prowell, T.M. and R. Pazdur, *Pathological complete response and accelerated drug approval in early breast cancer.* N Engl J Med, 2012. **366**(26): p. 2438-41.

42. Liedtke, C., et al., *Response to neoadjuvant therapy and long-term survival in patients with triple-negative breast cancer.* J Clin Oncol, 2008. **26**(8): p. 1275-81.

43. Wein, L. and S. Loi, *Mechanisms of resistance of chemotherapy in early-stage triple negative breast cancer (TNBC).* Breast, 2017.

44. Godwin, P., et al., *Targeting nuclear factor-kappa B to overcome resistance to chemotherapy.* Front Oncol, 2013. **3**: p. 120.

45. Tan, C. and T.A. Waldmann, *Proteasome inhibitor PS-341, a potential therapeutic agent for adult T-cell leukemia.* Cancer Res, 2002. **62**(4): p. 1083-6.

46. Croghan, G.A., et al., *A study of paclitaxel, carboplatin, and bortezomib in the treatment of metastatic malignant melanoma: a phase 2 consortium study.* Cancer, 2010. **116**(14): p. 3463-8.

47. Grassilli, E., et al., *Loss of MYC confers resistance to doxorubicin-induced apoptosis by preventing the activation of multiple serine protease- and caspase-mediated pathways.* J Biol Chem, 2004. **279**(20): p. 21318-26.

48. Deffie, A.M., et al., *Multifactorial resistance to adriamycin: relationship of DNA repair, glutathione transferase activity, drug efflux, and P-glycoprotein in cloned cell lines of adriamycin-sensitive and -resistant P388 leukemia.* Cancer Res, 1988. **48**(13): p. 3595-602.

49. Calcagno, A.M., et al., *Single-step doxorubicin-selected cancer cells overexpress the ABCG2 drug transporter through epigenetic changes.* Br J Cancer, 2008. **98**(9): p. 1515-24.

50. Sladek, N.E., et al., *Cellular levels of aldehyde dehydrogenases (ALDH1A1 and ALDH3A1) as predictors of therapeutic responses to cyclophosphamide-based chemotherapy of breast cancer: a retrospective study. Rational individualization of oxazaphosphorine-based cancer chemotherapeutic regimens.* Cancer Chemother Pharmacol, 2002. **49**(4): p. 309-21.

51. Sun, Y., *Tumor microenvironment and cancer therapy resistance.* Cancer Lett, 2016. **380**(1): p. 205-15.

52. Friedl, P. and S. Alexander, *Cancer invasion and the microenvironment: plasticity and reciprocity*. Cell, 2011. **147**(5): p. 992-1009.

53. Weaver, V.M., et al., *beta4 integrin-dependent formation of polarized three-dimensional architecture confers resistance to apoptosis in normal and malignant mammary epithelium.* Cancer Cell, 2002. **2**(3): p. 205-16.

54. Sun, Y., *Translational horizons in the tumor microenvironment: harnessing breakthroughs and targeting cures.* Med Res Rev, 2015. **35**(2): p. 408-36.

55. Seguin, L., et al., *An integrin beta(3)-KRAS-RalB complex drives tumour stemness and resistance to EGFR inhibition.* Nat Cell Biol, 2014. **16**(5): p. 457-68.

56. Goel, H.L., et al., *beta1 integrins mediate resistance to ionizing radiation in vivo by inhibiting c-Jun amino terminal kinase 1*. J Cell Physiol, 2013. **228**(7): p. 1601-9.

57. Olive, K.P., et al., *Inhibition of Hedgehog signaling enhances delivery of chemotherapy in a mouse model of pancreatic cancer*. Science, 2009. **324**(5933): p. 1457-61.

58. Fidler, I.J., *The pathogenesis of cancer metastasis: the 'seed and soil' hypothesis revisited.* Nat Rev Cancer, 2003. **3**(6): p. 453-8.

59. Weigelt, B., J.L. Peterse, and L.J. van 't Veer, *Breast cancer metastasis: markers and models.* Nat Rev Cancer, 2005. **5**(8): p. 591-602.

60. Gong, Y., et al., *Impact of molecular subtypes on metastatic breast cancer patients: a SEER population-based study.* Sci Rep, 2017. **7**: p. 45411.

61. Kimbung, S., N. Loman, and I. Hedenfalk, *Clinical and molecular complexity of breast cancer metastases.* Semin Cancer Biol, 2015. **35**: p. 85-95.

62. Minn, A.J., et al., *Genes that mediate breast cancer metastasis to lung.* Nature, 2005. **436**(7050): p. 518-24.

63. Bos, P.D., et al., *Genes that mediate breast cancer metastasis to the brain.* Nature, 2009. **459**(7249): p. 1005-9.

64. He, L. and G.J. Hannon, *MicroRNAs: small RNAs with a big role in gene regulation.* Nat Rev Genet, 2004. **5**(7): p. 522-31.

65. Singh, S.K., et al., *MicroRNAs--micro in size but macro in function.* FEBS J, 2008. **275**(20): p. 4929-44.

66. Inui, M., G. Martello, and S. Piccolo, *MicroRNA control of signal transduction.* Nat Rev Mol Cell Biol, 2010. **11**(4): p. 252-63.

67. Kozomara, A. and S. Griffiths-Jones, *miRBase: integrating microRNA annotation and deep-sequencing data.* Nucleic Acids Res, 2011. **39**(Database issue): p. D152-7.

68. Borchert, G.M., W. Lanier, and B.L. Davidson, *RNA polymerase III transcribes human microRNAs.* Nat Struct Mol Biol, 2006. **13**(12): p. 1097-101.

69. Bohnsack, M.T., K. Czaplinski, and D. Gorlich, *Exportin 5 is a RanGTP-dependent dsRNA-binding protein that mediates nuclear export of pre-miRNAs.* RNA, 2004. **10**(2): p. 185-91.

70. Winter, J., et al., *Many roads to maturity: microRNA biogenesis pathways and their regulation.* Nat Cell Biol, 2009. **11**(3): p. 228-34.

71. Orom, U.A., F.C. Nielsen, and A.H. Lund, *MicroRNA-10a binds the 5'UTR of ribosomal protein mRNAs and enhances their translation.* Mol Cell, 2008. **30**(4): p. 460-71.

72. Forman, J.J., A. Legesse-Miller, and H.A. Coller, *A search for conserved sequences in coding regions reveals that the let-7 microRNA targets Dicer within its coding sequence.* Proc Natl Acad Sci U S A, 2008. **105**(39): p. 14879-84.

73. Calin, G.A., et al., *Human microRNA genes are frequently located at fragile sites and genomic regions involved in cancers.* Proc Natl Acad Sci U S A, 2004. **101**(9): p. 2999-3004.

74. Ambros, V., *microRNAs: tiny regulators with great potential.* Cell, 2001. **107**(7): p. 823-6.

75. Friedman, R.C., et al., *Most mammalian mRNAs are conserved targets of microRNAs.* Genome Res, 2009. **19**(1): p. 92-105.

76. Raza, U., J.D. Zhang, and O. Sahin, *MicroRNAs: master regulators of drug resistance, stemness, and metastasis.* J Mol Med (Berl), 2014. **92**(4): p. 321-36.

77. Jin, H.Y., et al., *MicroRNA-17~92 plays a causative role in lymphomagenesis by coordinating multiple oncogenic pathways.* EMBO J, 2013. **32**(17): p. 2377-91.

78. D'Amato, N.C., E.N. Howe, and J.K. Richer, *MicroRNA regulation of epithelial plasticity in cancer.* Cancer Lett, 2013. **341**(1): p. 46-55.

79. Si, M.L., et al., *miR-21-mediated tumor growth.* Oncogene, 2007. **26**(19): p. 2799-803.

80. Gironella, M., et al., *Tumor protein 53-induced nuclear protein 1 expression is repressed by miR-155, and its restoration inhibits pancreatic tumor development.* Proc Natl Acad Sci U S A, 2007. **104**(41): p. 16170-5.

81. Johnson, C.D., et al., *The let-7 microRNA represses cell proliferation pathways in human cells.* Cancer Res, 2007. **67**(16): p. 7713-22.

82. Raver-Shapira, N., et al., *Transcriptional activation of miR-34a contributes to p53-mediated apoptosis.* Mol Cell, 2007. **26**(5): p. 731-43.

83. Blower, P.E., et al., *MicroRNAs modulate the chemosensitivity of tumor cells.* Mol Cancer Ther, 2008. **7**(1): p. 1-9.

84. Weeraratne, S.D., et al., *miR-34a confers chemosensitivity through modulation of MAGE-A and p53 in medulloblastoma.* Neuro Oncol, 2011. **13**(2): p. 165-75.

85. Takwi, A.A., et al., *miR-137 regulates the constitutive androstane receptor and modulates doxorubicin sensitivity in parental and doxorubicin-resistant neuroblastoma cells.* Oncogene, 2013.

86. Zhao, J.J., et al., *MicroRNA-221/222 negatively regulates estrogen receptor alpha and is associated with tamoxifen resistance in breast cancer.* J Biol Chem, 2008. **283**(45): p. 31079-86.

87. Miller, T.E., et al., *MicroRNA-221/222 confers tamoxifen resistance in breast cancer by targeting p27Kip1.* J Biol Chem, 2008. **283**(44): p. 29897-903.

88. Rao, X., et al., *MicroRNA-221/222 confers breast cancer fulvestrant resistance by regulating multiple signaling pathways.* Oncogene, 2011. **30**(9): p. 1082-97.

89. Ward, A., et al., *Re-expression of microRNA-375 reverses both tamoxifen resistance and accompanying EMT-like properties in breast cancer.* Oncogene, 2013. **32**(9): p. 1173-82.

90. Valastyan, S., et al., *Concurrent suppression of integrin alpha5, radixin, and RhoA phenocopies the effects of miR-31 on metastasis.* Cancer Res, 2010. **70**(12): p. 5147-54.

91. Keklikoglou, I., et al., *MicroRNA-520/373 family functions as a tumor suppressor in estrogen receptor negative breast cancer by targeting NF-kappaB and TGF-beta signaling pathways.* Oncogene, 2012. **31**(37): p. 4150-63.

92. Korpal, M., et al., *Direct targeting of Sec23a by miR-200s influences cancer cell secretome and promotes metastatic colonization.* Nat Med, 2011. **17**(9): p. 1101-8.

93. Tao, Z.H., et al., *miR-612 suppresses the invasive-metastatic cascade in hepatocellular carcinoma.* J Exp Med, 2013. **210**(4): p. 789-803.

94. Li, Z. and T.M. Rana, *Therapeutic targeting of microRNAs: current status and future challenges.* Nat Rev Drug Discov, 2014. **13**(8): p. 622-38.

95. Garzon, R., G. Marcucci, and C.M. Croce, *Targeting microRNAs in cancer: rationale, strategies and challenges.* Nat Rev Drug Discov, 2010. **9**(10): p. 775-89.

96. Janssen, H.L., et al., *Treatment of HCV infection by targeting microRNA.* N Engl J Med, 2013. **368**(18): p. 1685-94.

97. Bouchie, A., *First microRNA mimic enters clinic.* Nat Biotechnol, 2013. **31**(7): p. 577.

98. Agostini, M. and R.A. Knight, *miR-34: from bench to bedside.* Oncotarget, 2014. **5**(4): p. 872-81.

99. Yoo, B., et al., *Combining miR-10b-Targeted Nanotherapy with Low-Dose Doxorubicin Elicits Durable Regressions of Metastatic Breast Cancer.* Cancer Res, 2015. **75**(20): p. 4407-15.

100. Sanjana, N.E., O. Shalem, and F. Zhang, *Improved vectors and genome-wide libraries for CRISPR screening.* Nat Methods, 2014. **11**(8): p. 783-4.

101. Heigwer, F., G. Kerr, and M. Boutros, *E-CRISP: fast CRISPR target site identification.* Nat Methods, 2014. **11**(2): p. 122-3.

102. Fedchenko, N. and J. Reifenrath, *Different approaches for interpretation and reporting of immunohistochemistry analysis results in the bone tissue - a review.* Diagn Pathol, 2014. **9**: p. 221.

103. Smyth, G.K., *Linear models and empirical bayes methods for assessing differential expression in microarray experiments.* Stat Appl Genet Mol Biol, 2004. **3**: p. Article3.

104. Raza, U., et al., *The miR-644a/CTBP1/p53 axis suppresses drug resistance by simultaneous inhibition of cell survival and epithelial-mesenchymal transition in breast cancer*. Oncotarget, 2016. **7**(31): p. 49859-49877.

105. Ivshina, A.V., et al., *Genetic reclassification of histologic grade delineates new clinical subtypes of breast cancer.* Cancer Res, 2006. **66**(21): p. 10292-301.

106. Desmedt, C., et al., *Multifactorial approach to predicting resistance to anthracyclines.* J Clin Oncol, 2011. **29**(12): p. 1578-86.

107. Enerly, E., et al., *miRNA-mRNA integrated analysis reveals roles for miRNAs in primary breast tumors.* PLoS One, 2011. **6**(2): p. e16915.

108. Buffa, F.M., et al., *microRNA-associated progression pathways and potential therapeutic targets identified by integrated mRNA and microRNA expression profiling in breast cancer.* Cancer Res, 2011. **71**(17): p. 5635-45.

109. Sabatier, R., et al., *A gene expression signature identifies two prognostic subgroups of basal breast cancer.* Breast Cancer Res Treat, 2011. **126**(2): p. 407-20.

110. Esserman, L.J., et al., *Chemotherapy response and recurrence-free survival in neoadjuvant breast cancer depends on biomarker profiles: results from the I-SPY 1 TRIAL (CALGB 150007/150012; ACRIN 6657).* Breast Cancer Res Treat, 2012. **132**(3): p. 1049-62.

111. Hatzis, C., et al., *A genomic predictor of response and survival following taxane-anthracycline chemotherapy for invasive breast cancer.* JAMA, 2011. **305**(18): p. 1873-81.

112. Namlos, H.M., et al., *Modulation of the osteosarcoma expression phenotype by microRNAs.* PLoS One, 2012. **7**(10): p. e48086.

113. Xiao, D., et al., *Identifying mRNA, microRNA and protein profiles of melanoma exosomes.* PLoS One, 2012. **7**(10): p. e46874.

114. Avery-Kiejda, K.A., et al., *Decreased expression of key tumour suppressor microRNAs is associated with lymph node metastases in triple negative breast cancer.* BMC Cancer, 2014. **14**: p. 51.

115. Luo, D., et al., *A systematic evaluation of miRNA:mRNA interactions involved in the migration and invasion of breast cancer cells.* J Transl Med, 2013. **11**: p. 57.

116. Gruosso, T., et al., *Chronic oxidative stress promotes H2AX protein degradation and enhances chemosensitivity in breast cancer patients.* EMBO Mol Med, 2016. **8**(5): p. 527-49.

117. Lee, C.H., et al., *MicroRNA-regulated protein-protein interaction networks and their functions in breast cancer.* Int J Mol Sci, 2013. **14**(6): p. 11560-606.

118. Mudduluru, G., et al., *A Systematic Approach to Defining the microRNA Landscape in Metastasis.* Cancer Res, 2015. **75**(15): p. 3010-9.

119. Matamala, N., et al., *Tumor microRNA expression profiling identifies circulating microRNAs for early breast cancer detection.* Clin Chem, 2015. **61**(8): p. 1098-106.

120. Tofigh, A., et al., *The prognostic ease and difficulty of invasive breast carcinoma.* Cell Rep, 2014. **9**(1): p. 129-42.

121. Jezequel, P., et al., *Gene-expression molecular subtyping of triple-negative breast cancer tumours: importance of immune response.* Breast Cancer Res, 2015. **17**: p. 43.

122. Cabral, V., et al., *Targeted changes of the cell wall proteome influence Candida albicans ability to form single- and multi-strain biofilms.* PLoS Pathog, 2014. **10**(12): p. e1004542.

123. Gyorffy, B., et al., *An online survival analysis tool to rapidly assess the effect of 22,277 genes on breast cancer prognosis using microarray data of 1,809 patients.* Breast Cancer Res Treat, 2010. **123**(3): p. 725-31.

124. Curtis, C., et al., *The genomic and transcriptomic architecture of 2,000 breast tumours reveals novel subgroups.* Nature, 2012. **486**(7403): p. 346-52.

125. Huang da, W., B.T. Sherman, and R.A. Lempicki, *Systematic and integrative analysis of large gene lists using DAVID bioinformatics resources.* Nat Protoc, 2009. **4**(1): p. 44-57.

126. Xu, J., et al., *14-3-3zeta turns TGF-beta's function from tumor suppressor to metastasis promoter in breast cancer by contextual changes of Smad partners from p53 to Gli2.* Cancer Cell, 2015. **27**(2): p. 177-92.

127. Dancik, G.M. and D. Theodorescu, *Robust prognostic gene expression signatures in bladder cancer and lung adenocarcinoma depend on cell cycle related genes.* PLoS One, 2014. **9**(1): p. e85249.

128. Troester, M.A., et al., *Gene expression patterns associated with p53 status in breast cancer*. BMC Cancer, 2006. **6**: p. 276.

129. Drăghici, S., *Statistics and data analysis for microarrays using R and Bioconductor*. Chapman & Hall/CRC mathematical and computational biology. 2012, Boca Raton, FL: CRC Press. xlviii, 1042 p.

130. Jurmeister, S., et al., *MicroRNA-200c represses migration and invasion of breast cancer cells by targeting actin-regulatory proteins FHOD1 and PPM1F*. Mol Cell Biol, 2012. **32**(3): p. 633-51.

131. Kopp, F., et al., *miR-200c sensitizes breast cancer cells to doxorubicin treatment by decreasing TrkB and Bmi1 expression.* PLoS One, 2012. **7**(11): p. e50469.

132. Liu, L., et al., *miR-200c Inhibits invasion, migration and proliferation of bladder cancer cells through down-regulation of BMI-1 and E2F3.* J Transl Med, 2014. **12**(1): p. 305.

133. Jong, H.L., et al., *MicroRNA 299-3p modulates replicative senescence in endothelial cells.* Physiol Genomics, 2013. **45**(7): p. 256-67.

134. Willers, I.M., et al., *miR-127-5p targets the 3'UTR of human beta-F1-ATPase mRNA and inhibits its translation.* Biochim Biophys Acta, 2012. **1817**(5): p. 838-48.

135. Jordan, V.C., *Tamoxifen as the first targeted long-term adjuvant therapy for breast cancer.* Endocr Relat Cancer, 2014. **21**(3): p. R235-46.

136. Kobayashi, S., et al., *Transcriptional profiling identifies cyclin D1 as a critical downstream effector of mutant epidermal growth factor receptor signaling.* Cancer Res, 2006. **66**(23): p. 11389-98.

137. Bergman, L.M., et al., *CtBPs promote cell survival through the maintenance of mitotic fidelity.* Mol Cell Biol, 2009. **29**(16): p. 4539-51.

138. Birts, C.N., et al., *Expression of CtBP family protein isoforms in breast cancer and their role in chemoresistance.* Biol Cell, 2010. **103**(1): p. 1-19.

139. Pena, C., et al., *The expression levels of the transcriptional regulators p300 and CtBP modulate the correlations between SNAIL, ZEB1, E-cadherin and vitamin D receptor in human colon carcinomas.* Int J Cancer, 2006. **119**(9): p. 2098-104.

140. Vousden, K.H. and X. Lu, *Live or let die: the cell's response to p53.* Nat Rev Cancer, 2002. **2**(8): p. 594-604.

141. Grooteclaes, M., et al., *C-terminal-binding protein corepresses epithelial and proapoptotic gene expression programs.* Proc Natl Acad Sci U S A, 2003. **100**(8): p. 4568-73.

142. Di, L.J., et al., *Genome-wide profiles of CtBP link metabolism with genome stability and epithelial reprogramming in breast cancer.* Nat Commun, 2013. **4**: p. 1449.

143. Kovach, J.S., et al., *Mutation detection by highly sensitive methods indicates that p53 gene mutations in breast cancer can have important prognostic value.* Proc Natl Acad Sci U S A, 1996. **93**(3): p. 1093-6.

144. Murakami, I., et al., *p53 gene mutations are associated with shortened survival in patients with advanced non-small cell lung cancer: an analysis of medically managed patients.* Clin Cancer Res, 2000. **6**(2): p. 526-30.

145. Gyorffy, B., et al., *Online survival analysis software to assess the prognostic value of biomarkers using transcriptomic data in non-small-cell lung cancer.* PLoS One, 2013. **8**(12): p. e82241.

146. Humphries, J.D., A. Byron, and M.J. Humphries, *Integrin ligands at a glance.* J Cell Sci, 2006. **119**(Pt 19): p. 3901-3.

147. Bertucci, F., et al., *How basal are triple-negative breast cancers?* Int J Cancer, 2008. **123**(1): p. 236-40.

148. Wilson, W.R. and M.P. Hay, *Targeting hypoxia in cancer therapy.* Nat Rev Cancer, 2011. **11**(6): p. 393-410.

149. Erler, J.T., et al., *Lysyl oxidase is essential for hypoxia-induced metastasis.* Nature, 2006. **440**(7088): p. 1222-6.

150. Tredan, O., et al., *Drug resistance and the solid tumor microenvironment.* J Natl Cancer Inst, 2007. **99**(19): p. 1441-54.

151. Ben-Hamo, R. and S. Efroni, *MicroRNA regulation of molecular pathways as a generic mechanism and as a core disease phenotype.* Oncotarget, 2015. **6**(3): p. 1594-604.

152. Uhlmann, S., et al., *Global microRNA level regulation of EGFR-driven cell-cycle protein network in breast cancer.* Mol Syst Biol, 2012. **8**: p. 570.

153. Kozomara, A. and S. Griffiths-Jones, *miRBase: annotating high confidence microRNAs using deep sequencing data.* Nucleic Acids Res, 2014. **42**(Database issue): p. D68-73.

154. Diaz-Beya, M., et al., *MicroRNA expression at diagnosis adds relevant prognostic information to molecular categorization in patients with intermediate-risk cytogenetic acute myeloid leukemia.* Leukemia, 2014. **28**(4): p. 804-12.

155. Scheffer, A.R., et al., *Circulating microRNAs in serum: novel biomarkers for patients with bladder cancer?* World J Urol, 2014. **32**(2): p. 353-8.

156. Ostling, P., et al., *Systematic analysis of microRNAs targeting the androgen receptor in prostate cancer cells.* Cancer Res, 2011. **71**(5): p. 1956-67.

157. Zhang, J.X., et al., *Downregulation of MicroRNA-644a Promotes Esophageal Squamous Cell Carcinoma Aggressiveness and Stem Cell-like Phenotype via Dysregulation of PITX2*. Clin Cancer Res, 2017. **23**(1): p. 298-310.

158. Li, Y., et al., *miR-644a inhibits cellular proliferation and invasion via suppression of CtBP1 in gastric cancer cells.* Oncol Res, 2016.

159. Boyd, J.M., et al., *A region in the C-terminus of adenovirus 2/5 E1a protein is required for association with a cellular phosphoprotein and important for the negative modulation of T24-ras mediated transformation, tumorigenesis and metastasis.* EMBO J, 1993. **12**(2): p. 469-78.

160. Wang, R., et al., *Role of transcriptional corepressor CtBP1 in prostate cancer progression.* Neoplasia, 2012. **14**(10): p. 905-14.

161. Deng, H., et al., *CtBP1 is expressed in melanoma and represses the transcription of p16INK4a and Brca1*. J Invest Dermatol, 2013. **133**(5): p. 1294-301.

162. Zhang, X.L., et al., *CtBP1 is involved in epithelial-mesenchymal transition and is a potential therapeutic target for hepatocellular carcinoma.* Oncol Rep, 2013. **30**(2): p. 809-14.

163. Deng, Y., et al., *MicroRNA-137 targets carboxyl-terminal binding protein 1 in melanoma cell lines.* Int J Biol Sci, 2011. **7**(1): p. 133-7.

164. Haupt, S., et al., *Apoptosis - the p53 network.* J Cell Sci, 2003. **116**(Pt 20): p. 4077-85.

165. Fridman, J.S. and S.W. Lowe, *Control of apoptosis by p53.* Oncogene, 2003. **22**(56): p. 9030-40.

166. Herold, S., et al., *Negative regulation of the mammalian UV response by Myc through association with Miz-1*. Mol Cell, 2002. **10**(3): p. 509-21.

167. Seoane, J., H.V. Le, and J. Massague, *Myc suppression of the p21(Cip1) Cdk inhibitor influences the outcome of the p53 response to DNA damage.* Nature, 2002. **419**(6908): p. 729-34.

168. Raycroft, L., et al., *Analysis of p53 mutants for transcriptional activity.* Mol Cell Biol, 1991. **11**(12): p. 6067-74.

169. Wright, J.D. and C. Lim, *Mechanism of DNA-binding loss upon single-point mutation in p53.* J Biosci, 2007. **32**(5): p. 827-39.

170. Speidel, D., H. Helmbold, and W. Deppert, *Dissection of transcriptional and non-transcriptional p53 activities in the response to genotoxic stress.* Oncogene, 2006. **25**(6): p. 940-53.

171. Ryan, K.M. and K.H. Vousden, *Characterization of structural p53 mutants which show selective defects in apoptosis but not cell cycle arrest.* Mol Cell Biol, 1998. **18**(7): p. 3692-8.

172. Haupt, Y., et al., *Induction of apoptosis in HeLa cells by trans-activation-deficient p53.* Genes Dev, 1995. **9**(17): p. 2170-83.

173. He, M., et al., *A mutant P53 can activate apoptosis through a mechanism distinct from those induced by wild type P53.* FEBS Lett, 2002. **517**(1-3): p. 151-4.

174. Lee, C.G., et al., *MicroRNA-147 induces a mesenchymal-to-epithelial transition (MET) and reverses EGFR inhibitor resistance.* PLoS One, 2014. **9**(1): p. e84597.

175. Jin, W., et al., *Involvement of CtBP1 in the transcriptional activation of the MDR1 gene in human multidrug resistant cancer cells.* Biochem Pharmacol, 2007. **74**(6): p. 851-9.

176. Blevins, M.A., et al., *Small Molecule, NSC95397, Inhibits the CtBP1-Protein Partner Interaction and CtBP1-Mediated Transcriptional Repression.* J Biomol Screen, 2015. **20**(5): p. 663-72.

177. Oskarsson, T., *Extracellular matrix components in breast cancer progression and metastasis.* Breast, 2013. **22 Suppl 2**: p. S66-72.

178. Stewart, D.A., C.R. Cooper, and R.A. Sikes, *Changes in extracellular matrix (ECM) and ECM-associated proteins in the metastatic progression of prostate cancer.* Reprod Biol Endocrinol, 2004. **2**: p. 2.

179. Bonnans, C., J. Chou, and Z. Werb, *Remodelling the extracellular matrix in development and disease.* Nat Rev Mol Cell Biol, 2014. **15**(12): p. 786-801.

180. Rohwer, N. and T. Cramer, *Hypoxia-mediated drug resistance: novel insights on the functional interaction of HIFs and cell death pathways.* Drug Resist Updat, 2011. **14**(3): p. 191-201.

181. Sullivan, R., et al., *Hypoxia-induced resistance to anticancer drugs is associated with decreased senescence and requires hypoxia-inducible factor-1 activity.* Mol Cancer Ther, 2008. **7**(7): p. 1961-73.

182. Bondareva, A., et al., *The lysyl oxidase inhibitor, beta-aminopropionitrile, diminishes the metastatic colonization potential of circulating breast cancer cells.* PLoS One, 2009. **4**(5): p. e5620.

183. Kirschmann, D.A., et al., *A molecular role for lysyl oxidase in breast cancer invasion.* Cancer Res, 2002. **62**(15): p. 4478-83.

184. Lv, Y., et al., *Hypoxia-inducible factor-1alpha induces multidrug resistance protein in colon cancer*. Onco Targets Ther, 2015. **8**: p. 1941-8.

185. Wigerup, C., S. Pahlman, and D. Bexell, *Therapeutic targeting of hypoxia and hypoxia-inducible factors in cancer.* Pharmacol Ther, 2016. **164**: p. 152-69.

186. Trackman, P.C., *Enzymatic and non-enzymatic functions of the lysyl oxidase family in bone*. Matrix Biol, 2016. **52-54**: p. 7-18.

187. Cox, T.R., A. Gartland, and J.T. Erler, *Lysyl Oxidase, a Targetable Secreted Molecule Involved in Cancer Metastasis.* Cancer Res, 2016. **76**(2): p. 188-92.

188. Payne, S.L., M.J. Hendrix, and D.A. Kirschmann, *Paradoxical roles for lysyl oxidases in cancer--a prospect.* J Cell Biochem, 2007. **101**(6): p. 1338-54.

189. Barker, H.E., T.R. Cox, and J.T. Erler, *The rationale for targeting the LOX family in cancer*. Nat Rev Cancer, 2012. **12**(8): p. 540-52.

190. Cox, T.R., et al., *The hypoxic cancer secretome induces pre-metastatic bone lesions through lysyl oxidase.* Nature, 2015. **522**(7554): p. 106-110.

191. Le Calve, B., et al., *Lysyl oxidase family activity promotes resistance of pancreatic ductal adenocarcinoma to chemotherapy by limiting the intratumoral anticancer drug distribution.* Oncotarget, 2016. **7**(22): p. 32100-12.

192. Lu, P., V.M. Weaver, and Z. Werb, *The extracellular matrix: a dynamic niche in cancer progression.* J Cell Biol, 2012. **196**(4): p. 395-406.

193. Meng, X.N., et al., *Characterisation of fibronectin-mediated FAK signalling pathways in lung cancer cell migration and invasion.* Br J Cancer, 2009. **101**(2): p. 327-34.

194. Lv, M., et al., *An oncogenic role of miR-142-3p in human T-cell acute lymphoblastic leukemia (T-ALL) by targeting glucocorticoid receptor-alpha and cAMP/PKA pathways.* Leukemia, 2012. **26**(4): p. 769-77.

195. Xu, G., et al., *MiR-142-3p functions as a potential tumor suppressor in human osteosarcoma by targeting HMGA1*. Cell Physiol Biochem, 2014. **33**(5): p. 1329-39.

196. Zheng, Z., et al., *MiR-142 acts as a tumor suppressor in osteosarcoma cell lines by targeting Rac1*. Oncol Rep, 2015. **33**(3): p. 1291-9.

197. Xiao, P. and W.L. Liu, *MiR-142-3p functions as a potential tumor suppressor directly targeting HMGB1 in non-small-cell lung carcinoma.* Int J Clin Exp Pathol, 2015. **8**(9): p. 10800-7.

198. Jiang, D., et al., *MiR-142 inhibits the development of cervical cancer by targeting HMGB1*. Oncotarget, 2017. **8**(3): p. 4001-4007.

199. Shen, W.W., et al., *MiR-142-3p functions as a tumor suppressor by targeting CD133, ABCG2, and Lgr5 in colon cancer cells.* J Mol Med (Berl), 2013. **91**(8): p. 989-1000.

200. Schwickert, A., et al., *microRNA miR-142-3p Inhibits Breast Cancer Cell Invasiveness by Synchronous Targeting of WASL, Integrin Alpha V, and Additional Cytoskeletal Elements.* PLoS One, 2015. **10**(12): p. e0143993.

201. Cao, X.C., et al., *miR-142-3p inhibits cancer cell proliferation by targeting CDC25C.* Cell Prolif, 2016. **49**(1): p. 58-68.

202. Zhang, Y., Y. Liu, and X. Xu, *Upregulation of miR-142-3p Improves Drug Sensitivity of Acute Myelogenous Leukemia through Reducing P-Glycoprotein and Repressing Autophagy by Targeting HMGB1*. Transl Oncol, 2017. **10**(3): p. 410-418.

203. Chen, Y., et al., *MiR-142-3p Overexpression Increases Chemo-Sensitivity of NSCLC by Inhibiting HMGB1-Mediated Autophagy.* Cell Physiol Biochem, 2017. **41**(4): p. 1370-1382.

204. Blevins, M.A., M. Huang, and R. Zhao, *The Role of CtBP1 in Oncogenic Processes and Its Potential as a Therapeutic Target.* Mol Cancer Ther, 2017. **16**(6): p. 981-990.

205. Zhang, Y., Z. Wang, and R.A. Gemeinhart, *Progress in microRNA delivery*. J Control Release, 2013. **172**(3): p. 962-74.

206. Straza, M.W., et al., *Therapeutic targeting of C-terminal binding protein in human cancer*. Cell Cycle, 2010. **9**(18): p. 3740-50.

207. Birts, C.N., et al., *A cyclic peptide inhibitor of C-terminal binding protein dimerization links metabolism with mitotic fidelity in breast cancer cells.* Chemical Science, 2013. **4**(8): p. 3046-3057.

208. Parrales, A. and T. Iwakuma, *Targeting Oncogenic Mutant p53 for Cancer Therapy*. Front Oncol, 2015. **5**: p. 288.

209. Boufraqech, M., et al., *Lysyl Oxidase (LOX) Transcriptionally Regulates SNAI2 Expression and TIMP4 Secretion in Human Cancers.* Clin Cancer Res, 2016. **22**(17): p. 4491-504.

210. Narayanan, A.S., R.C. Siegel, and G.R. Martin, *On the inhibition of lysyl oxidase by -aminopropionitrile.* Biochem Biophys Res Commun, 1972. **46**(2): p. 745-51.

211. Granchi, C., et al., *Bioreductively activated lysyl oxidase inhibitors against hypoxic tumours.* ChemMedChem, 2009. **4**(10): p. 1590-4.

Appendix

Copyright permissions for Figures 1.2 and 1.3 can be found on the next 6 pages.

NATURE PUBLISHING GROUP LICENSE TERMS AND CONDITIONS

Sep 04, 2017

This Agreement between Bilkent university -- Umar Raza ("You") and Nature Publishing Group ("Nature Publishing Group") consists of your license details and the terms and conditions provided by Nature Publishing Group and Copyright Clearance Center.

License Number	4182201178461
License date	Sep 04, 2017
Licensed Content Publisher	Nature Publishing Group
Licensed Content Publication	Nature Reviews Cancer
Licensed Content Title	Breast cancer metastasis: markers and models
Licensed Content Author	Britta Weigelt, Johannes L. Peterse and Laura J. van't Veer
Licensed Content Date	Aug 1, 2005
Licensed Content Volume	5
Licensed Content Issue	8
Type of Use	reuse in a dissertation / thesis
Requestor type	academic/educational
Format	print and electronic
Portion	figures/tables/illustrations
Number of figures/tables/illustrations	1
High-res required	no
Figures	Figure 1
Author of this NPG article	no
Your reference number	
Title of your thesis / dissertation	Identifying and targeting coding/non-coding molecular switches regulating drug resistance and metastasis in breast cancer
Expected completion date	Sep 2017
Estimated size (number of pages)	200
Requestor Location	Bilkent university Ankara Ankara, Ankara 06800 Turkey Attn: Bilkent university
Billing Type	Invoice
Billing Address	Bilkent university Ankara

Ankara, Turkey 06800
Attn: Bilkent university

Total 0.00 USD

Terms and Conditions

Terms and Conditions for Permissions

Nature Publishing Group hereby grants you a non-exclusive license to reproduce this material for this purpose, and for no other use,subject to the conditions below:

1. NPG warrants that it has, to the best of its knowledge, the rights to license reuse of this material. However, you should ensure that the material you are requesting is original to Nature Publishing Group and does not carry the copyright of another entity (as credited in the published version). If the credit line on any part of the material you have requested indicates that it was reprinted or adapted by NPG with permission from another source, then you should also seek permission from that source to reuse the material.

2. Permission granted free of charge for material in print is also usually granted for any electronic version of that work, provided that the material is incidental to the work as a whole and that the electronic version is essentially equivalent to, or substitutes for, the print version.Where print permission has been granted for a fee, separate permission must be obtained for any additional, electronic re-use (unless, as in the case of a full paper, this has already been accounted for during your initial request in the calculation of a print run).NB: In all cases, web-based use of full-text articles must be authorized separately through the 'Use on a Web Site' option when requesting permission.

3. Permission granted for a first edition does not apply to second and subsequent editions and for editions in other languages (except for signatories to the STM Permissions Guidelines, or where the first edition permission was granted for free).

4. Nature Publishing Group's permission must be acknowledged next to the figure, table or abstract in print. In electronic form, this acknowledgement must be visible at the same time as the figure/table/abstract, and must be hyperlinked to the journal's homepage.

5. The credit line should read:
   Reprinted by permission from Macmillan Publishers Ltd: [JOURNAL NAME] (reference citation), copyright (year of publication)
   For AOP papers, the credit line should read:
   Reprinted by permission from Macmillan Publishers Ltd: [JOURNAL NAME], advance online publication, day month year (doi: 10.1038/sj.[JOURNAL ACRONYM].XXXXX)

   Note: For republication from the *British Journal of Cancer,* the following credit lines apply.
   Reprinted by permission from Macmillan Publishers Ltd on behalf of Cancer Research UK: [JOURNAL NAME] (reference citation), copyright (year of publication)For AOP papers, the credit line should read:
   Reprinted by permission from Macmillan Publishers Ltd on behalf of Cancer Research UK: [JOURNAL NAME], advance online publication, day month year (doi: 10.1038/sj.[JOURNAL ACRONYM].XXXXX)

6. Adaptations of single figures do not require NPG approval. However, the adaptation should be credited as follows:

   Adapted by permission from Macmillan Publishers Ltd: [JOURNAL NAME] (reference citation), copyright (year of publication)

   Note: For adaptation from the *British Journal of Cancer,* the following credit line applies.
   Adapted by permission from Macmillan Publishers Ltd on behalf of Cancer Research UK: [JOURNAL NAME] (reference citation), copyright (year of publication)

7. Translations of 401 words up to a whole article require NPG approval. Please visit http://www.macmillanmedicalcommunications.com for more information.Translations of up to a 400 words do not require NPG approval. The translation should be credited as follows:

   Translated by permission from Macmillan Publishers Ltd: [JOURNAL NAME] (reference citation), copyright (year of publication).

   Note: For translation from the *British Journal of Cancer,* the following credit line applies.
   Translated by permission from Macmillan Publishers Ltd on behalf of Cancer Research UK: [JOURNAL NAME] (reference citation), copyright (year of publication)

We are certain that all parties will benefit from this agreement and wish you the best in the use of this material. Thank you.

Special Terms:

v1.1

Questions? customercare@copyright.com or +1-855-239-3415 (toll free in the US) or +1-978-646-2777.

NATURE PUBLISHING GROUP LICENSE TERMS AND CONDITIONS

Aug 20, 2017

This Agreement between Bilkent university -- Umar Raza ("You") and Nature Publishing Group ("Nature Publishing Group") consists of your license details and the terms and conditions provided by Nature Publishing Group and Copyright Clearance Center.

License Number	4173090228897
License date	Aug 20, 2017
Licensed Content Publisher	Nature Publishing Group
Licensed Content Publication	Nature Cell Biology
Licensed Content Title	Many roads to maturity: microRNA biogenesis pathways and their regulation
Licensed Content Author	Julia Winter, Stephanie Jung, Sarina Keller, Richard I. Gregory and Sven Diederichs
Licensed Content Date	Mar 1, 2009
Licensed Content Volume	11
Licensed Content Issue	3
Type of Use	reuse in a dissertation / thesis
Requestor type	academic/educational
Format	electronic
Portion	figures/tables/illustrations
Number of figures/tables/illustrations	1
High-res required	no
Figures	Figure 1
Author of this NPG article	no
Your reference number	
Title of your thesis / dissertation	Identifying and targeting coding/non-coding molecular switches regulating drug resistance and metastasis in breast cancer
Expected completion date	Sep 2017
Estimated size (number of pages)	200
Requestor Location	Bilkent university Ankara Ankara, Ankara 06800 Turkey Attn: Bilkent university
Billing Type	Invoice
Billing Address	Bilkent university Ankara

Ankara, Turkey 06800
Attn: Bilkent university

Total 0.00 USD

Terms and Conditions

Terms and Conditions for Permissions

Nature Publishing Group hereby grants you a non-exclusive license to reproduce this material for this purpose, and for no other use,subject to the conditions below:

1. NPG warrants that it has, to the best of its knowledge, the rights to license reuse of this material. However, you should ensure that the material you are requesting is original to Nature Publishing Group and does not carry the copyright of another entity (as credited in the published version). If the credit line on any part of the material you have requested indicates that it was reprinted or adapted by NPG with permission from another source, then you should also seek permission from that source to reuse the material.

2. Permission granted free of charge for material in print is also usually granted for any electronic version of that work, provided that the material is incidental to the work as a whole and that the electronic version is essentially equivalent to, or substitutes for, the print version.Where print permission has been granted for a fee, separate permission must be obtained for any additional, electronic re-use (unless, as in the case of a full paper, this has already been accounted for during your initial request in the calculation of a print run).NB: In all cases, web-based use of full-text articles must be authorized separately through the 'Use on a Web Site' option when requesting permission.

3. Permission granted for a first edition does not apply to second and subsequent editions and for editions in other languages (except for signatories to the STM Permissions Guidelines, or where the first edition permission was granted for free).

4. Nature Publishing Group's permission must be acknowledged next to the figure, table or abstract in print. In electronic form, this acknowledgement must be visible at the same time as the figure/table/abstract, and must be hyperlinked to the journal's homepage.

5. The credit line should read:
   Reprinted by permission from Macmillan Publishers Ltd: [JOURNAL NAME] (reference citation), copyright (year of publication)
   For AOP papers, the credit line should read:
   Reprinted by permission from Macmillan Publishers Ltd: [JOURNAL NAME], advance online publication, day month year (doi: 10.1038/sj.[JOURNAL ACRONYM].XXXXX)

   Note: For republication from the *British Journal of Cancer,* the following credit lines apply.
   Reprinted by permission from Macmillan Publishers Ltd on behalf of Cancer Research UK: [JOURNAL NAME] (reference citation), copyright (year of publication)For AOP papers, the credit line should read:
   Reprinted by permission from Macmillan Publishers Ltd on behalf of Cancer Research UK: [JOURNAL NAME], advance online publication, day month year (doi: 10.1038/sj.[JOURNAL ACRONYM].XXXXX)

6. Adaptations of single figures do not require NPG approval. However, the adaptation should be credited as follows:

   Adapted by permission from Macmillan Publishers Ltd: [JOURNAL NAME] (reference citation), copyright (year of publication)

   Note: For adaptation from the *British Journal of Cancer,* the following credit line applies.
   Adapted by permission from Macmillan Publishers Ltd on behalf of Cancer Research UK:

[JOURNAL NAME] (reference citation), copyright (year of publication)

7. Translations of 401 words up to a whole article require NPG approval. Please visit http://www.macmillanmedicalcommunications.com for more information.Translations of up to a 400 words do not require NPG approval. The translation should be credited as follows:

   Translated by permission from Macmillan Publishers Ltd: [JOURNAL NAME] (reference citation), copyright (year of publication).

   Note: For translation from the *British Journal of Cancer*, the following credit line applies.
   Translated by permission from Macmillan Publishers Ltd on behalf of Cancer Research UK: [JOURNAL NAME] (reference citation), copyright (year of publication)

We are certain that all parties will benefit from this agreement and wish you the best in the use of this material. Thank you.

Special Terms:

v1.1

Questions? customercare@copyright.com or +1-855-239-3415 (toll free in the US) or +1-978-646-2777.